



Publicly Accessible Penn Dissertations


Fall 2010

A Study of Molecular Adsorption and Transport at Cell Membrane and Biologically Relevant Surfaces by Second Harmonic Generation

Jia Zeng

University of Pennsylvania, zengjia@sas.upenn.edu

Follow this and additional works at: <https://repository.upenn.edu/edissertations>

 Part of the [Biophysics Commons](#), and the [Physical Chemistry Commons](#)

Recommended Citation

Zeng, Jia, "A Study of Molecular Adsorption and Transport at Cell Membrane and Biologically Relevant Surfaces by Second Harmonic Generation" (2010). *Publicly Accessible Penn Dissertations*. 292.
<https://repository.upenn.edu/edissertations/292>

This paper is posted at ScholarlyCommons. <https://repository.upenn.edu/edissertations/292>
For more information, please contact repository@pobox.upenn.edu.

A Study of Molecular Adsorption and Transport at Cell Membrane and Biologically Relevant Surfaces by Second Harmonic Generation

Abstract

Most of the biological processes in living systems involve molecular adsorption and transport at biomembranes. It is highly desired to study the time-resolved transport kinetics through living cell membranes. In this thesis, an experimental means based on a nonlinear optical phenomenon, Second Harmonic Generation (SHG) has been demonstrated to detect the molecular adsorption and transport through living cell membranes in real time and to evaluate the salt ion effects on adsorption processes in biologically relevant colloidal systems. In the case of gram-negative bacteria, *E. coli*, a hydrophobic cation, Malachite Green (MG) has been observed to adsorb onto the cell surface and then sequentially transport across the double bilayer structures, the bacterial outer membrane and the cytoplasmic membrane. The adsorption characteristics as well as the transport rate constant at each of the membranes have been determined. In contrast to the prokaryotic *E. coli* cell, the molecular ion can adsorb onto the eukaryotic Murine Erythroleukemia (MEL) cell but cannot penetrate its membrane which has no hydrophobic ion permeable channels and is more tightly packed.

MG cation has been used as a SHG indicator to probe the effects of solvent ionic strength and ion specificity on molecular adsorption at model protein systems. Polystyrene sulfate (PSS) microspheres and polystyrene carboxyl (PSC) microspheres have been examined. The electrostatic force dominated molecule-surface interaction between MG cations and the sulfate terminations at PSS surface is largely affected by the ionic strength of the solution but is not sensitive to the ion identity. On the other hand, the hydrophobic force dominated molecule-surface interaction between hydrophobic regions of the MG dye and PSC microsphere shows pronounced specific ion effects but is less affected by ionic strength of the solution.

Degree Type

Dissertation

Degree Name

Doctor of Philosophy (PhD)

Graduate Group

Chemistry

First Advisor

Hai-Lung Dai

Keywords

cell membrane, molecular transport, ion channel, Hofmeister Series, hydrophobic interaction, Second Harmonic Generation

Subject Categories

Biophysics | Chemistry | Physical Chemistry

**A STUDY OF MOLECULAR ADSORPTION AND TRANSPORT
AT CELL MEMBRANE AND BIOLOGICALLY RELEVANT SURFACES
BY SECOND HARMONIC GENERATION**

Jia Zeng

A DISSERTATION

in

Chemistry

Presented to the Faculties of the University of Pennsylvania in Partial
Fulfillment of the Requirements for the Degree of Doctor of Philosophy

2010

Professor Hai-Lung Dai
Supervisor of Dissertation

Professor Gary Molander
Graduate Group Chair

Committee Members:

J. Kent Blasie, Walter H. & Leonore C. Annenberg Professor in the Natural Sciences
Robin Hochstrasser, Donner Professor of Physical Sciences
Michael L. Klein, Laura H. Carnell Professor of Science

A STUDY OF MOLECULAR ADSORPTION AND TRANSPORT
AT CELL MEMBRANE AND BIOLOGICALLY RELEVANT SURFACES
BY SECOND HARMONIC GENERATION

COPYRIGHT

2010

Jia Zeng

To My Youth

ACKNOWLEDGEMENTS

There are many people without whom this thesis would not be possible. First, I would express my sincere gratitude to Professor Hai-Lung Dai for his immeasurable support and encouragement during my life at UPenn. His inspiring guidance and good humor led me out the difficulty times in pursuing projects whose outcome was unpredictable. There have been many expected and unexpected obstacles since the first day we started to study the bio-related systems. His passion and creative thoughts on this project has been the strongest backing of me. Under his supervision, I received rigorous training required to become an independent researcher.

Second, I would like to thank the members of my committee: Professor J. Kent Blasie, Professor Robin Hochstrasser, and Professor Michael L. Klein for their priceless time, comments, and encouragements for my research. The questions they asked during my committee meeting every year helped me think further in my research projects.

I must mention the collaborative laboratories that offered help to my research projects. Without our previous neighbor Professor Mark Goulian's group (especially Dr. Tim Miyashiro), it wouldn't be possible for me to initiate *E.coli* experiments. And later Professor Gerd A. Blobel (especially Dr. Wulan Deng) was kind enough to provide us MEL cell line. Dr. Luca D'Agostino of Temple University assisted me with culturing techniques, for which I am very grateful.

I would also like to thank Professor Hongfei Wang for the useful discussion during his visit to Dai Group. His knowledge and rich experience in this area were of great help to me.

Special thanks goes out to Dr. Shih-Hui Jen for teaching me the precious hands-on tricks of how to handle the lasers, which actually helped my first step out on research.

I would also like to thank former and current Dai Group members, Heather Eckenrode, Wei Gan, Grazia Gonella, Jun Han, Jianqiang Ma, Matt Nikow, Rosa Qensinberry, Jonathan Smith, Michael Wilhelm, Bolei Xu, and Min Zhang for assistance and discussion in my projects.

Finally, I would like to thank my family, especially, my mother and my 90 year old grandmother for their continued and unselfish support all these years. I must also thank my fiancé, Jin Xu, for giving me the last push to get to the end of this thesis.

ABSTRACT

A STUDY OF MOLECULAR ADSORPTION AND TRANSPORT
AT CELL MEMBRANE AND BIOLOGICALLY RELEVANT SURFACES
BY SECOND HARMONIC GENERATION

Jia Zeng

Hai-Lung Dai

Most of the biological processes in living systems involve molecular adsorption and transport at biomembranes. It is highly desired to study the time-resolved transport kinetics through living cell membranes. In this thesis, an experimental means based on a nonlinear optical phenomenon, Second Harmonic Generation (SHG) has been demonstrated to detect the molecular adsorption and transport through living cell membranes in real time and to evaluate the salt ion effects on adsorption processes in biologically relevant colloidal systems. In the case of gram-negative bacteria, *E.coli*, a hydrophobic cation, Malachite Green (MG) has been observed to adsorb onto the cell surface and then sequentially transport across the double bilayer structures, the bacterial outer membrane and the cytoplasmic membrane. The adsorption characteristics as well as the transport rate constant at each of the membranes have been determined. In contrast to the prokaryotic *E.coli* cell, the molecular ion can adsorb onto the eukaryotic Murine Erythroleukemia (MEL) cell but cannot penetrate its membrane which has no hydrophobic ion permeable channels and is more tightly packed.

MG cation has been used as a SHG indicator to probe the effects of solvent ionic strength and ion specificity on molecular adsorption at model protein systems. Polystyrene sulfate (PSS) microspheres and polystyrene carboxyl (PSC) microspheres

have been examined. The electrostatic force dominated molecule-surface interaction between MG cations and the sulfate terminations at PSS surface is largely affected by the ionic strength of the solution but is not sensitive to the ion identity. On the other hand, the hydrophobic force dominated molecule-surface interaction between hydrophobic regions of the MG dye and PSC microsphere shows pronounced specific ion effects but is less affected by ionic strength of the solution.

TABLE OF CONTENTS

Chapter 1: Introduction	1
1.1 Colloidal Interfaces.....	1
1.2 Cell Membrane Interfaces.....	3
1.3 Interface Studies by Second Harmonic Generation.....	5
1.4 Aim and Scope of this Dissertation.....	8
Chapter 2: Second Harmonic Generation at Interfaces	22
2.1 Introduction.....	22
2.2 Theory of Second Harmonic Generation.....	23
2.2.1 Phenomenological Mode and Maxwell's Equation.....	25
2.2.2 Second Order Nonlinear Susceptibility.....	28
2.2.2.1 Molecular Energy Level and Second Order Nonlinear Susceptibility... 28	
2.2.2.2 Second Order Nonlinear Susceptibility Tensor.....	29
2.2.2.3 Electric Fields in the Interface Layer and Polarization Expressions of SHG.....	29
2.2.3 Transformation of Susceptibilities to Molecular Polarizabilities.....	31
2.3 Second Harmonic Generation at Colloidal Interfaces.....	35
Chapter 3: Molecular Adsorption and Time-Resolved Molecular Transport across <i>E.coli</i> Cell Membranes	48
3.1 Introduction.....	48
3.2 Experiment.....	51
3.2.1 The Laser System.....	51
3.2.2 Sample Flow-jet Circulation System.....	52

3.2.3 Malachite Green (MG) Dye	53
3.2.4 Cell Culture.....	54
3.3 Modified <i>Langmuir</i> Adsorption Model.....	54
3.3.1 Adsorption Isotherms.....	54
3.3.2 Modified <i>Langmuir</i> Adsorption Model.....	55
3.3.3 Application of the Modified <i>Langmuir</i> Model in Analyzing MG Adsorption under Physiological pH Value.....	56
3.3.4 Surface Coverage and SHG.....	58
3.4 Results and Discussion.....	59
3.4.1 Molecular Adsorption onto <i>E.coli</i> Cell Surface.....	59
3.4.2 Time-Resolved Molecular Transport through <i>E.coli</i> Membranes.....	62
3.4.3 Salt Effects on Molecular Adsorption at <i>E.coli</i> Cell Membrane.....	66
3.5 Summary.....	67
Chapter 4: Molecular Adsorption on Murine Erythroleukemia (MEL) Cell Membrane	89
4.1 Introduction.....	89
4.2 Experiment.....	93
4.3 Results and Analysis.....	94
4.4 Discussion.....	97
4.4.1. Driving Force of Molecular Adsorption is Charge-Charge Interaction.....	97
4.4.2. Adsorption Characteristics.....	99
4.4.3. Adsorbed Hydrophobic Ions Do Not Transport across MEL Cell Membrane	101
4.5 Summary.....	102

Chapter 5: Effects of Solvent Ionic Strength and Ion Specificity on Molecule-Surface Interactions in Aqueous Colloids	119
5.1 Introduction.....	119
5.2 Experiment.....	124
5.3 Standard <i>Langmuir</i> Adsorption Model.....	126
5.3.1 Standard <i>Langmuir</i> Adsorption Model.....	126
5.3.2 General Application of the Modified <i>Langmuir</i> Model by Global Fitting.....	127
5.4 Results and Discussion.....	129
5.4.1 Adsorption of MG on PSS/PSC Surfaces without Solvent Salts.....	129
5.4.2 Salt Ion Effects on MG Adsorption to Charged PSS Surface.....	131
5.4.3 Salt Ion Effects on MG Adsorption to Neutral PSC Surface.....	136
5.5 Summary.....	140
Chapter 6: Concluding Remarks	165
6.1 Perspective Applications.....	165
6.2 Feasibility.....	166

LIST OF TABLES

Table 1.1: Examples of different types of colloids based on the dispersed particles and the continuous medium.....13

Table 3.1: Specifications of Malachite Green.....80

Table 3.2: Adsorption and Transport Characteristics (a) at *E.coli* Outer Membrane, (b) at *E.coli* Cytoplasmic Membrane, and (c) Relative Results from Both Membranes in Comparison with the Liposome Results.....81

Table 3.3: Adsorption isotherms of MG ions on the *E.coli* cell under different salinities.....83

Table 4.1: Adsorption Characteristics of MG on MEL cell under Different Conditions.....111

Table 4.2: Adsorption Free Energy of MG on Polymeric Particles, Liposome and MEL Cell.....112

Table 5.1: Global fitting results versus individual fitting results of MG adsorption at PSS surface.....154

Table 5.2: Dependence of adsorption maximum density N_D^{\max} and free energy ΔG on NaCl concentration.....155

Table 5.3: Adsorption equilibrium constant and free energy of MG on PSS surface (1) without NaCl (0mM); (2) at NaCl concentration (44mM) where SH intensity reaches peak value; (3) at NaCl concentration (150mM) where SH intensity levels off.....156

Table 5.4: Adsorption equilibrium constant and free energy of MG on PSS surface at featured ionic strengths: (a) 50mM and (b) 150mM, for the anion series: I^- , Cl^- , SO_4^{2-} 157

Table 5.5: Adsorption equilibrium constant and free energy of MG on PSC surface at measured ionic strengths: (a) 50mM and (b) 150mM, the cation series: Li^+ , Na^+ , K^+ , NH_4^+ 158

LIST OF ILLUSTRATIONS

Figure 1.1: A schematic representative of colloidal systems according to their typical range of dimensions.....	12
Figure 2.1: Schematic of the typical phenomenological model to treat the second harmonic response from a planer interface between two isotropic bulk media.....	39
Figure 2.2: The energy diagram of SHG in which the SH frequency 2ω is in resonant enhancement with the electronic transition from the ground state $ g\rangle$ to the excited state $ f\rangle$	40
Figure 2.3: Schematic of the rotations to transform from molecular coordinates to lab coordinates using Euler angles.....	41
Figure 2.4: Schematic of SHG from two SH producing molecules adsorbed at centrosymmetric particles with opposite orientations.....	42
Figure 3.1: Schematic illustration of the experimental setup of the forward detection of SHG signal.....	69
Figure 3.2: MG structure and its spectral features.....	70
Figure 3.3: Spectrum of the two-photon absorption and the two-photon excited fluorescence for malachite green.....	71
Figure 3.4: System of isotherm classification	72
Figure 3.5: Typical <i>Langmuir</i> adsorption isotherm curve expressed in SH intensity versus molecular concentration.....	73
Figure 3.6: Illustration of the two membranes of the <i>E.coli</i> bacteria.....	74
Figure 3.7: Time profile of the SH intensity following addition of the MG ion (at $0.25\mu\text{M}$) to the <i>E.coli</i> bacteria solution.....	75

Figure 3.8: Nonlinear least-square fits (solid green lines) of the time profiles of the SH intensity (normalized) following addition of MG ions at various concentrations into solutions containing living <i>E.coli</i> cells.....	76
Figure 3.9: Time profiles of membrane surface coverage simulated using the kinetic model for MG=0.25 μ M.....	77
Figure 3.10: Adsorption isotherm expressed in SH intensity for MG ion on the <i>E.coli</i> cell.....	78
Figure 3.11: Adsorption isotherms of MG ions on the <i>E.coli</i> cell under different salinities. The solid lines are nonlinear least-square fits of a modified <i>Langmuir</i> model.....	79
Figure 4.1: Molecular Structures of (a) Malachite Green (MG); (b) Bromocresol Purple (BCP).....	104
Figure 4.2: SHG signal detected as a function of time following addition of MG ions into the MEL cell solution at neutral pH.....	105
Figure 4.3: Adsorption isotherms expressed in SH intensity for MG adsorbed on MEL cell membrane surface at different conditions: (a) acidic pH value (pH=4.5); (b) neutral pH value (pH=7.0); (c) MEL cell at a further differentiated stage.....	107
Figure 4.4: SH signal detected with increasing BCP concentration added into a solution containing MEL cells at acidic pH value (pH=4.5).....	108
Figure 4.5: Illustration of the MEL cell membrane structure.....	109
Figure 4.6: pH dependence of [COOH] and [COO ⁻] of polystyrene carboxyl microspheres in water.....	110

Figure 5.1: A theoretical simulation of the modified <i>Langmuir</i> model with the adsorption equilibrium constant set to a small value ($5 \times 10^7 \text{M}^{-1}$) for different maximum surface adsorption densities ($1 \mu\text{M}$ and $5 \mu\text{M}$).....	142
Figure 5.2: Theoretical simulations of the modified <i>Langmuir</i> isotherms expressed in SH intensity as a function of MG concentration: (a) isotherms at a fixed value of adsorption equilibrium constant ($K = 10^{10}$) by varying maximum adsorption density; (b) isotherms at a fixed value of maximum adsorption density ($N_{\text{max}} = 0.2 \mu\text{M}$) by varying adsorption equilibrium constant.....	143
Figure 5.3: An example of analyzing a set of adsorption isotherms of malachite green (MG) molecules on polystyrene sulfate (PSS) surface by Global Fitting.....	144
Figure 5.4: SH intensity detected as a function of MG concentration added in the colloidal solution of (a) charged polystyrene sulfate microspheres (PSS); and (b) neutral polystyrene carboxyl microspheres (PSC) particle surfaces, at $\text{pH} = 3.5 \pm 0.2$	145
Figure 5.5: SH intensity recorded as a function of NaCl concentration added in the MG fully covered PSS colloidal solutions.....	146
Figure 5.6: MG adsorption isotherms on PSS surfaces at different NaCl concentrations.....	147
Figure 5.7: Dependence of (a) adsorption maximum density N_D^{max} and (b) free energy ΔG on NaCl concentration.....	148
Figure 5.8: Titration profiles of a series of chloride salts: LiCl, NaCl, KCl, NH_4Cl into PSS colloids pre-covered with MG.....	149
Figure 5.9: (a) SH intensity recorded as a function of NaCl concentration added in the MG fully covered PSC colloidal solutions. Also displayed is the control trial titrated with	

blank solution without NaCl. (b) MG adsorption isotherms of PSC (1) without NaCl (0mM); (2) at NaCl concentration (44mM) where SH intensity reaches peak value; (3) at NaCl concentration (150mM) where SH intensity levels off.....150

Figure 5.10: SH intensities as function of salt concentrations of (a) sodium salts of different anions: I^- , Cl^- , SO_4^{2-} ; and (b) chlorides with different cations: Li^+ , Na^+ , K^+ , NH_4^+ ; applied into PSC colloids pre-saturated with MG molecules.....151

Figure 5.11: MG adsorption isotherms on PSC surfaces at featured ionic strengths for the anion series: I^- , Cl^- , SO_4^{2-} at (a) 50mM; (b) 150mM; and the cation series: Li^+ , Na^+ , K^+ , NH_4^+ at (c) 50mM; (d) 150mM.....153

CHAPTER ONE

INTRODUCTION

1.1 Colloidal Interfaces

Stone Age paintings with stabilized colloidal pigments could be the earliest evidence of man's use of colloids [1]. In 1845, Francesco Selmi first defined common properties of slightly turbid "pseudosolutions", which was later named as "colloid" by Thomas Graham in 1861 [1]. The low diffusion rates of colloidal particles implied the low end of the particle size to be at least 1nm in diameter while the failure of the particles to sediment under the influence of gravity implied the upper size limit to be approximately 1 μ m. Most of the studies are focused on the monodispersed objects of sizes ranging from 10nm to several micron meters [2-4]. Figure 1.1 is the schematic representative of various colloidal systems with their typical range and critical dimensions [5]. According to the chart, the upper limit of the critical dimension for colloid definition has been extended from 1 μ m to 100 μ m.

"Colloid" is no longer a modern term, however, colloidal science has become ubiquitous, which encompasses many chemical and biological systems and influences almost all technological processes [1, 6, 7]. Manipulation of colloidal systems can be date

back to our earliest technological processes, such as paper making, pottery making, and the fabrication of soaps and cosmetics. The extensive appearance of colloids in nature, biology and technology clearly demonstrated its importance. A variety of colloidal systems has long been fully developed industrial products, such as, papers, inks, paints, coatings, and ceramics in chemical industry and clays, minerals, aerosols, semiconductors and solar cells in material industry [8-20]. More recently, novel uses have been found for newly developed biological systems [21-32]. Listed in Table 1.1 is the examples of how colloids of all phases of matter are important in a highly industrialized society [1].

A typical colloidal system is often viewed as being comprised of two phases: the dispersed phase (the colloidal particle) and the dispersing medium (the solvent) separated by a well-defined interface. These interfaces are regions of high free energy, where many surface phenomena, such as adsorption and the formation of electrical double layers, take place; therefore, surface properties dominate the behavior of colloidal systems and play an integral role in colloidal science. To understand the observation of interfacial phenomenon is the key to solve practical issues and exploit the commercial use of colloidal systems. A primary concern in the application of colloidal systems is the dispersion stability, in which the inter-particle interactions and the particle-solvent interactions play an integral role. Therefore, structures and kinetic/dynamic processes at colloidal interfaces are of practical and fundamental interest.

Since the interfacial properties is deterministic for colloidal behavior, the most common practice to probe and modify the surface of the colloids is to have molecule species with specific properties (i.e., a surfactant, an emulsifier) adsorbed at the interface. Characterization of the molecular adsorption processes can therefore help to understand

and predict colloidal behaviors. Many investigations have focused on characterizing molecular adsorptions for the understanding of the effect of the molecular-interface interactions on colloidal behaviors as well as the nature of those adsorption processes [33-36]. One of the recent interests is to study the deterministic factors, such as the solvent ionic strength and ion specificity, which could influence molecular adsorption at colloidal surfaces. Both direct and indirect measurements of the characteristics of molecular adsorption has been conducted the details of which will be described in section 1.3.

1.2 Cell Membrane Interfaces

The interests in colloidal systems not only have technological reason but also have anthropological reason. Living systems are one of the most intriguing and challenging scientific area in the nature. Significant advances have been made in understanding and explaining various biological processes. It has long been recognized that the physiological conditions, size and structure, and the intrinsic properties of living systems makes it possible to be treated at the colloidal level from several perspectives:

Firstly, living systems are usually made up of proteins, polyelectrolytes, and amphiphilic molecules contained in an aqueous medium. Such molecules, by their size and structure, not necessary be classified as colloids, but do possess colloidal properties. They may further self-assemble into a great variety of organized structures that perform extremely sophisticated chemical and biological transformations. For example, many diseases are proved to be associated with malfunctions involving transformation of

colloidal assemblies [1]. To understand and control those life processes can be achieved by monitoring the characteristics and properties at the colloidal level.

Secondly, it has long been the research focus to exploit appropriate colloidal systems to achieve efficient drug delivery. More than one membrane must be permeated before a drug molecule passes from the outside into a capillary. The quantitative study of absorption, distribution, metabolism, and elimination of drugs is therefore closely associated with colloidal science. Most drug candidates often suffer from the First Pass Effect, that drugs may be metabolized (for example, by the liver) following absorption but before reaching systemic circulation. Another major limitation is that drug molecules as well as drug carriers usually get quickly removed from the blood, plasma or serum while effective drug delivery systems require sustained drug concentration. Applications of self-assembled vesicles as well as nanoparticles in controlled drug release have been reported [37, 38]. The control of targeted drug delivery and medical diagnostic systems are actually highly dependent on our ability to control fundamental colloidal interactions.

Last but not least, in this thesis, we consider cell suspensions as colloidal systems as well and characterize the interfacial properties of the cell membrane interfaces under different conditions. Almost all of the prokaryotic cells and a lot of the eukaryotic cells are within the size range of colloidal definition. Except that cells intend to stick to glass walls, they can be suspended in physiological buffers and stay as stable suspensions without sediment for a relatively long period of time. This is due to the specific composition and organization of the cell membrane structure, the lipid bilayer structures. The outer surface of the cell membrane is hydrophilic phosphate groups that favor the aqueous environment in living systems. The natural cell membrane interfaces turned out

to be one of the best defined colloidal interfaces. Some of the cells would even have special structures with the function to maintain certain cell shape. For example, the murein layer in Gram-negative bacteria cells and the network of proteins that forms the skeleton of the red blood cell (RBC) membrane. Uniformed cell shape makes cell suspension a better model for colloidal characterizations. Almost all of the life processes involve interfacial association with various molecules at the biological membranes as the initial step. Further interactions occur at the cell membrane or transport through the cell membranes can be all influenced by the very first interfacial adsorption processes. The investigation of the cell membrane interface related chemical and biological processes from a colloidal perspective will not only help to understand the intrinsic properties of specific cell membrane interfaces and the associated interactions, but also provide a model for predicting the general molecular adsorption and transport processes at biological membranes. The interfacial studies require experimental capabilities for characterizing the structure and kinetic/dynamic processes at the colloidal and biological membrane interfaces.

1.3 Interface Studies by Second Harmonic Generation

Many powerful techniques, such as LEED, XPS, IR, AFM, etc. [39], have been developed to study solid surfaces, providing information on adsorption geometry, surface chemical composition, as well as vibrational structures. However, UHV conditions are a requirement for these surface investigation techniques, which makes it a common limitation in terms of their application to buried interfaces, often involving liquid phases. Therefore, optical techniques rather than electronic methods are favored since buried

interfaces are accessible to light. These optical techniques include absorption and reflection spectroscopy, Raman and Infrared spectroscopy, fluorescence spectroscopy, ellipsometry and light scattering [40].

However, for scientists immersed in colloidal systems, the conventional optical techniques suffer the lack of surface sensitivity and selectivity. The barrier of probing molecular interactions at colloidal surfaces is due to the fact that the spectroscopic signal of a small surface population is often overwhelmed by a much larger contribution from bulk species. The surface information is thus buried if the molecules of interest are present both at the interface and in the bulk phase. However, the systems, including vesicles, micelles, emulsions, droplets and cell suspensions have great importance in nature and life sciences as discussed in the previous section. For these systems, the adsorption of molecules at interfaces is described by the Gibbs adsorption equation and the *Langmuir* adsorption isotherm. Only in very rare situations, the shifts in the spectra of interfacial adsorbed molecules are sufficient to allow differentiation from the bulk molecules [41-45], due to the inhomogeneous broadening in the condensed phase.

The arrival of interface specific non-linear optical techniques, i.e. Second Harmonic Generation (SHG) and Sum Frequency Generation (SFG), overcome the main obstacle of conventional linear optical techniques [46-50]. They are capable to achieve selectivity between interfacial and bulk molecules and furthermore, the frequency of the output optical signal lies in a different spectral region from that of the incident light, which enables easy discrimination and detection of the desired signal. Therefore, SHG and SFG have proven to be extremely useful in probing sub-monolayer of interfacial adsorbed molecules. By employing tunable and ultra-short laser pulses, ultrafast

molecular reaction and relaxation dynamic processes can be directly probed at interfaces [48, 49, 51].

The nonlinear optical technique used in this thesis is Second Harmonic Generation (SHG). SHG is the second order nonlinear optical process, in which two photons of one frequency (ω) simultaneously interact with a non-linear medium and generate radiation at the second harmonic frequency (2ω). Similar principle for the technique of Sum Frequency Generation (SFG) is that two frequencies (ω_1 and ω_2) of light interact with medium and the sum frequency ($\omega_1+\omega_2$) is generated. In this thesis, only SHG technique is employed to probe colloidal and biological interfaces. The production of SHG is sensitive to the symmetry of the medium. It is believed that SHG is electric-dipole forbidden in centrosymmetric media but allowed at interfaces where the inversion symmetry is broken down. SHG is generated only from the few layers which constitute the interface; therefore, the sensitivity of SHG technique is not determined by the optical penetration depth (optical wavelength) as conventional optical techniques. The symmetry sensitive nature of SHG makes it surface specific technique for the study of all kinds of interfaces.

The interface studies have been advancing rapidly with the interface specific nonlinear optical techniques, i.e. SHG and SFG. However, the application of SHG and SFG was restricted to planar surface for a long time. Given the fact that the SHG efficiency is usually small, for macroscopically flat interfaces, almost all of the SH photons generated from interfaces can be collected in order to achieve the sub-monolayer sensitivity. It was believed that the application of SHG to curved interfaces was not feasible due to the reduced coherence and cancelled orientations. It wasn't until 1996 that

Eisenthal group first reported the observation of SHG signal originated from the interface of spherical polystyrene particles with adsorbed dye molecules. Contrary to general thinking, SHG turned out to be dipole allowed for centrosymmetric media as long as the size scale is roughly within the range of tens of nanometers to microns. The light induced second order polarizations from the “opposite” sides of the colloidal particle do not have opposite phases and therefore do not cancel with each other. The investigation of buried interfaces, such as vesicles, micelles, emulsions, droplets and cell suspensions, began to grow since this major breakthrough. The effectiveness of SHG has been demonstrated on a full scope of colloidal systems, including polymer particles [36, 52-54], nanoparticles [55-58], carbon black particles [59], emulsions [53, 60], and living cells [61, 62].

1.4 Aim and Scope of this Dissertation

The non-destructive nature of SHG technique makes it ideal for the application to systems of biological nature in an in-situ manner. In this thesis, we reported works on investigating molecular adsorption at cell membrane interfaces as well as the subsequent molecular transport kinetics through the cell membranes. We also present study on the solvent salt effects on molecular adsorption at the colloidal interfaces. The study shed light on the understanding of the interaction driving forces that control biological processes and furthermore, the effects of local ionic conditions may have on interfacial association of molecules.

Chapter 2 is the framework of the general theory of Second Harmonic Generation (SHG) with the emphasis on interface studies. Both macroscopic and microscopic descriptions are elaborated.

In chapter 3, it is demonstrated for the first time that the nonlinear optical phenomenon Second Harmonic Generation (SHG) can be used to observe in real time the transport of molecules through living cell membranes. The adsorption and transport of a molecular ion at the *E.coli* outer and cytoplasmic membranes were recorded in sequence. Adsorption isotherms were obtained and analyzed to give molecular adsorption characteristics of free energy and adsorption density values. A kinetic model has been established to characterize the molecular transport processes through the double bilayer structures of the *E.coli* membranes. Transport of this hydrophobic ion through the outer membrane is much faster than the cytoplasmic membrane reflecting the effectiveness of ion transport porins. These observations illustrate that SHG can serve as an experimental means for studying interactions of small molecules with cell membranes, and the importance of the ionic nature and the detailed membrane structure in regulating molecular transport. The time resolved observations and characterizations have advanced the application of SHG technique to study the real time biological processes rather than limited to steady-state approximated equilibriums.

To highlight the possibility that different living cell membranes may have different molecular adsorption and transport properties, we examine a eukaryotic cell, the Murine Erythroleukemia (MEL) cell, in chapter 4. It is the first time to employ MEL cells as a model system for studying molecular interaction with eukaryotic cells. The size and shape of MEL cells favor SHG detection in the forward direction. Adsorption free energy as well as the maximum number density of model probe molecules has been determined under different conditions. Different cell membranes may have different constitutions and result in different interface characteristics as well as molecular transport mechanisms.

The collective behavior observed for molecular interactions with MEL cell interfaces together with those reported in chapter 3 for *E.coli* cell membrane interfaces, provides a new level of knowledge for the general understanding of molecular interactions at biological membrane interfaces.

In chapter 5, Second Harmonic Generation (SHG) – has been applied to investigate the solvent salt ion effects on molecule-surface interactions in aqueous colloids. Malachite Green (MG) cationic dye were used as a SHG indicator to probe ion effects on two model colloidal systems: the negatively charged polystyrene sulfate (PSS) microspheres and the neutral polystyrene carboxyl (PSC) microspheres in aqueous solutions at $\text{pH} < 4.0$. MG adsorption behavior under different ionic strength and ion specificity were examined. Modified and standard *Langmuir* models were employed to analyze the adsorption isotherms obtained for PSS and PSC, respectively. The electrostatic force dominated molecule-surface interaction between MG cations and the sulfate terminations at PSS surface is largely affected by the ionic strength of the solution but is not sensitive to the ion identity. The electrostatic contribution of the adsorption free energy depends on the interfacial electric potential, which can be related to ionic strength of the solvent salts through Gouy-Chapman model. On the other hand, the hydrophobic force dominated molecule-surface interaction between hydrophobic regions of the MG dye and PSC microsphere shows pronounced specific ion effects but is less affected by ionic strength of the solution. Surface acquired anions will provide extra adsorption sites for the cationic dye and the change in adsorption free energy reflects the electrostatic interaction between the dye and the surface acquired anions. The experimental

observations agree very well with both Hofmeister anion and cation series in the ability to precipitate.

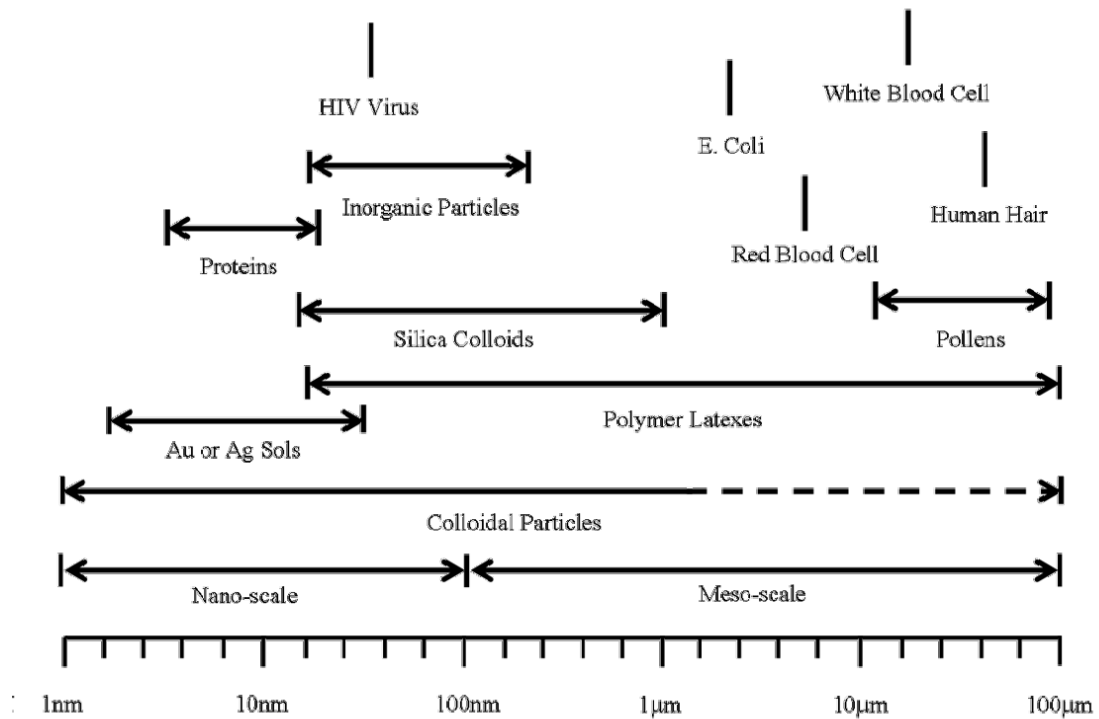


Figure 1.1: A schematic representative of colloidal systems according to their typical range of dimensions.

Table 1.1: Examples of different types of colloids based on the dispersed particles and the continuous medium.

Medium	Particle	Name	Examples		
			In Nature	Biological	Technical
Liquid	Solid	Colloidal sol	River water, glacial runoff, muddy water		Paint, ink Sol-Gel Processing
Liquid	Liquid	Emulsion (nonequilibrium) solution (equilibrium)		Fat digestion, biological membranes	Drug delivery, emulsion polymerization
Liquid	Gas	Foam	Polluted rivers	Vacuoles, insect excretions	Fire extinguishers, production of porous plastics
Gas	Solid	Aerosol	Volcanic smoke	Pollen	Inhalation of solid pharmaceuticals
Gas	Liquid	Aerosol	Clouds	Result of coughing	Hair spray, smog
Solid	Solid	Solid suspension	Wood	Bone	Composites
Solid	Liquid	Porus material	Oil reservoir rock, opals	Pearl	High impact plastics
Solid	Gas	Solid foam	Pumice	Loofah	Styrofoam, zeolites

Bibliography:

1. Evans, D.F. and H. Wennerström, *The Colloidal Domain- where physics, chemistry, biology, and technology meet*. 2nd ed. 1999, New York: Wiley-VCH.
2. Matijevic, E., *Preparation and properties of uniform size colloids*. Chem. Mat., 1993. **5**(4): p. 412-426.
3. Matijevic, E., *Uniform inorganic colloid dispersions - achievements and challenges*. Langmuir, 1994. **10**(1): p. 8-16.
4. Ozin, G.A., *Nanochemistry - synthesis in diminishing dimensions*. Adv. Mater., 1992. **4**(10): p. 612-649.
5. Xia, Y.N., et al., *Monodispersed colloidal spheres: old materials with new applications*. Adv. Mater., 2000. **12**(10): p. 693-713.
6. Antonietti, M., *Colloid Chemistry*. 2003, Springer: New York.
7. Everett, D.H., *Principles of Colloidal Science*. 1988, London: Royal Society of Chemistry.
8. Alivisatos, A.P., *Semiconductor clusters, nanocrystals, and quantum dots*. Science, 1996. **271**(5251): p. 933-937.
9. Bovey, F.A., *Emulsion Polymerization*. 1955, New York: Interscience.
10. Henglein, A., *Small-particle research -physicochemical properties of extremely small colloidal metal and semiconductor particles*. Chem. Rev., 1989. **89**(8): p. 1861-1873.
11. Idler, R.K., *The Chemistry of Silica*. 1979, New York: Wiley.
12. Pieranski, P., *Colloidal crystals*. Contemp. Phys., 1983. **24**(1): p. 25-73.

13. Pieranski, P., L. Strzelecki, and B. Pansu, *Thin colloidal crystals*. Phys. Rev. Lett., 1983. **50**(12): p. 900-903.
14. Schick, M.J., *Science and Technology of Polymer Colloids*, G.W. Poehlein, R.H. OTTEWILL, and J.W. Goodwin, Editors. 1983, Martinus Nijhoff: Amsterdam.
15. Schmid, G., *Large clusters and colloids - metals in the embryonic state*. Chem. Rev., 1992. **92**(8): p. 1709-1727.
16. Schmid, G. and L.F. Chi, *Metal clusters and colloids*. Adv. Mater., 1998. **10**(7): p. 515-526.
17. Schon, G. and U. Simon, *A fascinating new field in colloid science - small ligand-stabilized metal-clusters and possible application in microelectronics. 1. state-of-the-art*. Colloid Polym. Sci., 1995. **273**(2): p. 101-117.
18. Steigerwald, M.L. and L.E. Brus, *Semiconductor crystallites - a class of large molecules*. Accounts Chem. Res., 1990. **23**(6): p. 183-188.
19. Wang, Z.L., *Structural analysis of self-assembling nanocrystal superlattices*. Adv. Mater., 1998. **10**(1): p. 13-+.
20. Weller, H., *Colloidal semiconductor Q-particles - chemistry in the transition region between solid-state and molecules*. Angew. Chem.-Int. Edit. Engl., 1993. **32**(1): p. 41-53.
21. Kataoka, K., A. Harada, and Y. Nagasaki, *Block copolymer micelles for drug delivery: design, characterization and biological significance*. Adv. Drug Deliv. Rev., 2001. **47**(1): p. 113-131.

22. Moghimi, S.M., A.C. Hunter, and J.C. Murray, *Long-circulating and target-specific nanoparticles: theory to practice*. Pharmacol. Rev., 2001. **53**(2): p. 283-318.
23. Brigger, I., C. Dubernet, and P. Couvreur, *Nanoparticles in cancer therapy and diagnosis*. Adv. Drug Deliv. Rev., 2002. **54**(5): p. 631-651.
24. Martinek, K., et al., *Micellar enzymology*. Eur. J. Biochem., 1986. **155**(3): p. 453-468.
25. Parak, W.J., et al., *Biological applications of colloidal nanocrystals*. Nanotechnology, 2003. **14**(7): p. R15-R27.
26. Yguerabide, J. and E.E. Yguerabide, *Light-scattering submicroscopic particles as highly fluorescent analogs and their use as tracer labels in clinical and biological applications - I. Theory*. Anal. Biochem., 1998. **262**(2): p. 137-156.
27. Stolnik, S., L. Illum, and S.S. Davis, *Long circulating microparticulate drug carriers*. Adv. Drug Deliv. Rev., 1995. **16**(2-3): p. 195-214.
28. Kakizawa, Y. and K. Kataoka, *Block copolymer micelles for delivery of gene and related compounds*. Adv. Drug Deliv. Rev., 2002. **54**(2): p. 203-222.
29. Otsuka, H., Y. Nagasaki, and K. Kataoka, *PEGylated nanoparticles for biological and pharmaceutical applications*. Adv. Drug Deliv. Rev., 2003. **55**(3): p. 403-419.
30. Janes, K.A., P. Calvo, and M.J. Alonso, *Polysaccharide colloidal particles as delivery systems for macromolecules*. Adv. Drug Deliv. Rev., 2001. **47**(1): p. 83-97.

31. Chiou, P.Y., A.T. Ohta, and M.C. Wu, *Massively parallel manipulation of single cells and microparticles using optical images*. *Nature*, 2005. **436**(7049): p. 370-372.
32. Penn, S.G., L. He, and M.J. Natan, *Nanoparticles for bioanalysis*. *Curr. Opin. Chem. Biol.*, 2003. **7**(5): p. 609-615.
33. Radovic, L.R., et al., *An experimental and theoretical study of the adsorption of aromatics possessing electron-withdrawing and electron-donating functional groups by chemically modified activated carbons*. *Carbon*, 1997. **35**(9): p. 1339-1348.
34. Matijevic, E., *Interactions of solutes with monodispersed colloids - practical aspects*, in *Adsorption and Its Applications in Industry and Environmental Protection, Vol I: Applications in Industry*. 1999, Elsevier Science Publ B V: Amsterdam. p. 847-878.
35. Aray, Y., et al., *Electrostatics for exploring the nature of water adsorption on the laponite sheets' surface*. *J. Phys. Chem. B*, 2003. **107**(34): p. 8946-8952.
36. Eckenrode, H.M., et al., *Adsorption of a cationic dye molecule on polystyrene microspheres in colloids: Effect of surface charge and composition probed by second harmonic generation*. *J. Phys. Chem. B.*, 2005. **109**(10): p. 4646-4653.
37. Chambers, E. and S. Mitragotri, *Prolonged circulation of large polymeric nanoparticles by non-covalent adsorption on erythrocytes*. *J. Control. Release*, 2004. **100**(1): p. 111-119.

38. Chambers, E. and S. Mitragotri, *Long circulating nanoparticles via adhesion on red blood cells: mechanism and extended circulation*. *Exp. Biol. Med.*, 2007. **232**(7): p. 958-966.
39. Somorjai, G.A., *Chemistry in Two Dimensions: Surfaces*. 1981, Ithaca: Cornell Univeristy Press.
40. *Light scattering by liquid surfaces and complementary techniques* D. Langevin, Editor. 1992, M. Dekker, Inc.: New York.
41. Zachariasse, K.A., N. Vanphuc, and B. Kozankiewicz, *Investigation of micelles, micro-emulsions, and phospholipid-bilayers with the pyridinium n-phenolbetaine ET(30), a polarity probe for aqueous interfaces*. *J. Phys. Chem.*, 1981. **85**(18): p. 2676-2683.
42. Warr, G.G. and D.F. Evans, *Spectroscopic determination of the effective dielectric-constant of micelle water interfaces between 15 and 85-degrees-C*. *Langmuir*, 1988. **4**(1): p. 217-224.
43. Ueda, M. and Z.A. Schelly, *Reverse micelles of aerosol-ot in benzene. 4. investigation of the micropolarity using 1-methyl-8-oxyquinolinium betaine as a probe*. *Langmuir*, 1989. **5**(4): p. 1005-1008.
44. Varadaraj, R., et al., *Micropolarity and water penetration in micellar aggregates of linear and branched hydrocarbon surfactants*. *Langmuir*, 1990. **6**(8): p. 1376-1378.
45. Zhu, D.M., X. Wu, and Z.A. Schelly, *Reverse micelles and water in oil microemulsions of triton X-100 in mixed-solvents of benzene and n-hexane -*

- dynamic light-scattering and turbidity studies*. Langmuir, 1992. **8**(6): p. 1538-1540.
46. Shen, Y.R., *Optical 2nd harmonic-generation at interfaces*. Annu. Rev. Phys. Chem., 1989. **40**: p. 327-350.
47. Richmond, G.L., J.M. Robinson, and V.L. Shannon, *2nd harmonic-generation studies of interfacial structure and dynamics*. Prog. Surf. Sci., 1988. **28**(1): p. 1-70.
48. Eisenthal, K.B., *Equilibrium and dynamic processes at interfaces by 2nd harmonic and sum frequency generation*. Annu. Rev. Phys. Chem., 1992. **43**: p. 627-661.
49. Corn, R.M. and D.A. Higgins, *Optical 2nd-harmonic generation as a probe of surface-chemistry*. Chem. Rev., 1994. **94**(1): p. 107-125.
50. Shen, Y.R., *Surface-properties probed by 2nd-harmonic and sum-frequency generation*. Nature, 1989. **337**(6207): p. 519-525.
51. Dai, H.-L. and W. Ho, eds. *Laser spectroscopy and photochemistry on metal surfaces 1995*, World Scientific: Singapore ; River Edge, N.J. .
52. Wang, H., et al., *Second harmonic generation from the surface of centrosymmetric particles in bulk solution*. Chem. Phys. Lett., 1996. **259**(1-2): p. 15-20.
53. Wang, H.F., et al., *Energetics and population of molecules at microscopic liquid and solid surfaces*. J. Phys. Chem. B, 1998. **102**(23): p. 4446-4450.

54. Eckenrode, H.M. and H.L. Dai, *Nonlinear optical probe of biopolymer adsorption on colloidal particle surface: Poly-L-lysine on polystyrene sulfate microspheres*. *Langmuir*, 2004. **20**(21): p. 9202-9209.
55. Malvezzi, A.M., et al., *Melting-induced enhancement of the second-harmonic generation from metal nanoparticles*. *Phys. Rev. Lett.*, 2002. **89**(8).
56. Russier-Antoine, I., et al., *Multipolar contributions of the second harmonic generation from silver and gold nanoparticles*. *J. Phys. Chem. C*, 2007. **111**(26): p. 9044-9048.
57. Jen, S.H. and H.L. Dai, *Probing molecules adsorbed at the surface of nanometer colloidal particles by optical second-harmonic generation*. *J. Phys. Chem. B*, 2006. **110**(46): p. 23000-23003.
58. Jen, S.H., G. Gonella, and H.L. Dai, *The effect of particle size in second harmonic generation from the surface of spherical colloidal particles. I: experimental observations*. *J. Phys. Chem. A*, 2009. **113**(16): p. 4758-4762.
59. Wang, H.F., et al., *Adsorption at a carbon black microparticle surface in aqueous colloids probed by optical second-harmonic generation*. *J. Phys. Chem. C*, 2007. **111**(25): p. 8708-8715.
60. Yan, E.C.Y., Y. Liu, and K.B. Eisenthal, *New method for determination of surface potential of microscopic particles by second harmonic generation*. *J. Phys. Chem. B*, 1998. **102**(33): p. 6331-6336.
61. Zeng, J., H.M. Eckenrode, and H.-L. Dai, *Time-Resolved Molecular Transport across Living Cell Membranes*. to be submitted.

62. Zeng, J., H.M. Eckenrode, and H.-L. Dai, *Molecular interaction with murine erythroleukemia (MEL) cell membrane probed by second harmonic generation.* to be submitted.

CHAPTER TWO

SECOND HARMONIC GENERATION AT INTERFACES

2.1 Introduction

Generally, polarization of the medium by an electromagnetic field can be expressed as a power series [1]:

$$\vec{P} = \chi^{(1)} \vec{E}_\omega + \chi^{(2)} \vec{E}_\omega \vec{E}_\omega + \chi^{(3)} \vec{E}_\omega \vec{E}_\omega \vec{E}_\omega + \dots \quad (2.1)$$

where $\chi^{(1)}$ represents the linear susceptibility, $\chi^{(2)}$ the second order susceptibility, etc. and E_ω is the incoming electric field of frequency ω . The interaction of weak light field with matter is dominated by linear process, but with intense field, higher order nonlinear terms, second harmonic generation, third harmonic generation, etc. become observable.

Second harmonic generation (SHG) is a nonlinear process where a photon at the frequency 2ω is generated from the interaction between intense light at frequency ω and a nonlinear medium. In 1961, shortly after the invention of the optical laser as intense light source, the first observation of optical second harmonic generation (SHG) was made from the noncentrosymmetric quartz crystal [2]. SHG generated from the centrosymmetric calcite crystal was also reported [3]. The field of nonlinear optics started to grow. Experiments were conducted in other bulk media and SHG was observed from

metal surface [4] and the liquid-air interface [5]. On the other hand, in order to interpret the experimental observations, the theoretical treatments were also developed for homogeneous nonlinear media [6] as well as the boundary of two centrosymmetric media [7]. Initially, it was believed that the quadrupolar term in the nonlinear polarization that acts as the source of SHG. However, observation of SH signal from the adsorbed layers at silver surfaces showed that an additional surface dipole term must contribute. Since then, theoretical description has started to attribute the origin of SHG to the symmetry-breaking nature of the surface [8]. It was not until early 1980s that the basic SHG theory was sophisticated enough to relate the experimental observables to the surface molecular properties [9-12]. Exhibiting strong sensitivity and selectivity to the interfacial region, SHG has been developed into a powerful technique for interface studies. SHG has been successfully applied to all kinds of planar interfaces as well as buried colloidal surfaces. Much attention has been given to the molecular adsorption at these interfaces. A variety of dye molecules [13-15], surfactants [16-18], proteins [19], and other biomolecules [20, 21] have been investigated. Only recently has SHG been extended to biomembrane surfaces. Comprehensive reviews have been written on the extensive applicability of this technique [22-30].

2.2 Theory of Second Harmonic Generation

When intense light interacts with a nonlinear medium, higher order polarization terms are induced in addition to the linear polarization. Second harmonic generation is the nonlinear process that two photons at frequency ω are coupled to produce one photon

at the second harmonic frequency 2ω . As was described in the previous section, the induced second order polarization $P^{(2)}$ can be expressed by itself as [9-12]:

$$P^{(2)} = \chi^{(2)} E_\omega E_\omega \quad (2.2)$$

Since the second order polarization $P^{(2)}$ and the incoming electric field E_ω at frequency ω are vectors, and $\chi^{(2)}$ is a second order $3 \times 3 \times 3$ tensor, a more rigorous expression for eq. 2.2 is:

$$P_i^{(2)} = \sum_{j,k} \chi_{ijk}^{(2)} E_\omega^j E_\omega^k \quad (2.3)$$

where i, j, k are the three normal coordinates of laboratory system, respectively.

As an even order term in the polarization expression, second harmonic generation, is sensitive to the symmetry of the medium. An inversion symmetry operation will change both polar vectors' sign: the second order polarization $P^{(2)}$ and the electric field E_ω . However, for a centrosymmetric medium with inversion symmetry $\chi^{(2)}$ does not change sign upon inversion. Therefore, the expression for $P^{(2)}$ in a centrosymmetric medium after inversion is:

$$-P^{(2)} = \chi^{(2)} (-E_\omega)(-E_\omega) \quad (2.4)$$

Comparison of equation 2.2 and 2.4 implies $\chi^{(2)} = -\chi^{(2)}$, which is impossible unless $\chi^{(2)} = 0$. Therefore, $\chi^{(2)}$ vanishes in isotropic media and second harmonic generation is forbidden. However, at interfaces where inversion symmetry is no longer conserved, $\chi^{(2)}$ is not necessarily equal to zero upon inversion operation, which makes SHG an intrinsic interface specific technique.

Complete treatment of SHG can be found in literature [6, 7, 10, 11, 25]. In this chapter, we will focus on the theory of second harmonic generation at interfaces, from both macroscopic and microscopic perspectives. The macroscopic second order nonlinear response of the interface to the applied optical field is described by the macroscopic second order nonlinear susceptibility, $\chi^{(2)}$, which can be obtained from the experimental observables. On the other hand, in order to obtain the microscopic properties of the interface down to the molecular orientation level, we need to relate to the microscopic hyperpolarizability $\beta^{(2)}$ of the molecules at interface.

In the following sections, we first discuss the radiation from a sheet of polarization governed by the Maxwell's equations. Then a discussion on the second order nonlinear susceptibility and how it relates to the molecular energy level structures. Finally, the transformation of in the molecular coordinates at system into with the experimental laboratory coordinates is presented.

2.2.1 Phenomenological Mode and Maxwell's Equation

The typical phenomenological model that widely adopted to treat the second harmonic response from a planer interface is shown in Fig. 2.1. The interfacial region is in between two centrosymmetric bulk media. The incoming electric field E_ω at frequency ω passes through medium 1 and gives rise to a nonlinear polarization $P^{(2)} = P^{NL}$ at frequency 2ω in the interfacial region. A small amount of fundamental is converted into 2ω in both the reflected direction in medium 1 and the transmitted direction in medium 2. It is the former one we are going to consider here.

The interfacial region usually occurs over a distance of only a few Angstroms, consisting of only one or several molecular layers, the thickness of which is much smaller than the wavelength of the incoming light. We consider the nonlinearity of the interface as a sheet of the nonlinear source polarization imbedded in a dielectric medium with a dielectric constant as ϵ' shown in Fig. 2.1. The induced nonlinear polarization of the sheet is described by:

$$P^{(2)}(2\omega) = \delta(z)\chi^{(2)}E_\omega E_\omega \quad (2.5)$$

where $\delta(z)$ is a delta function representing the thickness of the interfacial layer.

The nonlinear polarization $P^{(2)} = P^{NL}$ generated from the interface is governed by the Maxwell's equations, from which the wave equation can be derived as [1]:

$$\nabla \times (\nabla \times \vec{E}^{2\omega}) + \frac{\epsilon^{2\omega}}{c^2} \frac{\partial^2 \vec{E}^{2\omega}}{\partial t^2} = \frac{-4\pi}{c^2} \frac{\partial^2 P^{NL}}{\partial t^2} \quad (2.6)$$

and

$$\nabla \epsilon E = -4\pi \nabla P^{NL} \quad (2.7)$$

Satisfying boundary conditions[10]:

$$\Delta B_x = -4\pi i \frac{2\omega}{c} P_y \quad (2.8)$$

$$\Delta B_y = +4\pi i \frac{2\omega}{c} P_x \quad (2.9)$$

$$\Delta B_z = 0 \quad (2.10)$$

$$\Delta E_x = -\frac{4\pi}{\epsilon'} \frac{\partial P_z}{\partial x} \quad (2.11)$$

$$\Delta E_y = -\frac{4\pi}{\epsilon'} \frac{\partial P_z}{\partial y} \quad (2.12)$$

$$\Delta D_z = -4\pi\left(\frac{\partial P_x}{\partial x} + \frac{\partial P_y}{\partial y}\right) \quad (2.13)$$

Where ΔB_x represents the difference of B_x across the interface:

$$\Delta B_x = B_x(z=0^+) - B_x(z=0^-) \quad (2.14)$$

And similar relations for all other boundary condition terms in eq. 2.9-2.13, respectively.

Solving the Maxwell's equations (eq. 2.6 and 2.7) with boundary conditions (eq. 2.8 -2.13) gives the expressions for the p- (parallel to the table) and s- (perpendicular to the laboratory table) polarized components of the reflected second harmonic electric field, and, respectively [10]:

$$E_p^{2\omega} = \frac{i4\pi k_1}{\varepsilon_2 k_{1z} + \varepsilon_1 k_{2z}} (k_{2z} P_x^{NL} + \frac{\varepsilon_2}{\varepsilon_1} k_x P_z^{NL}) \quad (2.15)$$

$$E_s^{2\omega} = \frac{i4\pi k_1}{k_{1z} + k_{2z}} \frac{k_1}{\varepsilon_1} P_y^{NL} \quad (2.16)$$

$k_{1z} = k_1 \cos \theta_i$, $k_{2z} = k_2 \cos \theta_r$, and $k_{2x} = k_2 \sin \theta_r$, where k_1 and k_2 are the wave vectors of $E_{2\omega}$ in media 1 and 2; the subscripts x, y, and z denote x-, y-, and z- components in the laboratory coordinate system; θ_i is the incident angle and θ_r the refractive angle. P_x^{NL} , P_y^{NL} and P_z^{NL} are the Cartesian components of the second order nonlinear polarization.

The nonlinear polarization, P^{NL} at 2ω , should be expressed in terms of the local electric field E_ω^{iL} in the layer of polarization sheet, which is different from the input optical fields:

$$P^{NL} = \chi^{(2)} : E_\omega^{iL} E_\omega^{iL} \quad (2.17)$$

The components of P^{NL} , i.e., P_x^{NL} , P_y^{NL} and P_z^{NL} , can be expressed with the susceptibility tensor elements, $\chi_{ijk}^{(2)}$, as:

$$P_i^{NL} = \sum_{j,k} \chi_{ijk}^{(2)} E_j^{L}(\omega) E_k^{L}(\omega) \quad (2.18)$$

The tensor elements $\chi_{ijk}^{(2)}$ as well as the local field E_ω^{L} need to be examined to give the explicit expressions for the Cartesian components of the polarization P^{NL} , i.e., P_x^{NL} , P_y^{NL} and P_z^{NL} , which will be presented later in this chapter.

2.2.2 Second Order Nonlinear Susceptibility

2.2.2.1 Molecular Energy Level and Second Order Nonlinear Susceptibility

Second order nonlinear susceptibility $\chi^{(2)}$ describes the response of the medium to the applied field. This macroscopic property of the interface can be related to the molecular energy level structures [1]. The full expression for the nonlinear susceptibilities under dipolar approximation can be expressed as [31]:

$$\chi^{(2)} = \sum_{i,f} \frac{\langle g | \mu | i \rangle \langle i | \mu | f \rangle \langle f | \mu | g \rangle}{[(\omega_{gi} - \omega) - i\gamma_{ig}][(\omega_{gf} - 2\omega) - i\gamma_{fg}]} \quad (2.19)$$

Where $\langle g | \mu | i \rangle$ represents the transition dipole moment from g to i state, ω_{gi} is the corresponding optical frequency of the transition, γ_{ig} is the linewidth associated with the transition, etc. Eq. 2.17 clearly demonstrated that the magnitude of the $\chi^{(2)}$ will be greatly enhanced when the fundamental or the second harmonic frequency is in resonance with that of a molecular transition. This condition can be satisfied by selecting proper fundamental wavelength so that ω or 2ω is close to ω_{gi} or ω_{gf} . Illustrated in Fig. 2.2 is

an energy diagram in which the SH frequency 2ω is in resonant enhancement with the electronic transition from the ground state to the excited state.

2.2.2.2 Second Order Nonlinear Susceptibility Tensor

The second order nonlinear susceptibility $\chi^{(2)}$ is a third rank tensor with $3 \times 3 \times 3 = 27$ elements. Symmetry operations can reduce the number of the elements [32, 33]. For an isotropic interface, though the inversion symmetry is broken along axis z, other symmetries are still preserved. Due to the rotational symmetry around axis z, which makes x and y indistinguishable, many components disappear. Only 7 non-vanishing tensor elements survive, with 4 independent values [32]:

$$\chi_{zzz}^{(2)} \tag{2.20a}$$

$$\chi_{zxx}^{(2)} = \chi_{zyy}^{(2)} \tag{2.20b}$$

$$\chi_{xzx}^{(2)} = \chi_{yzy}^{(2)} \tag{2.20c}$$

$$\chi_{xxz}^{(2)} = \chi_{yyz}^{(2)} \tag{2.20d}$$

For SHG, the number can be further reduced by recognizing the fact that the order of the input electric fields does not matter since they are identical, $\chi_{ijk}^{(2)} = \chi_{ikj}^{(2)}$. Plus the equivalence of x and y at an isotropic surface, we have:

$$\chi_{xzx}^{(2)} = \chi_{yzy}^{(2)} = \chi_{xxz}^{(2)} = \chi_{yyz}^{(2)} \tag{2.20e}$$

Altogether 3 independent tensor elements remain: eq. 2.20a, 2.20b and 2.20e.

2.2.2.3 Electric Fields in the Interface Layer and Polarization Expressions of SHG

Given eq. 2.20, the expressions for the three Cartesian components of the polarization from eq.2.18 are simplified into:

$$P_x^{NL} = 2\chi_{xx}^{(2)} E_z^L(\omega) E_x^L(\omega) \quad (2.21a)$$

$$P_y^{NL} = 2\chi_{yy}^{(2)} E_z^L(\omega) E_y^L(\omega) \quad (2.21b)$$

$$P_z^{NL} = \chi_{zz}^{(2)} E_z^L(\omega)^2 + \chi_{zx}^{(2)} (E_x^L(\omega)^2 + E_y^L(\omega)^2) \quad (2.21c)$$

Here the electric fields $E_x^L(\omega)$, $E_y^L(\omega)$, and $E_z^L(\omega)$ in the interface layer are different from the input optical fields E_ω^s and E_ω^p . The relation between the two are given by the Fresnel transmission coefficients, and the appropriate continuity conditions [32].

As was shown in Figure 2.1, the incoming electric field comes from medium 1 to the interface at an angle θ_i , and is then refracted into medium 2 at an angle θ_r . θ_r can be obtained by Snell's Law:

$$n_i \sin \theta_i = n_r \sin \theta_r \quad (2.22)$$

The Fresnel transmission coefficients (which are the ratio of the transmitted to incident fields) are given by [34]:

$$T_s = \frac{E_2^s}{E_1^s} = \frac{2 \cos \theta_i \sin \theta_r}{\sin(\theta_i + \theta_r)} \quad (2.23a)$$

$$T_p = \frac{E_2^p}{E_1^p} = \frac{2 \cos \theta_i \sin \theta_r}{\sin(\theta_i + \theta_r) \cos(\theta_i - \theta_r)} \quad (2.23b)$$

Since E is continuous between the interface and medium 2, at the boundary the continuity conditions yield:

$$E_x^2(\omega) = E_x^L(\omega) \quad (2.24a)$$

$$E_y^2(\omega) = E_y^L(\omega) \quad (2.24b)$$

$$E_{\perp}^2(\omega) = -\frac{\varepsilon'}{\varepsilon_2} E_{\perp}^L(\omega) \quad (2.24c)$$

Therefore, for expressions of the components of E^L , we have:

$$E_x^L(\omega) = T_p E_{\omega}^p \cos \theta_r \quad (2.25a)$$

$$E_y^L(\omega) = T_s E_{\omega}^s \quad (2.25b)$$

$$E_z^L(\omega) = -\frac{\varepsilon_2}{\varepsilon'} T_p E_{\omega}^p \sin \theta_r \quad (2.25c)$$

The expressions in eq. 2.25 may be substituted into eq. 2.21, and then into eq. 2.15 and 2.16 to obtain the overall expressions for second harmonic field components $E_p^{2\omega}$ and $E_s^{2\omega}$ as functions of input field components E_{ω}^s and E_{ω}^p . The macroscopic nonlinear susceptibility $\chi^{(2)}$ can be extracted by selecting the incoming optical fields and measuring the s- and p- polarized second harmonic generation components.

2.2.3 Transformation of Susceptibilities to Molecular Polarizabilities

The macroscopic susceptibility elements $\chi_{ijk}^{(2)}$ can be written as the sum of the individual molecular polarizabilities $\beta_{i'j'k}^{(2)}$, through a statistical average over molecular orientations:

$$\chi^{(2)} = N_s \langle \beta^{(2)} \rangle \quad (2.26)$$

where N_s is the number density of adsorbates at the interface and the brackets denote an average over the orientation distribution of the adsorbates. Eq. 2.26 is valid for coherent processes such as SHG from an interface, where the in phase individual oscillating dipoles act as a collective oscillating dipole.

In order to find out the individual components $\chi_{ijk}^{(2)}$, a relationship is needed between the laboratory frame of reference (x, y, z) and the molecular frame of reference (x', y', z'). As is illustrated in Figure 2.3, the transformation between the two sets of coordinates may be made using a matrix T defined by three Euler angles, θ , ϕ , and ψ , where $\theta \in (0, \pi)$ is the angle between z and z', $\phi \in (0, 2\pi)$ is the azimuthal angle about z axis of the laboratory coordinate system, and $\psi \in (0, 2\pi)$ is the azimuthal angle about z' axis of the molecular coordinate system. The two sets of coordinates are related:

$$\begin{pmatrix} x \\ y \\ z \end{pmatrix} = T \begin{pmatrix} x' \\ y' \\ z' \end{pmatrix} = \begin{pmatrix} T_{xx'} & T_{xy'} & T_{xz'} \\ T_{yx'} & T_{yy'} & T_{yz'} \\ T_{zx'} & T_{zy'} & T_{zz'} \end{pmatrix} \begin{pmatrix} x' \\ y' \\ z' \end{pmatrix} \quad (2.27)$$

Where the transformation matrix T can be obtained by performing three counterclockwise rotations of the molecule as illustrated in Figure 2.3:

(1) Rotate molecule about the z-axis to obtain ϕ , represented by:

$$T(\phi) = \begin{pmatrix} \cos \phi & \sin \phi & 0 \\ -\sin \phi & \cos \phi & 0 \\ 0 & 0 & 1 \end{pmatrix}$$

(2) Rotate molecule about the x'-axis to obtain θ , represented by:

$$T(\theta) = \begin{pmatrix} 1 & 0 & 0 \\ 0 & \cos \theta & \sin \theta \\ 0 & -\sin \theta & \cos \theta \end{pmatrix}$$

(3) Rotate about the z'-axis to obtain ψ , represented by:

$$T(\psi) = \begin{pmatrix} \cos \psi & \sin \psi & 0 \\ -\sin \psi & \cos \psi & 0 \\ 0 & 0 & 1 \end{pmatrix}$$

The complete transformation matrix is the product of all three rotation matrices:

$$\begin{aligned}
T &= T(\phi)T(\theta)T(\psi) \\
&= \begin{pmatrix} \cos \psi \cos \phi - \cos \theta \sin \phi \sin \psi & \cos \psi \sin \phi - \cos \theta \cos \phi \sin \psi & \sin \theta \sin \psi \\ -\sin \psi \cos \phi - \cos \theta \sin \phi \cos \psi & -\sin \psi \sin \phi + \cos \theta \cos \phi \cos \psi & \sin \theta \cos \psi \\ \sin \theta \sin \phi & -\sin \theta \cos \phi & 1 \end{pmatrix} \quad (2.28)
\end{aligned}$$

Therefore, the relationship between $\chi_{ijk}^{(2)}$ and $\beta_{i'j'k'}^{(2)}$ is:

$$\chi_{ijk}^{(2)} = N_s \sum_{i'j'k'} \langle T_{ii'} T_{jj'} T_{kk'} \rangle \beta_{i'j'k'}^{(2)} \quad (2.29)$$

Where $T_{ii'} T_{jj'} T_{kk'}$ is the product of the possible combinations of the elements of the transformation matrix T which can be found in eq. 2.28.

If the Hamiltonian of a certain orientation (θ, ϕ, ψ) is $H = E(\theta, \phi, \psi)$, the above average will be:

$$\chi_{ijk}^{(2)} = N_s \sum_{i'j'k'} \beta_{i'j'k'}^{(2)} \frac{\int T_{ii'} T_{jj'} T_{kk'}(\theta, \phi, \psi) e^{-\beta E(\theta, \phi, \psi)} d\Omega}{\int e^{-\beta E(\theta, \phi, \psi)} d\Omega} \quad (2.30)$$

where $d\Omega$ is the integral element of the solid angle $\Omega(\theta, \phi, \psi)$.

For centrosymmetric medium, $E(\theta, \phi, \psi) = 0$ indicates that all orientation states are equally favorable. By integrating over the whole solid angle range $\theta \in (0, \pi)$, $\phi \in (0, 2\pi)$, and $\psi \in (0, 2\pi)$ we have $\chi_{ijk}^{(2)} = 0$.

The general case at an interface is that for a uniaxial molecule, which has a well defined molecular axis and its nonlinear polarizability tensor $\beta^{(2)}$ is dominated by a single element $\beta_{z'z'z'}^{(2)}$, with z' along the molecular axis. The interface has a rotational symmetry along the interface normal, therefore, $E(\theta, \phi, \psi) = E(\theta)$, which indicates that the orientation in ϕ and ψ are random. As was described before that only three

independent non-zero elements of $\chi^{(2)}$ survive (eq. 2.20). Both ϕ and ψ get averaged out and leaves the expressions for nonlinear susceptibility as a function of θ alone:

$$\chi_{zzz}^{(2)} = N_s \beta_{z'z'z'}^{(2)} \langle \cos^3 \theta \rangle \quad (2.31a)$$

$$\chi_{zxx}^{(2)} = \frac{1}{2} N_s \beta_{z'z'z'}^{(2)} \langle \cos \theta - \cos^3 \theta \rangle \quad (2.31b)$$

$$\chi_{xzx}^{(2)} = \frac{1}{2} N_s \beta_{z'z'z'}^{(2)} \langle \cos \theta - \cos^3 \theta \rangle \quad (2.31c)$$

Generally, if the interfacial molecule is in resonance with the incoming light or SHG light, only one transition is dominant, we can consider it uniaxial along the transition axis. For molecules which are not uniaxial, the expressions of the elements of $\chi^{(2)}$ can be worked out similarly, given the knowledge of the possible non-zero elements of the molecular nonlinear polarizability $\beta^{(2)}$ from the molecular symmetry [32]. Later in this thesis, a molecule Malachite Green (MG), which has a C_{2v} symmetry, will be used as a probe molecule. For MG, $\beta_{z'x'x'}^{(2)}$ is the dominant tensor element. The three independent elements of $\chi^{(2)}$ can be expressed as:

$$\chi_{zzz}^{(2)} = N_s \beta_{z'x'x'}^{(2)} \langle \cos \theta \sin^2 \theta \sin^2 \psi \rangle \quad (2.32a)$$

$$\chi_{zxx}^{(2)} = \frac{1}{2} N_s \beta_{z'x'x'}^{(2)} \langle \cos \theta - \cos \theta \sin^2 \theta \sin^2 \psi \rangle \quad (2.32b)$$

$$\chi_{xzx}^{(2)} = \frac{1}{2} N_s \beta_{z'x'x'}^{(2)} \langle -\cos \theta \sin^2 \theta \sin^2 \psi \rangle \quad (2.32c)$$

2.3 Second Harmonic Generation at Colloidal Interfaces

Second harmonic generation is only allowed, in the electric dipole approximation, in the symmetry broken systems [35-37], such as surfaces and interfaces, but is generally thought to be forbidden, in centrosymmetric system such as bulk liquids. In the previous sections, generation of SHG from a planer surface has been described. It was believed that, as centrosymmetric system, surfaces of colloids cannot be investigated using SHG. In 1996, Eisenthal and coworkers first demonstrated that SHG can occur at the surface of spherical colloidal particles when the surface is adsorbed with molecules with detectable second-order polarizabilities [38].

A sophisticated description of the interference of the SH fields generated from molecules adsorbed at all regions of the particle and the SH signal scattered in all solid angles can be fully analyzed using the nonlinear Rayleigh-Gans-Debye (NLRGD) theory. Angular resolved measurements and size effects studies of SHG from spherical colloidal particle surfaces have been reported [39-41].

In this thesis, the dimensions of the colloidal and biological objects under investigation are of micron size. A simple, yet illustrative model firstly presented by Eisenthal and coworkers [38] can be used to explain the generation of SHG from a micron sized centrosymmetric colloidal suspension.

Individual, isolated, non-centrosymmetric molecules can generate second harmonic radiation [42]. When two molecules near each other are oppositely oriented, the radiated field generated will cancel one another. Therefore, for the molecules dissolved in the bulk solution, the net coherent radiated field from such a collection of randomly

oriented molecules is zero for symmetry reasons. This can be understood through the fact that for each molecule oriented in a given direction, there is another one oriented in the opposite direction and located at a distance which is much less than the coherence length of the process. The nonlinear polarization from the bulk species are out of phase with each other, the statistical sum of which is zero, resulting in no coherent second harmonic generation.

In contrast, it must be mentioned that, incoherent second order light scattering called hyper-Rayleigh scattering can be observed from the centrosymmetric bulk solution [43]. This phenomenon originates from the fluctuations in orientation and density of the molecules in the bulk solution, which disrupt the phase cancellation mentioned above. This contribution does not have a surface origin and is small enough in our experiments to be neglected.

The phase cancellation is only true for particles of the size much smaller than the incident wavelength. For particles of the size comparable or larger than the wavelength of the incoming beam, the elimination of the phase cancellation occurs due to the symmetry broken on a microscopic scale. Consider a simple model of a spherical particle with only two identical molecules, separated by the particle diameter L and adsorbed with opposite orientations, as is shown in Figure 2.4. The oppositely oriented molecules have nonlinear polarizabilities $\beta^{(2)}$, of opposite sign. And also in this simple model, the SH signal is generated along the fundamental beam propagation direction. Therefore, the total second harmonic field $E_{2\omega}$ at the forward direction detector due to these two particles is of the form:

$$E_{2\omega} \propto \beta^{(2)} E_{\omega} E_{\omega} (1 - e^{-i\Delta\vec{k}\cdot\vec{L}}) \quad (2.33)$$

where the scattering vector $\Delta\vec{k}$ is defined as

$$\Delta\vec{k} = \vec{k}_{2\omega} - 2\vec{k}_{\omega} \quad (2.34)$$

And $\vec{k}_{2\omega}$ and \vec{k}_{ω} are the light propagation vectors for the second harmonic at 2ω and fundamental at ω , respectively. The amplitude of the scattering vector can be calculated as:

$$\Delta k = \frac{4\pi(n_{\omega} - n_{2\omega})}{\lambda_{\omega}} = \frac{4\pi\Delta n}{\lambda_{\omega}} \quad (2.35)$$

From eq. 2.33-2.35, it is clear that if the separation of the two oppositely oriented molecules L is much less than the wavelength λ_{ω} of the fundamental beam, then $\Delta\vec{k}\cdot\vec{L} \ll 1$ and $E_{2\omega} = 0$. On the other hand, if the separation of the two molecules is comparable to the wavelength of the incoming beam, then $\Delta\vec{k}\cdot\vec{L} \sim 1$, which means constructive interference of the SH polarization from the two molecules. In fact, when the magnitude of $\Delta\vec{k}\cdot\vec{L}$ equals π , $E_{2\omega}$ will be at a maximum, which is of twice that of the individual molecule.

Take one step further, if the propagation directions of the fundamental and SH lights are no longer parallel to each other, i.e. there is an angle between the two beams θ_s . In this case, the total second harmonic field from the two oppositely oriented molecules is of the same form in eq. 2.33, however, the amplitude of the scattering vector should be calculated differently:

$$\Delta k = 2k_{2\omega} \sin \frac{\theta_s}{2} = \frac{4\pi n_{2\omega}}{\lambda_{2\omega}} \sin \frac{\theta_s}{2} \quad (2.36)$$

The condition for constructive interference (phase matching) is:

$$\Delta k \cdot L = \frac{4\pi n_{2\omega}}{\lambda_{2\omega}} \sin \frac{\theta_s}{2} \cdot L = \pi \quad (2.37)$$

Eq. 2.37 clearly demonstrated that the phase matched SH intensity appears at larger scattering angles with decreasing particle sizes.

Colloidal particles and living cells used for the studies in this thesis are of micron-size dimensions. The size is close to the 840nm fundamental light that is used, which favors forward direction detection of the coherent SHG signal generated. The principle and method described in this section allows the investigation of complex interfacial systems. This major breakthrough in colloidal and interface science now shows its power in investigating biological systems at a colloidal level.

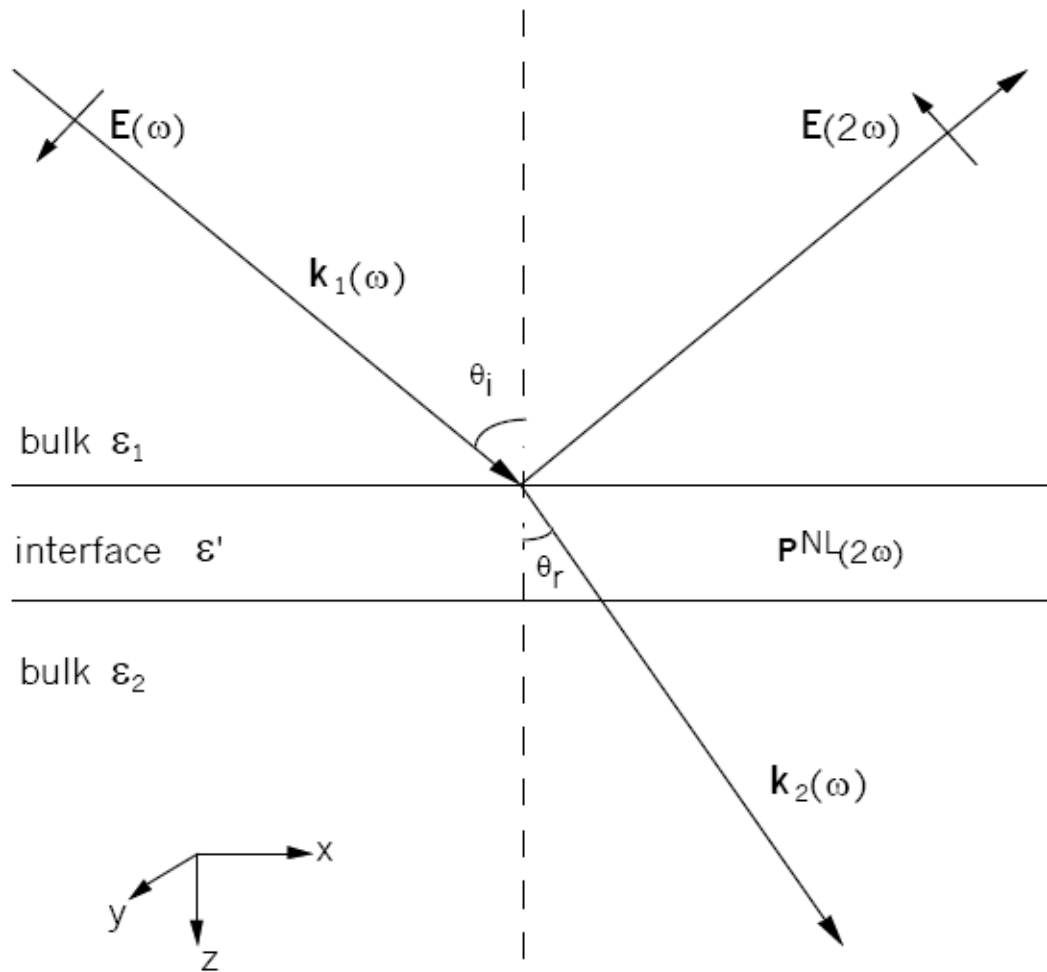


Figure 2.1: Schematic of the typical phenomenological model to treat the second harmonic response from a planer interface between two isotropic bulk media

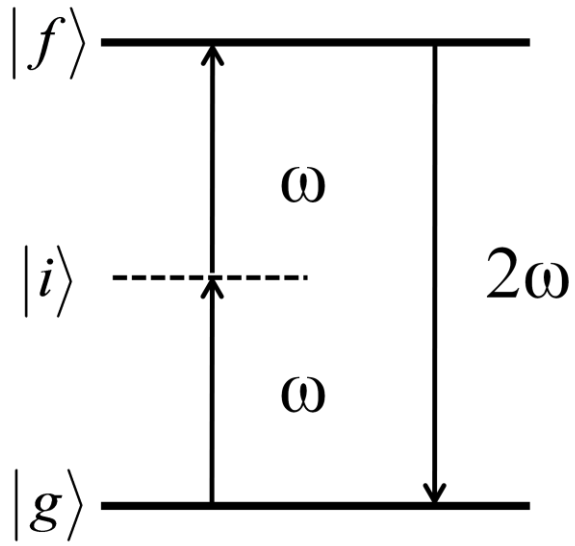


Figure 2.2: The energy diagram of SHG in which the SH frequency 2ω is in resonant enhancement with the electronic transition from the ground state $|g\rangle$ to the excited state $|f\rangle$.

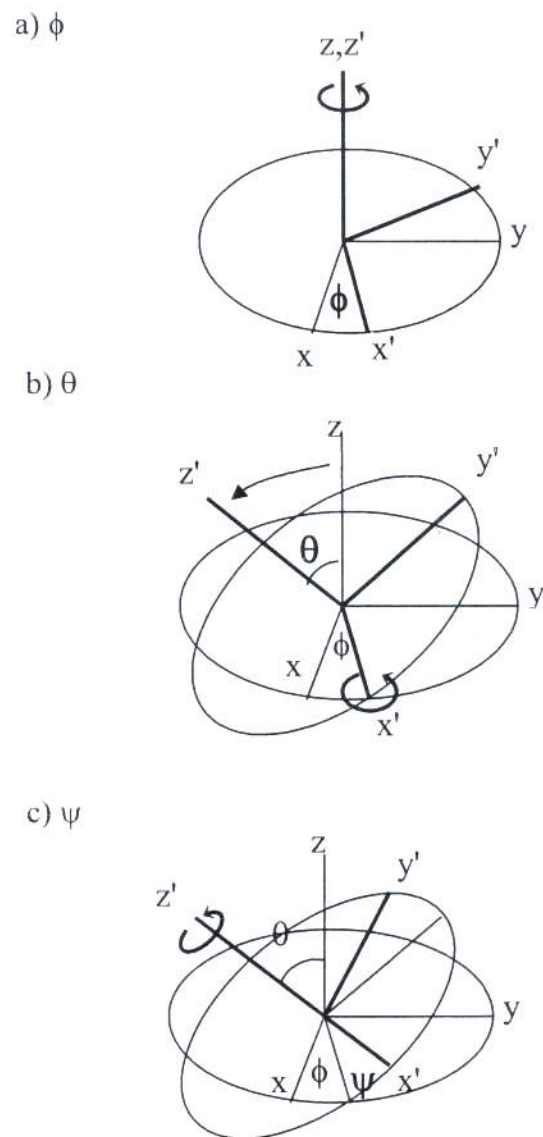


Figure 2.3: Schematic of the rotations to transform from molecular coordinates to lab coordinates using Euler angles [44].

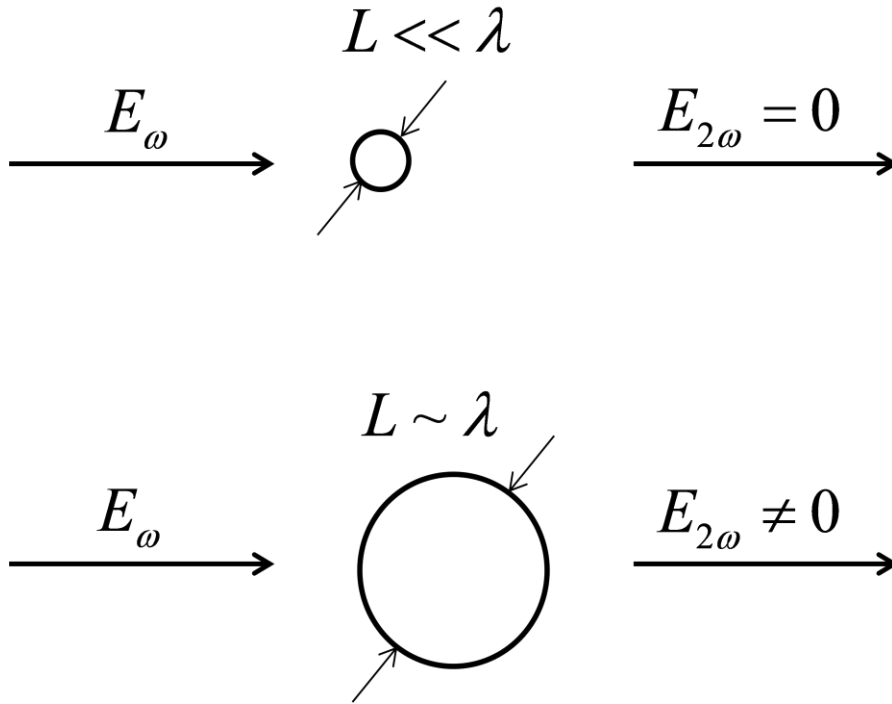


Figure 2.4: Schematic of SHG from two SH producing molecules adsorbed at centrosymmetric particles with opposite orientations. The upper panel is the case when the particle size is much less than the wavelength of the incident light, while the lower case is the particle size comparable to the coherent length.

Bibliography

1. Boyd, R.W., *Nonlinear Optics*. 1992, New York: Academic Press.
2. Franken, P.A., et al., *Generation of optical harmonics*. Phys. Rev. Lett., 1961. **7**(4): p. 118-119.
3. Terhune, R.W., P.D. Maker, and C.M. Savage, *Optical harmonic generation in calcite*. Phys. Rev. Lett., 1962. **8**(10): p. 404-406.
4. Brown, F., R.E. Parks, and A.M. Sleeper, *Nonlinear optical reflection from a metallic boundary*. Phys. Rev. Lett., 1965. **14**(25): p. 1029-1031.
5. Wang, C.C., *Second-harmonic generation of light at boundary of anisotropic medium*. Phys. Rev., 1969. **178**(3): p. 1457-1460.
6. Bloembergen, N. and P.S. Pershan, *Light waves at boundary of nonlinear media*. Phys. Rev., 1962. **128**(2): p. 606-622.
7. Bloembergen, N., et al., *Optical second-harmonic generation in reflection from media with inversion symmetry*. Phys. Rev. , 1968. **174**(3): p. 813-822.
8. Rudnick, J. and E.A. Stern, *Second-harmonic radiation from metal surfaces*. Phys. Rev. B, 1971. **4**(12): p. 4274-4290.
9. Shen, Y.R. and F. deMartini, *Surface polaritons: electromagnetic waves at surfaces and interfaces*. 1982, New York: Elsevier Science Pub. Co.
10. Heinz, T.F., *Nonlinear optics of surfaces and adsorbates*. 1982, University of California at Berkeley.
11. Sipe, J.E. and G.I. Stegman, *Surface polaritons: electromagnetic waves at surfaces and interfaces*. 1982, New York: Elsevier Science Pub. Co.

12. Fukui, M. and G.I. Stegman, *Electromagnetic surface modes*. 1982, New York: Wiley.
13. Li, J.W., G. He, and Z. Xu, *Determination of the ratio of nonlinear optical tensor components at solid-liquid interfaces using transmission second-harmonic generation (TSHG)*. J. Phys. Chem. B, 1997. **101**(18): p. 3523-3529.
14. Piron, A., P.F. Brevet, and H.H. Girault, *Surface second harmonic generation monitoring of the anion methyl orange during ion transfer reactions across a polarised water vertical bar 1,2-dichloroethane interface*. J. Electroanal. Chem., 2000. **483**(1-2): p. 29-36.
15. Uchida, T., et al., *Observation of molecular association at liquid/liquid and solid/liquid interfaces by second harmonic generation spectroscopy*. J. Phys. Chem. B, 2000. **104**(51): p. 12091-12094.
16. Motschmann, H. and K. Lunkenheimer, *Phase transition in an adsorption layer of a soluble surfactant at the air-water interface*. J. Colloid Interface Sci., 2002. **248**(2): p. 462-466.
17. Wang, H.F., et al., *In situ, nonlinear optical probe of surfactant adsorption on the surface of microparticles in colloids*. Langmuir, 2000. **16**(6): p. 2475-2481.
18. Moller, G., et al., *Influence of a base electrolyte on the adsorption behavior of an anionic surfactant as observed by second harmonic generation*. Langmuir, 2000. **16**(10): p. 4594-4598.
19. Petralli-Mallow, T.P., et al., *Cytochrome c at model membrane surfaces: exploration via second harmonic generation-circular dichroism and surface-enhanced resonance Raman spectroscopy*. Langmuir, 2000. **16**(14): p. 5960-5966.

20. Perrenoud-Rinuy, J., P.F. Brevet, and H.H. Girault, *Second harmonic generation study of myoglobin and hemoglobin and their protoporphyrin IX chromophore at the water/1,2-dichloroethane interface*. Phys. Chem. Chem. Phys., 2002. **4**(19): p. 4774-4781.
21. Kim, B.M., et al., *Collagen structure and nonlinear susceptibility: effects of heat, glycation, and enzymatic cleavage on second harmonic signal intensity*. Lasers Surg. Med., 2000. **27**(4): p. 329-335.
22. Shen, Y.R., *Surface 2nd harmonic-generation - a new technique for surface studies*. Annu. Rev. Mater. Sci., 1986. **16**: p. 69-86.
23. Shen, Y.R., *Surface-properties probed by 2nd-harmonic and sum-frequency generation*. Nature, 1989. **337**(6207): p. 519-525.
24. Shen, Y.R., *Optical 2nd harmonic-generation at interfaces*. Annu. Rev. Phys. Chem, 1989. **40**: p. 327-350.
25. Heinz, T.F. and G.A. Reider, *Surface studies with optical 2nd-harmonic generation*. Trac-Trends Anal. Chem., 1989. **8**(6): p. 235-242.
26. Corn, R.M. and D.A. Higgins, *Optical 2nd-harmonic generation as a probe of surface-chemistry* OPTICAL 2ND-HARMONIC GENERATION AS A PROBE OF SURFACE-CHEMISTRY. Chem. Rev., 1994. **94**(1): p. 107-125.
27. Eisenthal, K.B., *Equilibrium and dynamic processes at interfaces by 2nd harmonic and sum frequency generation*. Ann. Rev. Phys. Chem., 1992. **43**: p. 627-661.
28. Eisenthal, K.B., *Liquid interfaces*. Acc. Chem. Res., 1993. **26**(12): p. 636-643.

29. Eiseenthal, K.B., *Liquid interfaces probed by second-harmonic and sum-frequency spectroscopy*. Chem. Rev., 1996. **96**(4): p. 1343-1360.
30. Eiseenthal, K.B., *Second harmonic spectroscopy of aqueous nano- and microparticle interfaces*. Chem. Rev., 2006. **106**(4): p. 1462-1477.
31. Wang, H., *Second harmonic generation studies of chemistry at liquid interfaces*. 1996, Columbia University.
32. Guyotsionnest, P., W. Chen, and Y.R. Shen, *General-considerations on optical 2nd-harmonic generation from surfaces and interfaces*. Phys. Rev. B, 1986. **33**(12): p. 8254-8263.
33. Sipe, J.E., D.J. Moss, and H.M. Vandriel, *Phenomenological theory of optical 2nd-harmonic and 3rd-harmonic generation from cubic centrosymmetric crystals*. Phys. Rev. B, 1987. **35**(3): p. 1129-1141.
34. Hecht, E., *Optics*. 3rd ed. 1998, New York: Addison Wesley Longman, Inc.
35. Shen, Y.R., *The principles of Nonlinear Optics*. 1984, New York: Wiley.
36. Bloembergen, N., *Nonlinear Optics*. 1965, New York: W.A. Benjamin, Inc.
37. Heinz, T.F., *Second order nonlinear optical effects at surfaces and interfaces*, in *Nonlinear surface electromagnetic phenomena*, H.E. Ponath and S. G.I., Editors. 1991, Elsevier Science Publishers.
38. Wang, H., et al., *Second harmonic generation from the surface of centrosymmetric particles in bulk solution*. Chem. Phys. Lett., 1996. **259**(1-2): p. 15-20.

39. Jen, S.H. and H.L. Dai, *Probing molecules adsorbed at the surface of nanometer colloidal particles by optical second-harmonic generation*. J. Phys. Chem. B, 2006. **110**(46): p. 23000-23003.
40. Jen, S.H., H.L. Dai, and G. Gonella, *The effect of particle size in second harmonic generation from the surface of spherical colloidal particles. II: the nonlinear Rayleigh-Gans-Debye model*. J. Phys. Chem. C, 2010. **114**(10): p. 4302-4308.
41. Jen, S.H., G. Gonella, and H.L. Dai, *The effect of particle size in second harmonic generation from the surface of spherical colloidal particles. I: experimental observations*. J. Phys. Chem. A, 2009. **113**(16): p. 4758-4762.
42. Buckingham, A.D. and B.J. Orr, *Molecular hyperpolarisabilities*. Q. Rev., 1967. **21**(2): p. 195.
43. Terhune, R.W., P.D. Maker, and C.M. Savage, *Measurements of nonlinear light scattering*. Phys. Rev. Lett., 1965. **14**(17): p. 681.
44. Goldstein, H., *Classical Mechanics*. 1980, New York: Addison-Wesley.

CHAPTER THREE

MOLECULAR ADSORPTION AND TIME-RESOLVED MOLECULAR TRANSPORT ACROSS E.COLI CELL MEMBRANES

3.1 Introduction

Biological membranes possess unique structures and perform specific biochemical functions that are necessary for protecting the living cells and maintaining bio-activities of the organism. A primary role of the cell membrane as a boundary between the cell interior and the outside environment is to regulate transport of ions, nutrients, metabolites, peptides, and proteins into and out of the cell. Numerous studies have been done on revealing the transmembrane movements of essential metal ions [1-3] such as Na^+ , K^+ , and Ca^{2+} as well as organic nutrients like amino acids, sugars, and nucleotides [4-6]. A substantial knowledge base has been established for understanding transport of small ions through cell membranes. This, however, is not the case for molecules in general.

The importance of gaining fundamental understanding on what are the factors determining the adsorption and penetration of molecules at cell membranes has inspired the development of a variety of experimental approaches. In addition to contributing to fundamental knowledge, experimental capability for characterizing kinetic processes taking place at the cell membrane carries also practical significance. Transport characteristics of small and medium molecules are crucial for rational drug design in pharmacology as well as for understanding important cell membrane relevant phenomena in environmental science.

The investigation of the adsorption and transport of small and medium size molecules has been conducted for decades through a variety of methods including electrical relaxation [7, 8], voltage-clamp [9], fluorescence [10], EPR spin label [11], and assay [12, 13]. These methods rely on measurements of in-cell and out-of-cell concentrations of the molecule of interest for deducing what is happening at the cell membrane. Real time measurement of concentration in the solution phase, but not at the membrane, can be achieved but only under harsh restrictions. For example, the electrical relaxation approach requires application of exterior voltage so that it is best performed only on flat membrane systems. The voltage-clamp technique involves a clamp voltage which is highly perturbing to membranes. The fluorescence technique, on the other hand, cannot directly distinguish the molecules adsorbed on the membrane from those in the bulk solution. Overall, studies of molecular transport of intact, *living* cells have been restricted to steady-state measurements of solution, not membrane, characteristics without time-resolution.

We report in this chapter the use of the nonlinear optical phenomenon - Second Harmonic Generation (SHG) – for studying molecular transport through living cell membranes with real time-resolution. The SHG method has the advantage of directly differentiating molecules adsorbed on the cell membrane from those in the bulk solution. We demonstrate the effectiveness of the method by characterizing the transport of a hydrophobic ion through living *E.coli* cell membranes. Transport rate constant and adsorption density and energy on both the inner and outer membranes of the *E.coli* cell have been determined.

The first demonstration of the detection of SHG from dye molecules adsorbed on the surface of micro-colloidal particles was performed by Eisenthal and coworkers [14]. More recently it has been shown that SHG arising from nanoparticles with diameters much smaller than the optical coherence length can still be detected at specific phase matching angles [15]. Eisenthal and coworkers have also shown that this SHG technique can be used to measure in real time molecular transport through a vesicle liposome membrane [16-20]. The measurement is based on the anticipation that as the dye molecules adsorb on the opposite sides of a membrane they would have exactly opposite orientation and subsequently the SH fields generated from the two sides of the membrane cancel each other out. Consequently during the diffusion stage following the initial adsorption of the dye molecules at the outside surface, the SHG signal displayed a decrease as dye molecules enter the vesicle and adsorb to the inside wall of the membrane.

3.2 Experiment

3.2.1 The Laser System

A schematic illustration of the experimental setup is shown in Fig. 3.1. The laser source for the fundamental light we used for the Second Harmonic Generation was provided by a Ti: Sapphire femtosecond laser (Coherent Mira Seed, oscillator only) pumped by an Ar ion laser (Coherent Innova 310). The laser combination generates nominally 50 fs laser pulses with less than 4 nJ pulse energy at 76 MHz repetition rate with tunable wavelength from 780nm to 840nm. The operating wavelength was set at 840nm whose second harmonic is in resonance with the electronic transition of the malachite green (MG) dye molecule to get resonantly enhanced SHG signal. The details of malachite green will be given in Chapter 3.2.3.

The femtosecond laser pulses were used because they provided the high peak power necessary for the nonlinear optical process, while on the other hand, the heating and photochemical effects from light absorption could be kept at the minimum due to the low pulse energy. The 1mm diameter fundamental laser beam, with an averaged output power of 0.4W, was focused with a 2 in. fl lens into the sample liquid jet, resulting in an approximate peak intensity of $4 \times 10^9 \text{W/cm}^2$ inside the sample. A long pass filter (Schott RG695) was placed before the lens to get rid of any possible SHG from the components in the optical path up to the sample which ensured the collected SHG signal was all generated from our sample. The laser beam, after exiting the sample, was collected with a 2 in. fl lens and collimated by an 8 in.-4 in. lens assembly. The total light collected consisted of fundamental and second harmonic in the same forward direction, then passed through a set of band-pass filters (Schott BG39) for filtering out the fundamental as

much as possible before entered a monochromator (Jarrel-Ash 1/4m) where only the second harmonic wavelength was allowed to pass through. The monochromator with 1mm slit at both entrance and exit was set at 420nm with 2nm bandwidth. The combination of the BG39 filters and the monochromator effectively eliminated fluorescence and scattering light at other wavelengths. The rectangular nature of the monochromator slit restricted the light collected within $\pm 20^\circ$ in the vertical direction and only $\pm 2^\circ$ in the horizontal direction to enter the monochromator. The signal was then detected by a photomultiplier (Hamamatsu R585). The output was then preamplified with a Stanford Research Systems SR 440 amplifier and processed through a correlated photon counting system (SRS SR400). The discrimination voltage for suppression of the statistical random noise was set at -100mV when the PMT was powered at -1300 V. The signal collected was averaged over 1 sec.

3.2.2 Sample Flow-jet Circulation System

The cell sample was prepared in a flow/titration system (Fig. 3.1). The cell suspension was pumped with a small motorized liquid pump to form a liquid jet through a nozzle made out of pressed stainless steel tubing with 1/16 in. inner diameter. The cell suspension in the reservoir was forced out and collected back through Nalgene tubing connected to the nozzle and was continuously stirred using a magnetic stirrer. The cell suspension volume in the circulation tubing was kept small enough compared to the total sample volume to prevent significant error of the concentration reading. The laser intercepted the center of the jet perpendicularly and passed through the jet with approximately 1mm path length. The windowless liquid jet prevented SHG from background materials and improved the S/N. Aqueous solutions of MG dye at know high

concentrations were added into the cell suspension reservoir by a digital titration buret (CAT Contiburet) This allowed synchronized data collection with titration and enables the collection of SH intensity as a function of dye concentration added. A 4-sec interval in the titration experiment was allowed between the dye aliquots to ensure the equilibrium state of the sample was reached. The effect of the volume change caused by the titration amount was included in the analysis.

3.2.3 Malachite Green (MG) Dye

MG dye used was Malachite Green oxalate salt purchased from Sigma-Aldrich and used without further purification. The basic specifications of MG are tabulated in Table 3.1[21]. Malachite Green is a water-soluble cationic triphenylmethane dye. When dissolved in aqueous solutions, MG adopts different ionic forms depending on the pH of the solution [21, 22]. MG is in its single-charged cationic form between pH 2 and 7. The structure of MG cation and its spectral feature is illustrated in Figure 3.2. The z' polarized transition arises from exciting of an electron from nonbonding molecular orbital to the second highest occupied bonding orbital and appears electronic transition $S_2 \leftarrow S_0$ at around 420nm. Spectrum of two photon absorption and excited fluorescence are shown in Fig. 3.3. The peak of two-photon absorption is around 430nm and the fluorescence is centered at 460nm, is an unrelaxed emission from the second excited state S_2 to the ground state S_0 . The two photon fluorescence from bulk MG ($\lambda_{\text{max}} \sim 460\text{nm}$) therefore has only a small tail extending to the second harmonic wavelength (420nm).

3.2.4 Cell Culture

The *E.coli* MC4100 strain was grown at 37°C in Terrific Broth until saturation. The cells were centrifuged, washed and re-suspended in distilled water for use in the SHG experiments, typically with a concentration of $2\sim 4\times 10^7$ cells/ml.

3.3 Modified *Langmuir* Adsorption Model

3.3.1 Adsorption Isotherms

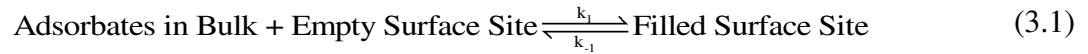
The conventional way to characterize adsorption processes is to monitor the adsorption isotherm. There are four major classes of adsorption isotherms (Figure 3.4) [23] according to the initial slope. The four main classes are names: the S, L (“*Langmuir*”), H (“high affinity”), and C (“constant partition”) isotherms. The S class represents the adsorption type with side-by-side association between adsorbed molecules. The L class is the best known *Langmuir* adsorption isotherm, which assumes no inter-adsorbate attractions. The H class is a special case of L curve, in which the adsorbate has such high affinity that in dilute solutions it is completely adsorbed, or at least there is no measurable amount remaining in solution. The initial part of the isotherm is therefore vertical. The C class describes the constant partition of adsorbates between solution and substrate, right up to the maximum possible adsorption, where an abrupt change to a horizontal plateau occurs. The variations in the four classes are further divided into sub-divisions according to the amount that adsorbs. Sub-division 1 represents adsorption of less than a monolayer, while 2 shows monolayer adsorption. 3 and 4 represent multilayer adsorption and 5 occurs when there is association between the adsorbates in solution. The

adsorption processes investigated in this thesis can be best described by the L2 class, the details of which will be discussed in the following sections.

3.3.2 Modified *Langmuir* Adsorption Model

The *Langmuir* adsorption model was developed by Irving Langmuir in 1916 [24]. There are three assumptions: 1) adsorption is limited to a monolayer, 2) the surface is divided into sites for adsorption with equal probability of adsorption to each site, and 3) there are no inter-adsorbate interactions [25].

The *Langmuir* kinetics describes the adsorption as the “reaction” between the adsorbates in the bulk solution and those on the colloidal surface.



where k_1 and k_{-1} is the rate constant for adsorption and desorption, respectively. The kinetic equation is as follow:

$$\frac{dN}{dt} = k_1 \frac{(C - N)}{55.5} (N_{\max} - N) - k_{-1}N \quad (3.2)$$

where N is the number of adsorbed molecules on the surface, N_{\max} is the maximum adsorption density, C is the total concentration of the adsorbate molecules, including both the molecules in the bulk and adsorbed on the surface. 55.5 is the molarity of water.

At equilibrium:

$$\frac{dN}{dt} = 0 \quad (3.3)$$

The expression for surface coverage θ can be related to C , N_{\max} and the equilibrium constant K , defined as $K = k_1 / k_{-1}$:

$$\theta = \frac{N}{N_{\max}} = \frac{(C + N_{\max} + \frac{55.5}{K}) - \sqrt{(C + N_{\max} + \frac{55.5}{K})^2 - 4CN_{\max}}}{2N_{\max}} \quad (3.4)$$

The model can be used to analyze the adsorption isotherm of dye adsorption at colloidal surface. K and N_{\max} can be obtained from a fit of the adsorption isotherm. K can then be used to determine the adsorption free energy of the adsorbate molecule on the surface using $\Delta G = -RT \ln K$.

The modified *Langmuir* model is actually the complete form of *Langmuir* model without further assumptions. Generally, for micro surfaces, such as microparticles and emulsion surfaces, the effective surface area can be very large. Hence, N can be comparable to C most of the time and cannot be neglected from the $(C - N)$ term in equation 3.2. Therefore, in most cases, the modified *Langmuir* model should be used to analyze adsorption isotherms obtained for colloidal systems. In the following section, we will show the application of the model in a specific case, the molecular adsorption of MG at *E.coli* cell membrane surface under physiological pH.

3.3.3 Application of the Modified *Langmuir* Model in Analyzing MG Adsorption under Physiological pH Value

The *E.coli* experiments presented in this chapter were performed under physiological pH = 7.4±0.1 while the literature reported pK_a of MG cation is 6.80 [22], therefore, at pH=7.4 only a fraction of MG molecules exist in cationic form, but it is the MG cation that gives resonantly enhanced and readily detectable SH signal as described

in chapter 3.2.3. In this situation, we need to consider both equilibriums involving MG in the system:



The kinetic equations are:

$$\frac{dN}{dt} = k_1 \frac{[MG^+]}{55.5} (N_{\max} - N) - k_{-1}N \quad (3.7)$$

$$\begin{aligned} \frac{d[MG^+]}{dt} = & -k_1 \frac{[MG^+]}{55.5} (N_{\max} - N) + k_{-1}N \\ & -k_a[MG^+] + k_{-a}[H^+][MG \cdot OH] \end{aligned} \quad (3.8)$$

where $C = [MG \cdot OH] + [MG^+] + N$. $[MG \cdot OH]$, $[MG^+]$ and N is the number of $MG \cdot OH$ in bulk, MG^+ cations in bulk, and MG^+ cations adsorbed on the cell membrane surface, respectively. k_a and k_{-a} the rate constant for the equilibrium between MG cations and neutral form.

At equilibrium, the expression of the surface coverage θ for the pH-adjusted *Langmuir* model can be derived as follow:

$$\theta = \frac{N}{N_{\max}} = \frac{(C + N_{\max} + \frac{55.5}{\alpha K}) - \sqrt{(C + N_{\max} + \frac{55.5}{\alpha K})^2 - 4CN_{\max}}}{2N_{\max}} \quad (3.9)$$

where $K = \frac{k_1}{k_{-1}}$; $K_a = \frac{k_a}{k_{-a}}$; and $\alpha = \frac{[H^+]}{K_a + [H^+]}$. Therefore, a nonlinear least-square fitting

of the adsorption isotherm will allow the determination of αK and N_{\max} . K can then be calculated at the given pH value, and then be used to calculate the adsorption free energy $\Delta G = -RT \ln K$. In order to analyze the adsorption isotherms obtained as the SH

intensity I_{SH} versus MG concentration, one last step is to relate I_{SH} to the surface coverage θ , details of which will be given in the following section.

3.3.4 Surface Coverage and SHG

The theoretical model for analyzing the adsorption isotherms recorded as SH intensity versus molecule concentration measured from the colloidal system has been established and reported [26, 27]. As is learned from previous studies, the SH intensity I_{SH} is related to the adsorbate coverage θ on the particle surface and can be generally represented as

$$I_{SH} = B + (b + a\theta e^{i\varphi})^2 \quad (3.10)$$

The interface contribution to SHG has two sources: the contribution from the bulk and bare surface depicted by parameter b and the contribution from the surface adsorbed dye depicted by the term $a\theta e^{i\varphi}$. In the surface contribution term $a\theta e^{i\varphi}$, a corresponds to the SH polarization at full surface dye coverage, θ is the surface dye coverage as a fraction of the full coverage. The two sources may interfere and $e^{i\varphi}$ is the phase factor between the particle surface SHG contribution b and the surface adsorbed dye SHG contribution a . All other incoherent contributions detected as signal that are not related to the liquid-colloidal interface are summarized in background noise term B .

For our experiments, equation 3.10 can be simplified with b and φ set to zero, since the SHG contribution from the bulk colloidal surface is negligible. A typical adsorption isotherm should look like Figure 3.5, equation 3.9 and 3.10 together can be used to relate the SHG intensity I_{SH} to C , and a nonlinear least-square fit of the

experimentally measured SH intensity I_{SH} as a function of C can give parameters N_{\max} and K .

3.4 Results and Discussion:

3.4.1 Molecular Adsorption onto *E.coli* Cell Surface

For demonstrating the utility of this nonlinear optical technique for examining molecular transport through living cell membrane, we choose gram-negative bacteria *E.coli* which has two cell membranes (Fig. 3.6): a cytoplasmic lipid-bilayer inner membrane and an outer membrane which is asymmetric in the bilayer structure with an outer leaflet covered by long polysaccharide chains and a phospholipid inner leaflet. The *E.coli* cell is typically a rod 2 μm long with 1 μm diameter. For this size particle, the surface generated SH light can be amply detected at the forward scattering direction [28, 29].

The molecule for study is the positively charged hydrophobic ion, the malachite green (MG) dye. Its structure mimics many small/medium size hydrophobic ions. The charge is surrounded by propeller-like hydrophobic groups (Fig. 3.2) and is delocalized by symmetry so the molecule binds to and readily permeates through lipid membranes in a simple diffusion mechanism [7, 30]. At the wavelength we chose for the SHG measurement, the MG ion gives resonantly enhanced and readily detectable SH signal.

We anticipate this hydrophobic ion to diffuse through the polysaccharide chains and adsorb onto the negatively charged outer membrane surface. The hydrophobic ion, with molecular weight 329.4 Da, may then penetrate through the outer membrane either

through the porin channels or directly through the phospholipid bilayer. The classic porin trimer, the *ompF*, contains three channels each with a $7 \times 11 \text{ \AA}^2$ bottleneck known to exclude uncharged hydrophobic solutes but permits passive diffusion of hydrophilic compounds with molecular weight smaller than 600 Da [31]. Diffusion of the MG ion through the outer membrane results in MG concentration inside the cell. Subsequent adsorption to the inner surface of the outer membrane, adsorption to the outer surface of the inner membrane, diffusion through the inner membrane, and adsorption onto the inner surface of the inner membrane may occur, Fig. 3.6. It is expected that adsorption onto the outer surfaces of the two membranes will lead to increase of the SHG signal while adsorption onto the inner surfaces, following membrane diffusions, will result in decrease in the SHG signal, Fig. 3.7.

The MG dye in solution form was mixed into the *E.coli* solution to reach a selected initial concentration at $t=0$. As expected, a rapid initial rise in the SH signal was observed due to adsorption of MG ions onto the cell, Fig. 3.7. As time proceeds, the hydrophobic ions penetrate the bacteria membrane and bind to its inner leaflet, resulting in the decay of the signal. However, instead of a monotonic decay, another rise and decay appear in the signal, reflecting occurrence of subsequent adsorption and transport processes at the inner cytoplasmic membrane.

It is found that the time-profile of the SH signal depends on the MG concentration applied, Fig. 3.8. There is an apparent second rise when the MG concentration is relatively low, from $0.25 \text{ }\mu\text{M}$ to $1.00 \text{ }\mu\text{M}$. The magnitude of the second rise decreases when the MG concentration is increased to higher values. In the following we extract the molecular transport rate constants of each membrane from analyzing the time-resolved

traces. But first we determine the adsorption characteristics of the MG ion on the *E.coli* cell membrane.

In Fig. 3.8 the initial SH intensity is proportional to the square of the coverage of the MG ion on the cell membrane prior to its diffusion into the cell. By plotting the intensity of the SH signal at $t=0$ as a function of the MG concentration as in Fig. 3.9, we obtain the adsorption isotherm which can be quantitatively described by a modified *Langmuir* Model (chapter 3.3.2). The experiments were performed under physiological $\text{pH} = 7.4 \pm 0.1$. In the model analysis, the influence of the pH on the MG-MG ion equilibrium [22] has to be included (chapter 3.3.3).

A nonlinear least-square fit of the SHG-expressed adsorption isotherm yields the maximum adsorption density of MG ion on the cell as $N_{\text{max}} = (7.4 \pm 1.2) \times 10^7 / \text{cell}$ or $(1.2 \pm 0.2) \times 10^7 / \mu\text{m}^2$ and the adsorption free energy $\Delta G = - (13.6 \pm 0.4) \text{ kcal/mol}$. The MG ion binds to the *E.coli* membrane with a 6.3 times higher density and much stronger energy in comparison with the lipid vesicle membrane: $(1.9 \pm 0.1) \times 10^6 / \mu\text{m}^2$ and $\Delta G = - (8.6 \pm 0.2) \text{ kcal/mol}$ [18]. On the bacterial surface the density corresponds to an 8.3 \AA^2 area for each adsorbed MG ion, which is comparable to the molecular size of $\sim 10 \text{ \AA}^2$. This is likely due to the complexity of the cell surface, Fig. 3.6: there are negatively charged groups in the “hair-like” polysaccharide chains [32, 33], which in addition to the lipid membrane also provide adsorption sites for positively charged MG ions. The dominant driving force for MG adsorption at *E.coli* cell membrane under physiological $\text{pH} 7.4$ is electrostatic interaction while that for MG adsorption at liposome surface is hydrophobic interaction since the later experiments were reported under acidic $\text{pH} 4$ at which the negative charges at the liposome surface was neutralized [18]. Therefore, the

electrostatic interactions driving MG adsorption at the cell membrane surface results in a much larger magnitude of adsorption free energy compared to the hydrophobic interaction driving adsorption at liposome surface.

3.4.2 Time-Resolved Molecular Transport through *E.coli* Membranes

A kinetic model, illustrated in Fig. 3.6, that incorporates all the adsorption and transport processes at both membranes is constructed for quantitative account of the observed time-resolved SH intensity. The sharp rise of the SH signal following addition of MG at $t=0$ indicates that the adsorption rate of the MG ion onto the outer surface of the outer membrane (OM) is much larger than the translocation rate through the membrane. Following the transport of MG ions across the outer membrane, the adsorption and transport processes proceed to populate the membrane surfaces as well as the periplasmic space between the two membranes and the cytoplasmic space inside the inner membrane (IM). In the kinetic model, the adsorption/desorption rate constants, the transport constants, and the maximum adsorption densities on all four membrane surfaces, are variables to be determined through nonlinear least-squares fitting of the SH intensity as a function of time.

The kinetic model that incorporates all the adsorption and transport processes at both membranes of *E.coli* can be evaluated numerically to obtain the surface coverage at all membrane surfaces as a function of time. The total adsorption/desorption and transport physical process can be expressed as:





where M , M_1 , M_2 represents MG molecules in the bulk solution outside the cell membrane, in the periplasmic space in between the two membranes, and in the cytoplasmic space inside the inner membrane, respectively; while E_{1o} , E_{1i} , E_{2o} , E_{2i} denotes the empty adsorption sites on the outer surface of the outer membrane, on the inner surface of the outer membrane, on the outer surface of the cytoplasmic membrane, and on the inner surface of the cytoplasmic membrane, respectively. k_i / k_{-i} ($i=1, 3, 4$) are the adsorption/desorption rate constant on the respective cell membrane surfaces; while k_2 and k_5 is the transport rate constant through the outer membrane and the cytoplasmic membrane, respectively. In the above kinetic model, we assume equal forward/backward transport rate constant for both membranes. Due to the symmetry of the cytoplasmic membrane, it is also reasonable to assume equal characteristics (rate constants and maximum number density) for both sides of the cytoplasmic membrane.

The physical model can be written-up as differential equations:

$$\frac{dM}{dt} = -k_1 \cdot M \cdot (N_{1o}^{\max} - N_{1o}) + k_{-1} \cdot M_{H_2O} \cdot N_{1o} \quad (3.17)$$

$$\frac{dN_{1o}}{dt} = k_1 \cdot M \cdot (N_{1o}^{\max} - N_{1o}) - k_{-1} \cdot M_{H_2O} \cdot N_{1o} - k_2 \cdot (N_{1o} - N_{1i}) \quad (3.18)$$

$$\frac{dN_{1i}}{dt} = k_2 \cdot (N_{1o} - N_{1i}) + k_3 \cdot M_1 \cdot (N_{1i}^{\max} - N_{1i}) - k_{-3} \cdot M_{H_2O} \cdot N_{1i} \quad (3.19)$$

$$\begin{aligned} \frac{dM_1}{dt} = & -k_3 \cdot M_1 \cdot (N_{1i}^{\max} - N_{1i}) + k_{-3} \cdot M_{H_2O} \cdot N_{1i} \\ & -k_4 \cdot M_1 \cdot (N_{2o}^{\max} - N_{2o}) + k_{-4} \cdot M_{H_2O} \cdot N_{2o} \end{aligned} \quad (3.20)$$

$$\frac{dN_{2o}}{dt} = k_4 \cdot M_1 \cdot (N_{2o}^{\max} - N_{2o}) - k_{-4} \cdot M_{H_2O} \cdot N_{2o} - k_5 \cdot (N_{2o} - N_{2i}) \quad (3.21)$$

$$\frac{dN_{2i}}{dt} = k_5 \cdot (N_{2o} - N_{2i}) + k_4 \cdot M_2 \cdot (N_{2i}^{\max} - N_{2i}) - k_{-4} \cdot M_{H_2O} \cdot N_{2i} \quad (3.22)$$

$$\frac{dM_2}{dt} = -k_4 \cdot M_2 \cdot (N_{2i}^{\max} - N_{2i}) + k_{-4} \cdot M_{H_2O} \cdot N_{2i} \quad (3.23)$$

where N_{1o}^{\max} , N_{1i}^{\max} , N_{2o}^{\max} , N_{2i}^{\max} are the maximum number densities on all four surfaces and M_{H_2O} is the water molarity 55.5M. The kinetic model allows incremental determination of the surface coverage N_{1o} , N_{1i} , N_{2o} , N_{2i} as a function of time. Eventually, the SH intensity I_{SH} is related to these surface MG ions as:

$$I_{SH} = c(N_{1o} - N_{1i} + N_{2o} - N_{2i})^2 \quad (3.24)$$

The experimentally observed SH signal as a function of time can be fitted through a nonlinear least-square program for the determination of adsorption equilibrium constant $K_i = k_i / k_{-i}$ ($i=1, 3, 4$) ($K_{1i}=K_3$, $K_{2o=2i}=K_4$); the transport rate constant $k_{1l}=k_2$ and $k_{l2}=k_5$; as well as the maximum surface coverage N_{1o}^{\max} , N_{1i}^{\max} , N_{2o}^{\max} , N_{2i}^{\max} .

Some of the fitting traces are shown in Fig. 3.8 and simulation of surface coverage time profiles are illustrated in Fig. 3.9. As a test to the reliability of the model, the maximum adsorption density at the outermost cell surface obtained as a variable in the model fitting, $(1.07 \pm 0.06) \times 10^7 \mu\text{m}^{-2}$ (Table 3.2) is in good agreement with that determined from the adsorption isotherm, $(1.2 \pm 0.2) \times 10^7 \mu\text{m}^{-2}$. Furthermore, the maximum adsorption density at the inner surface of the OM and at the outer surface of

the IM, $(1.52 \pm 0.08) \times 10^6 \mu\text{m}^{-2}$ and $(1.55 \pm 0.17) \times 10^6 \mu\text{m}^{-2}$ (Table 3.2) are identical within errors, as expected due to the similar composition of the two membrane leaflets.

The rate constants of transport through the outer and inner membranes are determined respectively as $(3.62 \pm 0.79) \times 10^{-2} \text{ s}^{-1}$ and $(6.58 \pm 4.41) \times 10^{-4} \text{ s}^{-1}$ (Table 3.2). The transport rate constant of MG ions through the outer membrane is more than one order of magnitude larger than the one for the inner membrane. It appears that the hydrophobic ions can, in addition to simple diffusion [34], transport through the porin channels. The porins of *E. coli* are known to exclude uncharged lipophilic solutes but enable hydrophilic solutes to transport with permeability inversely proportional to their hydrophobicity [31]. Though MG ion is hydrophobic, it is positively charged and the size is relatively small, therefore, it still permeates through porin.

The importance of the ion channels is also born out in comparison with other works. We noted very limited prior work done on small/medium molecules transport across the bacterial outer membrane. The celebrated study by Zimmermann and Rosset in 1970s [12] using enzyme assay method has determined the transport of benzylpenicillin, in its negatively charged acidic form, through *E. coli* outer membrane with a rate constant of $1.9 \times 10^{-4} \text{ s}^{-1}$, two orders of magnitude smaller than the transport rate constant we determined for the MG ion. Considering the comparable size of the two molecules, this comparison confirms that the ionic nature of a molecule is deterministic for transport through a cell membrane that has ion transport channels. It has been reported that the classic porins show a preference for cations over anions, presumably because of the presence of interior-negative Donnan potential and of the presence of a high concentration of negatively charged LPS molecules on the surface [35, 36].

The transport rate constant determined for the cytoplasmic membrane which has a straightforward lipid bilayer structure is one order of magnitude smaller than that of the lipid bilayer membrane [18], $9.5 \times 10^{-3} \text{ s}^{-1}$ presumably due to the more tightly packed cell membrane than the artificial liposome membrane. The adsorption free energies of MG ions on the inner surface of the OM and on the outer surface of the IM, $-(10.9 \pm 0.4)$ kcal/mole and $-(12.1 \pm 0.6)$ kcal/mole (Table 3.2), are comparable with variations, magnitudes of which are higher than the one measured for the liposome membrane [18]. The results for liposome were reported under acidic pH 4, at which the negatively charged phosphate groups at the liposome surface were neutralized, while our cell results were obtained under physiological pH 7.4, at which the membrane surface is negatively charged. Therefore, the dominant driving force for MG adsorption at cell surface is charge-charge interactions while that for the liposome surface is hydrophobic interactions, which explains well the much larger magnitude of adsorption free energy from the former than the later. Also noticed is that both magnitudes of adsorption free energy for the membrane surfaces inside the cell are smaller than that determined for the outermost cell membrane surface. This phenomenon is due to the high ionic strength in the periplasm and cytoplasm inside the cell [37]. The effect of solution ionic strength on MG ion adsorption on *E.coli* cell surface has been confirmed, the experimental results and analysis are illustrated in the following section.

3.4.3 Salt Effects on Molecular Adsorption at *E.coli* Cell Membrane

Adsorption isotherms of MG ions on *E.coli* cell membrane surface under different ionic strengths (Figure 3.10) were obtained. The analysis by modified *Langmuir* model yields adsorption free energy and maximum density, the values of which are listed in

Table 3.3. The results clearly demonstrated that the higher the ionic strength, the lower the adsorption free energy. On the other hand, as the salinity increases, the maximum adsorption density also increases. Further investigation of solvent ionic effects on molecular adsorption will be shown in chapter 5.

3.5 Summary

In summary, we've demonstrated that the nonlinear optical phenomenon Second Harmonic Generation can be used to observe the adsorption and transport of molecules through living cell membranes in real time. In the case of the gram-negative bacteria *E.coli*, the adsorption onto and transport across the two membranes of a hydrophobic molecular cation with molecular weight of 329.4 Da are individually observed in sequence in time. The adsorption density and free energy as well as the transport rate constant at each of the membranes have been determined. It is observed that the transport rate of this molecular ion through the outer membrane with ion channel porins is more than one order of magnitude faster than the transport through the inner lipid bilayer membrane. In contrast to the *E.coli* cell, the molecular ion can adsorb onto the MEL cell but cannot penetrate its membrane which has no hydrophobic ion permeable channels and is more tightly packed.

The biggest advantage of SHG is to directly differentiate molecules associated to the cell membrane surface from those in the bulk cell compartmentations and the time evolution of membrane-associated populations allows quantitative determination of transmembrane movement kinetics of small molecules. The molecular transport mechanisms as well as the deterministic local environment factors can be evaluated.

The value of the SHG technique is not limited to identify a specific transport mechanism for a specific molecule, but to provide fundamental knowledge concerning transmembrane movement of small molecules and quantitatively characterize molecular transport kinetics. Although the SHG technique so far has only been used on two types of cell membranes, *E.coli* and MEL, for probing molecular adsorption and transport kinetics, the results point to a general understanding of how small molecules associate with cell membranes, and the importance of the ionic nature and the detailed membrane structure in regulating molecular transport. The study demonstrates an experimental capability that can be broadly applied for studies aiming at establishing fundamental understanding of interactions of molecules with the membranes of living cells and for characterization pharmacological mechanism of specific molecules.

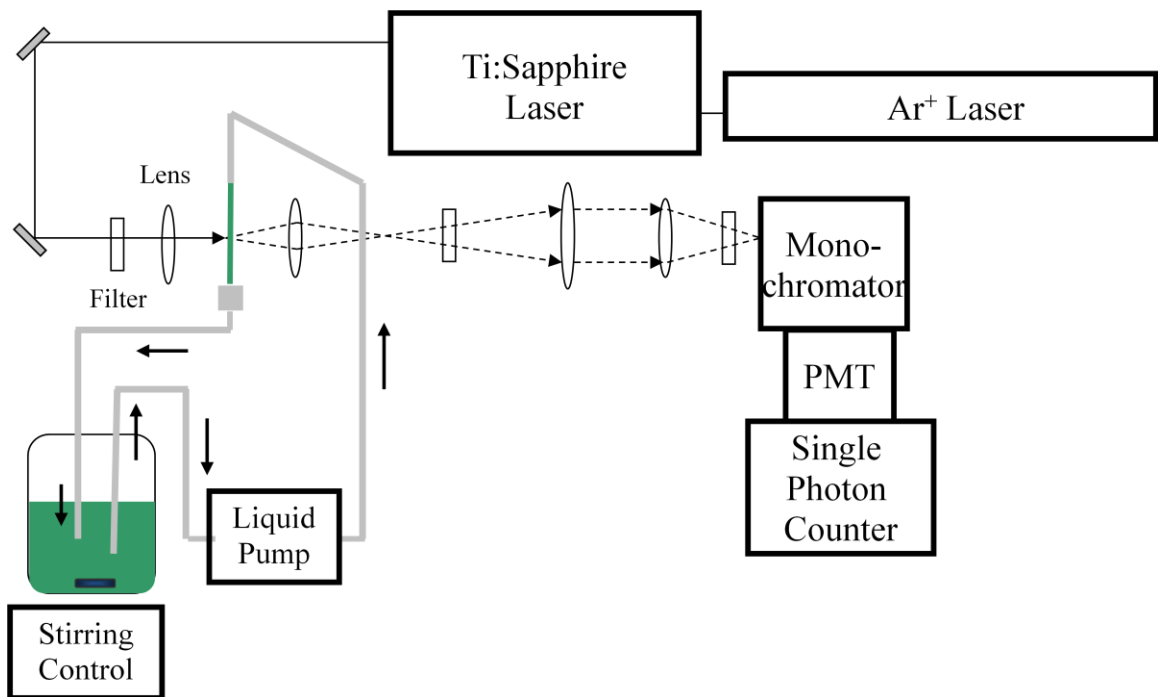


Figure 3.1: Schematic illustration of the experimental setup of the forward detection of SHG signal.

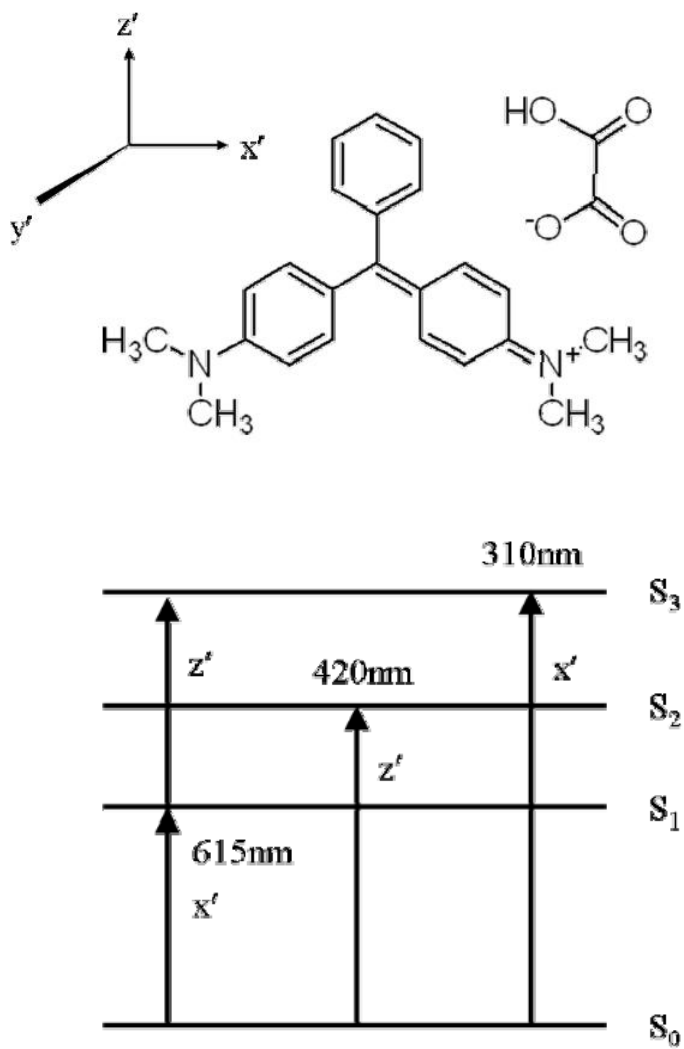


Figure 3.2: MG structure and its spectral features

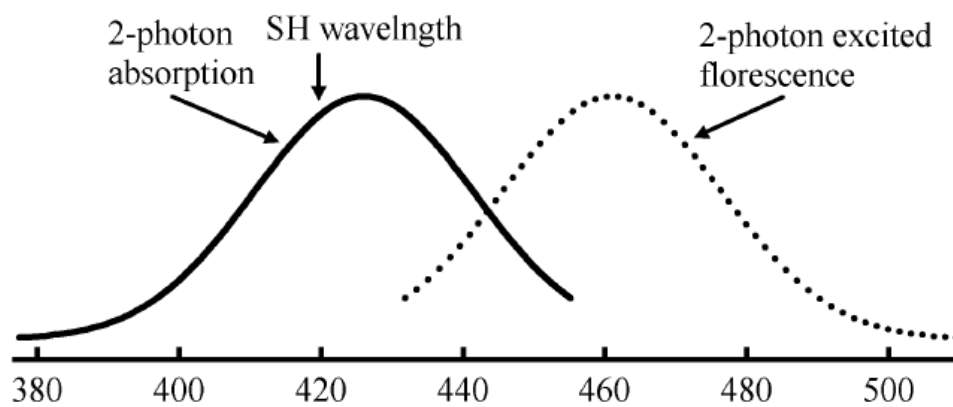


Figure 3.3: Spectrum of the two-photon absorption and the two-photon excited fluorescence for malachite green

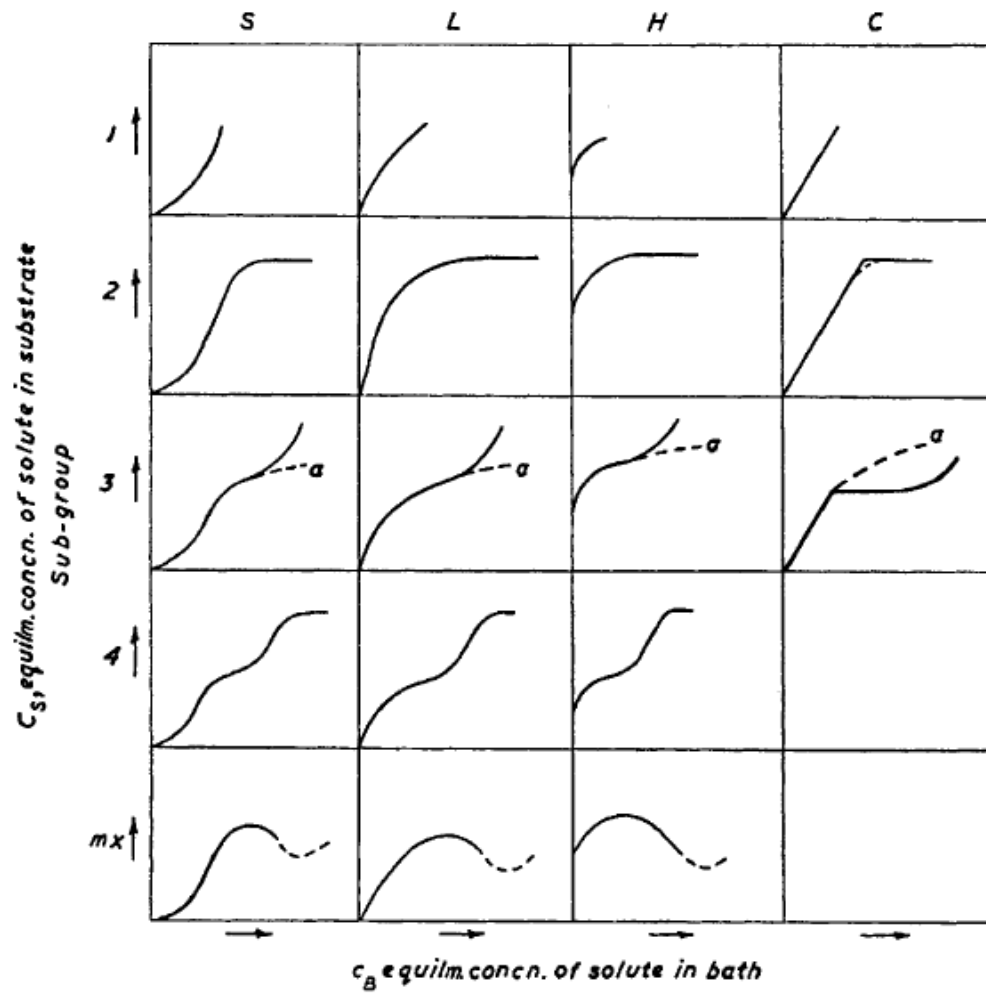


Figure 3.4: System of isotherm classification [ref]. L2 represents the *Langmuir* isotherm.

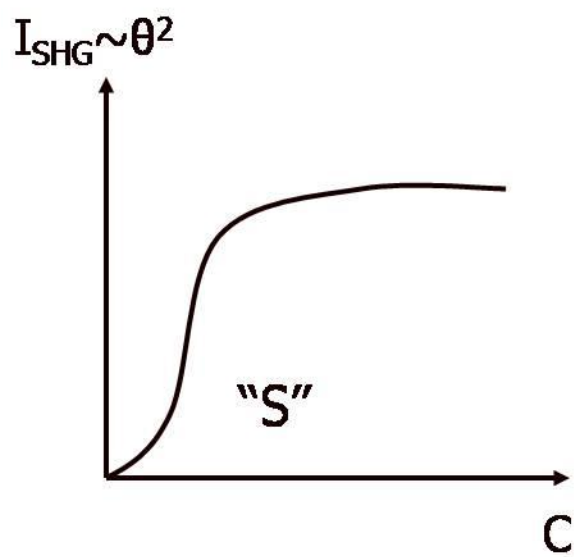


Figure 3.5: Typical *Langmuir* adsorption isotherm curve expressed in SH intensity versus molecular concentration.

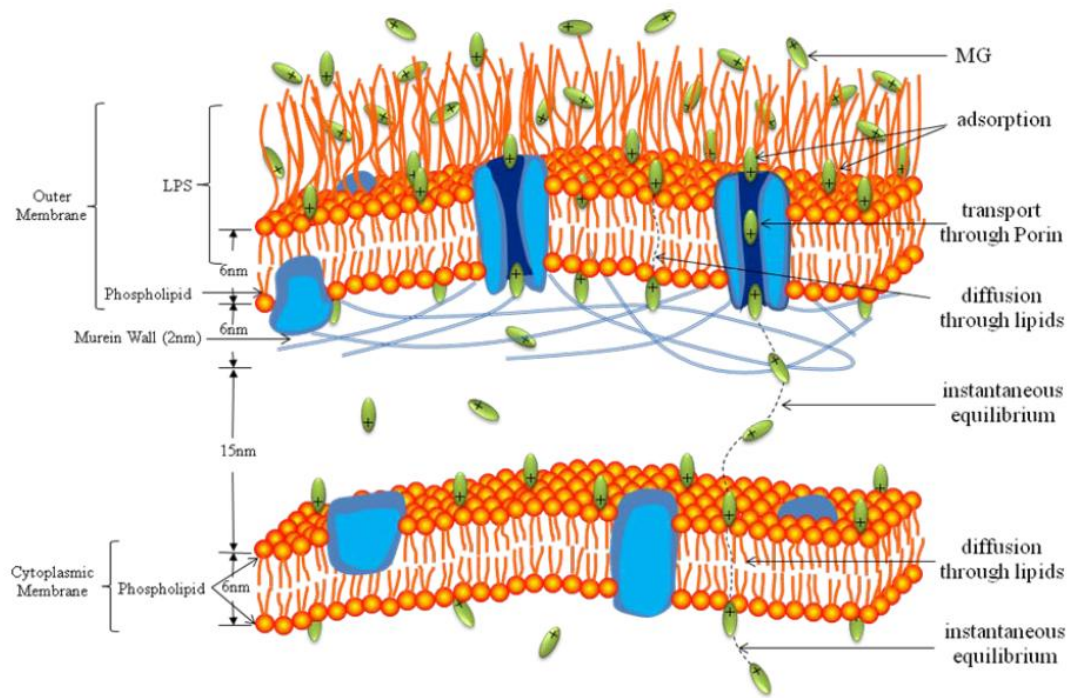


Figure 3.6: Illustration of the two membranes of the *E.coli* bacteria. Types of interactions of the molecular ion (in green color) with the membranes are listed on the right side.

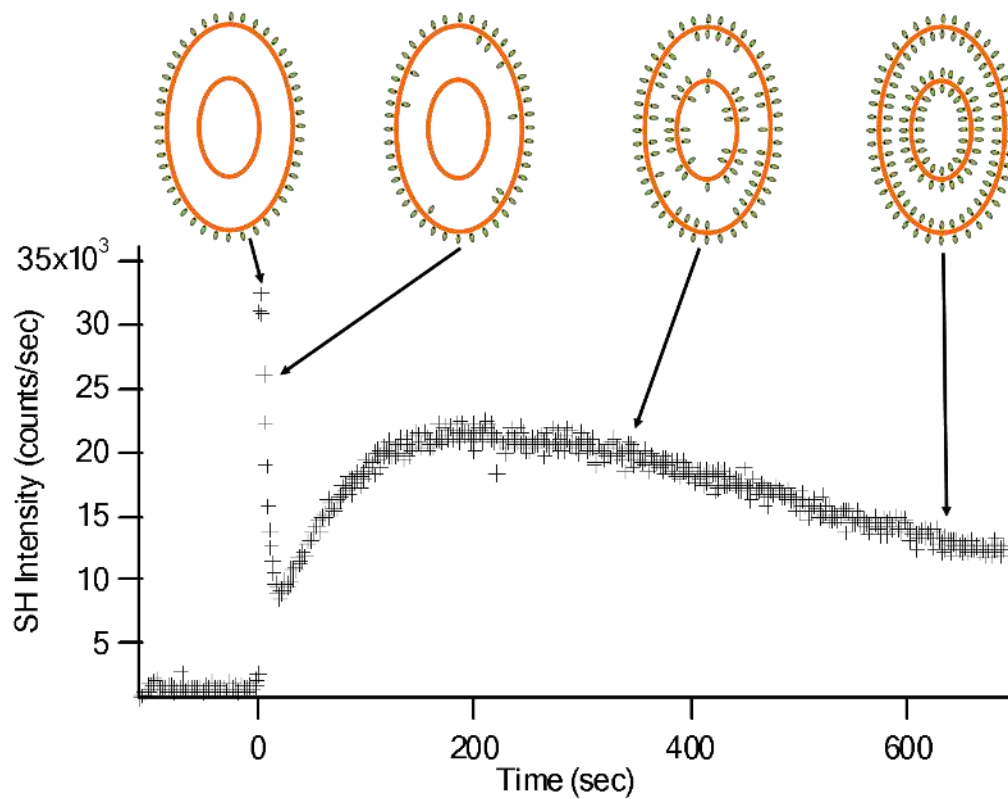


Figure 3.7: Time profile of the SH intensity following addition of the MG ion (at $0.25\mu\text{M}$) to the *E.coli* bacteria solution. Displayed at the top are schematic representations of the corresponding states of adsorption and transport of the MG ions at the two membranes.

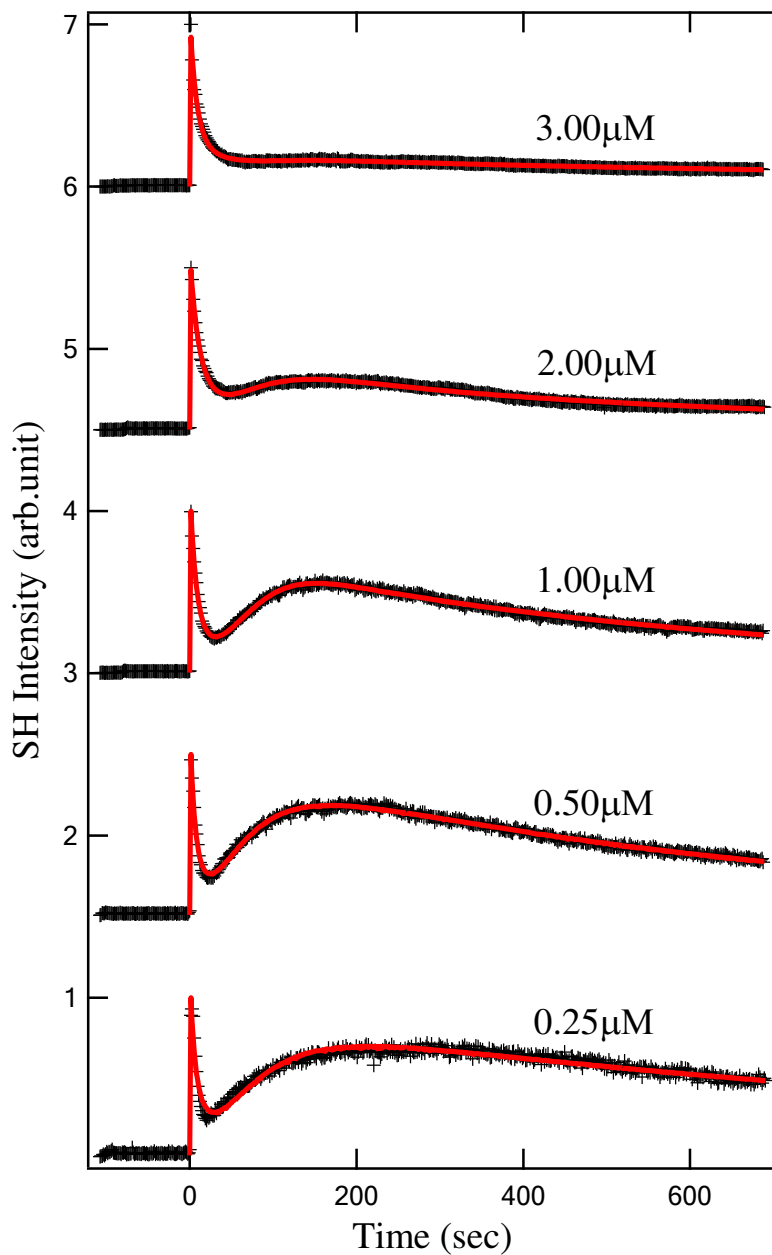


Figure 3.8: Nonlinear least-square fits (solid red lines) of the time profiles of the SH intensity (normalized) following addition of MG ions at various concentrations into solutions containing living *E.coli* cells.

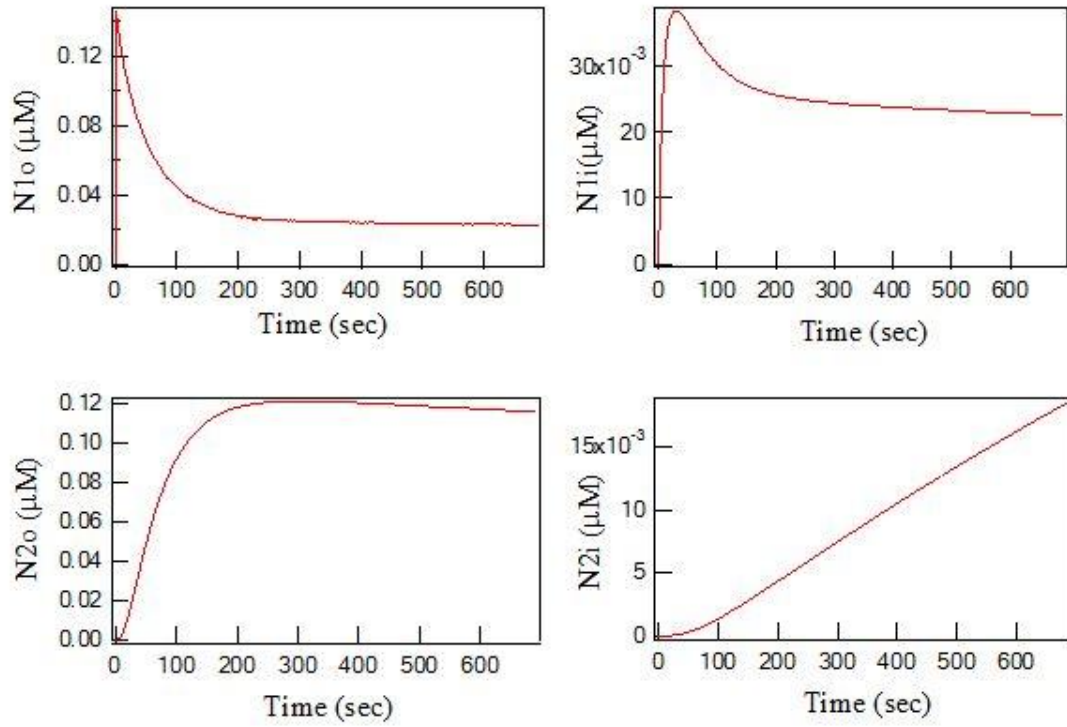


Figure 3.9: Time profiles of membrane surface coverage simulated using the kinetic model for $MG=0.25\mu\text{M}$.

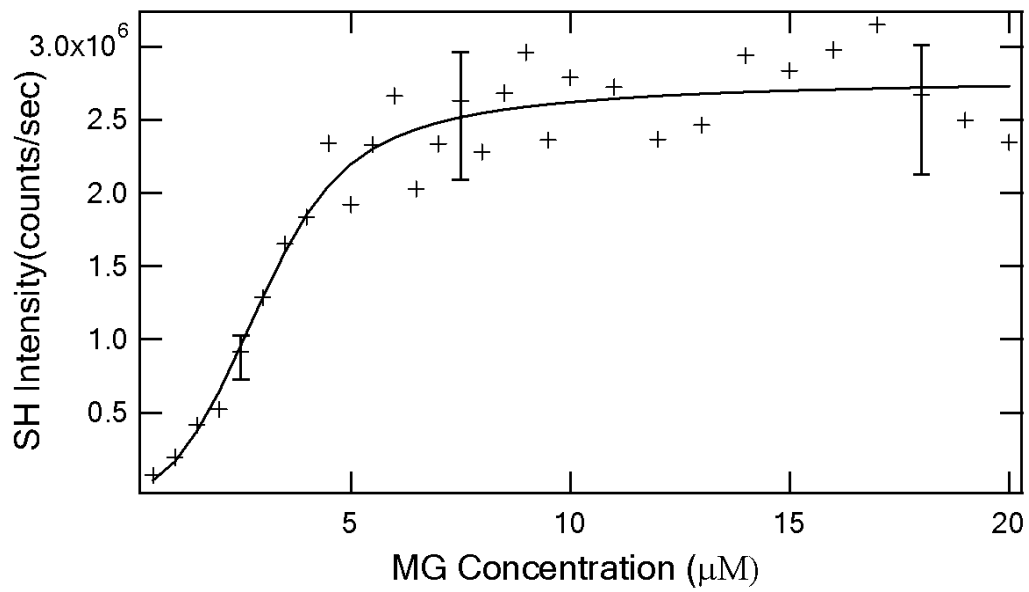


Figure 3.10: Adsorption isotherm expressed in SH intensity for MG ion on the *E.coli* cell. The solid line is a nonlinear least-square fit of a modified *Langmuir* model; error bars indicate s.d..

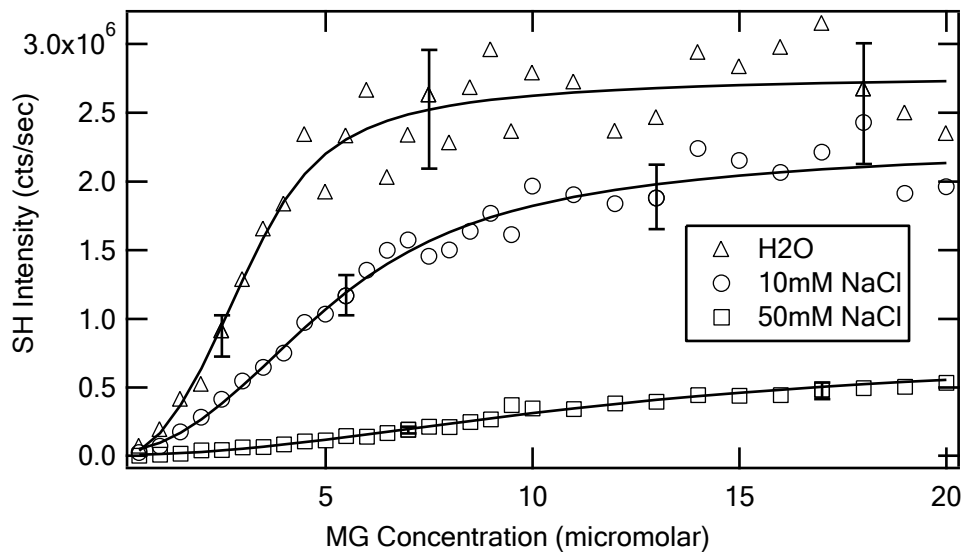


Figure 3.11: Adsorption isotherms of MG ions on the *E.coli* cell under different salinities.

The solid lines are nonlinear least-square fits of a modified *Langmuir* model.

Table 3.1: Specifications of Malachite Green

Product name	Malachite Green oxalate salt, certified by the Biological Stain Commission
CAS number	2437-29-8
Sigma Aldrich Product NO.	M9015
Molecular formula	$C_{46}H_{50}N_4 \cdot 2HC_2O_4 \cdot C_2H_2O_4$
Molecular weight	927.03
Appearance	Green powder
Solubility	Dark blue solution at 4 mg plus 4 mL of water
Dye content	Minimum 90%

Table 3.2: Adsorption and Transport Characteristics (a) at *E.coli* Outer Membrane, (b) at *E.coli* Cytoplasmic Membrane, and (c) Relative Results from Both Membranes in Comparison with the Liposome Results [18]

(a)

	0.25μM	0.50 μM	1.00 μM	2.00 μM	3.00 μM
$k_{r1}(\times 10^{-2} s^{-1})$	3.88 \pm 0.04	4.14 \pm 0.03	3.45 \pm 0.03	2.83 \pm 0.01	3.82 \pm 0.01
$K_{li}(\times 10^8)$	0.52 \pm 0.06	0.96 \pm 0.03	1.15 \pm 0.11	1.35 \pm 0.02	1.64 \pm 0.02
$-\Delta G_{li}(kcal / mol)$	10.5 \pm 0.1	10.9 \pm 0.1	11.0 \pm 0.1	11.1 \pm 0.1	11.2 \pm 0.1
$N_{io}^{max}(\times 10^7 \mu m^{-2})$	1.12 \pm 0.01	1.10 \pm 0.01	1.10 \pm 0.01	1.04 \pm 0.01	1.01 \pm 0.01
$N_{li}^{max}(\times 10^6 \mu m^{-2})$	1.57 \pm 0.09	1.60 \pm 0.03	1.50 \pm 0.03	1.47 \pm 0.03	1.47 \pm 0.03

(b)

	0.25μM	0.50 μM	1.00 μM	2.00 μM	3.00 μM
$k_{r2}(\times 10^{-2} s^{-1})$	3.63 \pm 0.05	6.05 \pm 0.03	7.87 \pm 0.05	11.0 \pm 0.1	4.37 \pm 0.04
$K_{2o=2i}(\times 10^8)$	3.65 \pm 0.41	8.11 \pm 0.22	21.4 \pm 1.9	2.13 \pm 0.04	14.1 \pm 0.1
$-\Delta G_{2o=2i}(kcal / mol)$	11.7 \pm 0.1	12.2 \pm 0.1	12.7 \pm 0.1	11.4 \pm 0.1	12.5 \pm 0.1
$N_{2o=2i}^{max}(\times 10^6 \mu m^{-2})$	1.50 \pm 0.06	1.50 \pm 0.03	1.54 \pm 0.03	1.72 \pm 0.03	1.50 \pm 0.03

(c)

	$N_{\max} (\mu\text{m}^{-2})$	$-\Delta G (\text{kcal/mol})$	$k_t (\text{s}^{-1})$
OM (outer surface)	$(1.07 \pm 0.06) \times 10^7$	13.6 ± 0.4	$(3.62 \pm 0.79) \times 10^{-2}$
OM (inner surface)	$(1.52 \pm 0.08) \times 10^6$	10.9 ± 0.4	
IM	$(1.55 \pm 0.17) \times 10^6$	12.1 ± 0.6	$(6.58 \pm 4.41) \times 10^{-4}$
Liposome [18]	$(1.9 \pm 0.1) \times 10^6$	8.6 ± 0.2	9.5×10^{-3}

Table 3.3: Adsorption isotherms of MG ions on the *E.coli* cell under different salinities

	N_{\max} (cell ⁻¹)	$K(M^{-1})$	$-\Delta G(\text{kcal/mol})$
0mM NaCl (H₂O)	$(7.4 \pm 1.2) \times 10^7$	$(1.3 \pm 0.8) \times 10^{10}$	13.6 ± 0.4
10mM NaCl	$(1.0 \pm 0.2) \times 10^8$	$(3.7 \pm 1.1) \times 10^9$	12.9 ± 0.2
50mM NaCl	$(1.8 \pm 0.4) \times 10^8$	$(9.1 \pm 2.5) \times 10^8$	12.1 ± 0.2

Bibliography

1. Slepko, E.R., et al., *Structural and functional analysis of the Na⁺/H⁺ exchanger*. Biochem. J., 2007. **401**: p. 623-633.
2. Noskov, S.Y. and B. Roux, *Ion selectivity in potassium channels*. Biophys. Chem., 2006. **124**(3): p. 279-291.
3. Lewis, R.S., *The molecular choreography of a store-operated calcium channel*. Nature, 2007. **446**(7133): p. 284-287.
4. Dunlop, J. and J.A. Butera, *Ligands targeting the excitatory amino acid transporters (EAATs)*. Curr. Top. Med. Chem., 2006. **6**(17): p. 1897-1906.
5. Guan, L.K., H. Ronald., *Glucose/sugar transport in bacteria*, in *Encyclopedia of Biological Chemistry* 2004, Elsevier Ltd: Oxford, UK. p. 204-207.
6. Visser, W.F., et al., *Metabolite transport across the peroxisomal membrane*. Biochem. J., 2007. **401**: p. 365-375.
7. Ketterer, B., B. Neumcke, and P. Läuger, *Transport mechanism of hydrophobic ions through lipid bilayer membranes*. J. Membrane Biol., 1971. **5**(3): p. 225-245.
8. Benz, R., P. Läuger, and K. Janko, *Transport kinetics of hydrophobic ions in lipid bilayer membranes - charge-pulse relaxation studies*. Biochim. Biophys. Acta, 1976. **455**(3): p. 701-720.
9. Hamill, O.P., et al., *Improved patch-clamp techniques for high-resolution current recording from cells and cell-free membrane patches*. Pflug. Arch.-Eur. J. Phy., 1981. **391**(2): p. 85-100.

10. Eidelman, O. and Z.I. Cabantchik, *Continuous monitoring of transport by fluorescence on cells and vesicles*. Biochim. Biophys. Acta, 1989. **988**(3): p. 319-334.
11. Cafiso, D.S. and W.L. Hubbell, *Spin-label detection of electrogenic proton fluxes in phospholipid-vesicles*. Biophys. J., 1981. **33**(2): p. A114.
12. Zimmermann, W. and A. Rosselet, *Function of outer membrane of Escherichia coli as a permeability barrier to beta-lactam antibiotics*. Antimicrob. Agents Ch., 1977. **12**(3): p. 368-372.
13. Plesiat, P. and H. Nikaido, *Outer membranes of Gram-negative bacteria are permeable to steroid probes*. Mol. Microbiol., 1992. **6**(10): p. 1323-1333.
14. Wang, H., et al., *Second harmonic generation from the surface of centrosymmetric particles in bulk solution*. Chem. Phys. Lett., 1996. **259**(1-2): p. 15-20.
15. Jen, S.H. and H.L. Dai, *Probing molecules adsorbed at the surface of nanometer colloidal particles by optical second-harmonic generation*. J. Phys. Chem. B, 2006. **110**(46): p. 23000-23003.
16. Srivastava, A. and K.B. Eisenthal, *Kinetics of molecular transport across a liposome bilayer*. Chem. Phys. Lett., 1998. **292**(3): p. 345-351.
17. Yan, E.C.Y. and K.B. Eisenthal, *Effect of cholesterol on molecular transport of organic cations across liposome bilayers probed by second harmonic generation*. Biophys. J., 2000. **79**(2): p. 898-903.

18. Liu, Y., E.C.Y. Yan, and K.B. Eisenthal, *Effects of bilayer surface charge density on molecular adsorption and transport across liposome bilayers*. *Biophys. J.*, 2001. **80**(2): p. 1004-1012.
19. Shang, X.M., et al., *Effects of counterions on molecular transport across liposome bilayer: probed by second harmonic generation*. *J. Phys. Chem. B*, 2001. **105**(51): p. 12816-12822.
20. Liu, J., et al., *Antibiotic assisted molecular ion transport across a membrane in real time*. *Faraday Discuss.*, 2005. **129**: p. 291-299.
21. Green, F.J., *The Sigma-Aldrich Handbook of Stains, Dyes and Indicators*. 1990, Milwaukee, WI: Aldrich Chemical Co., Inc.
22. Anthony-Barbier, A.M., P. Rumpf, and C. Viel, *Spectrophotometric study of ionization equilibriums of a diaminated triphenylcarbinol*. , in *Bulletin de la Societe Chimique de France* 1959. p. 1474-1481.
23. Giles, C.H., et al., *Studies in adsorption. 11. A system of classification of solution adsorption isotherms, and its use in diagnosis of adsorption mechanisms and in measurement of specific surface areas of solids*. *J.Chem. Soc. Abstr.*, 1960(OCT): p. 3973-3993.
24. Langmuir, I., *The constitution and fundamental properties of solids and liquids. part I. solids*. *J. Am. Chem. Soc.*, 1916. **38**: p. 2221-2295.
25. Evans, D.F. and H. Wennerström, *The Colloidal Domain- where physics, chemistry, biology, and technology meet*. 2nd ed. 1999, New York: Wiley-VCH.
26. Wang, H.F., et al., *Energetics and population of molecules at microscopic liquid and solid surfaces*. *J. Phys. Chem. B*, 1998. **102**(23): p. 4446-4450.

27. Wang, H.F., et al., *In situ, nonlinear optical probe of surfactant adsorption on the surface of microparticles in colloids*. Langmuir, 2000. **16**(6): p. 2475-2481.
28. Jen, S.H., G. Gonella, and H.L. Dai, *The effect of particle size in second harmonic generation from the surface of spherical colloidal particles. I: experimental observations*. J. Phys. Chem. A, 2009. **113**(16): p. 4758-4762.
29. Jen, S.H., H.L. Dai, and G. Gonella, *The effect of particle size in second harmonic generation from spherical colloidal particle surface. II: the non-linear Rayleigh-Gans-Debye model*. J. Phys. Chem. C (in press).
30. Flewelling, R.F. and W.L. Hubbell, *Hydrophobic ion interactions with membranes - thermodynamic analysis of tetraphenylphosphonium binding to vesicles*. Biophys. J., 1986. **49**(2): p. 531-540.
31. H. Nikaido, E.Y.R., *Effect of solute size on diffusion rates through the transmembrane pores of the outer membrane of Escherichia coli*. J. Gen. Physiol., 1981. **77**: p. 121-135.
32. Reeves, P., *Biosynthesis and assembly of lipopolysaccharides*, in *New Comprehensive Biochemistry*. 1994, Elsevier: Amsterdam. p. 281-317.
33. K. Takayama, N.Q., *Chemical structure of lipid A*, in *Bacterial Endotoxic Lipopolysaccharides*. 1992, CRC Press. p. 44-65.
34. M. Vaara, W.Z.P., H. Nikaido, *Partitioning of hydrophobic probes into lipopolysaccharide bilayers*. Biochim. Biophys. Acta, 1990. **1024**: p. 152-158.
35. Benz, R., K. Janko, and P. Läuger, *Ionic selectivity of pores formed by the matrix protein (porin) of Escherichia-coli*. Biochim. Biophys. Acta, 1979. **551**(2): p. 238-247.

36. Nikaido, H., *Outer Membrane*, in *Escherichia-coli and Salmonella - Cellular and Molecular Biology*, F. Neidhardt, Editor. 1996, ASM Press: Washington, DC. p. 29-47.
37. Oliver, D.B., *Periplasm*, in *Escherichia-coli and Salmonella - Cellular and Molecular Biology* F. Neidhardt, Editor. 1996, ASM Press: Washington, DC. p. 88-103.

CHAPTER FOUR

MOLECULAR ADSORPTION ON MURINE

ERYTHROLEUKEMIA (MEL) CELL MEMBRANE

4.1 Introduction

Murine Erythroleukemia (MEL) cells are virus transformed erythroid cells blocked in an immature stage in the differentiation pathway. The conventional interest in MEL cells is based on the nature of the cell lines that they are easily induced to initiate erythroid differentiation at a much greater level, which makes MEL cells a valuable model system for analyzing the erythroid differentiation process [1, 2].

It has been established that the most notable morphological changes during the MEL cell differentiation to its end stage normoblasts, are reduction of cell size, condensation of nucleus and extrusion of nucleoli [3]. Though differentiating MEL cells undergo numerous biochemical and structural changes, studies have shown that there is no significant changes of the cell membrane structure [4]. Therefore, the information concerning molecular interaction with the MEL cell membrane surface, which largely depends on the cell surface characteristics, can represent, reliably, the molecular interaction at the regular red blood cell (RBC) surface.

RBC membrane is one of the most extensively investigated cell membrane for its physiological functions and therapeutic use. Studies of Hemoglobin (Hb) O₂ binding and blood gas (O₂ and CO₂) transport have provided fundamental understandings of the respiratory function of blood [5, 6]. As a regulatory barrier, the transport of specific anions [7, 8] and cations [9, 10] across the RBC membrane has been well characterized, and a vast knowledge base of ion channels on RBC membrane has been established. Various RBC membrane components carry different categories of blood group antigens on cell surface, the structure and functions of which are being gradually revealed [11, 12]. For RBC, a particular interest of the cell membrane surface lies in the fact that the surface characteristics and properties are critical to the problems associated with blood transfusion as well as blood storage. It has been reported that one function of the carbohydrate-rich protein coat on the surface of RBC is to sterically stabilize cells against nonspecific interactions and enabling specific biological recognitions [13]. In order to stabilize blood cells, specific recognitions at the cell surface also need to be prevented. Various efforts have been made to achieve stabilization of RBC, some of which involve introducing molecules to associate with the RBC membrane. For example, block copolymers adsorbed on the RBC membrane can prevent settling and aggregation of the cells [14].

In this report, MEL cells are used as a model system for studying molecular interaction with eukaryotic cells. It has long been recognized that the glycocalyx of the erythrocyte membrane plays an important role in preventing spontaneous red cell-red cell and red cell-endothelial interactions during blood circulation. The aggregability of erythrocytes is mainly determined by the amount of the net negative charges at the cell

surface, which is determined by collectively all charge bearing functional groups present or close to the cell surface. The possible charged functional groups include the carboxyl group (COO^-) from sialic acid, carboxyl group (COO^-) of proteins, sulfate group (SO_4^-) of condition sulfate, and phosphate group (PO_4^-) of phospholipids, of which sialic acid comprises 90% of the total [15-17]. Information such as surface charge densities and properties pertaining to molecular adsorption at the cell membrane are critical for understanding cell-cell interaction which subsequently is important for defining conditions for blood storage and for cell-cell adhesion which might cause coagulation in blood vessels under certain pathological conditions.

Studying molecular interaction with the cell membrane surface also has applications in drug delivery. Drug molecules and drug carriers often suffer from one major limitation that they are quickly removed from the blood while effective drug delivery systems require sustained blood concentration. It is recently proposed that hitchhiking on red blood cells can prolong the circulating lifetime of the drug molecules [18, 19]. From this perspective, studying molecular interaction with MEL cell membrane, which morphologically resembles proerythroblasts, should provide insights useful to development of efficient drug delivery systems.

A variety of methods, including electrophoresis [20, 21], fluorescence [22-24], SPR spectroscopy [25], FTIR spectroscopy [26]. have been used to investigate molecular interactions at biomembrane surface, ranging from the binding of small ions [20] to the association of polymer particles as drug carriers [18, 19], with a most concentrated interest on the adsorption of peptides and proteins [21, 23-25, 27-29]. Almost all studies so far were performed on predesigned artificial lipid membrane model systems implanted

with synthesized hosts for the guest probes. In these studies, either centrifugation for the binding measurements [28] or assays for differentiating surface adsorbed vs. bulk quantities has been used.

It has been shown that the nonlinear optical technique Second Harmonic Generation (SHG) can be used to study the adsorption and transport of certain small/medium size molecules at membrane of living biological cells with real time resolution [30]. The SHG signal is detected at twice the frequency 2ω of the incident fundamental light with frequency ω . SHG through dipole allowed polarizability is surface sensitive: It is dipole forbidden in centrosymmetric media but allowed in non-centrosymmetric media such as at the surface. For molecules that are noncentrosymmetric each individual molecule would have non-zero second-order polarizability for SHG. The nonlinear polarization from an ensemble of these molecules in a bulk solution will be zeroed out due to their random orientation. However, as these molecules adsorb at a surface with an ordered orientation, the ensemble average of the polarization will add up constructively to give SHG. Subsequently, the SHG signal detected from a solution containing both the cells and the molecules is from solely the molecules at the cell membrane but not in the liquid bulk.

Since the first demonstration of detecting SHG from dye molecules adsorbed on micro-colloidal particles by Eisenthal and coworkers [31], SHG has proven to be an effective technique for quantitative characterization of molecular adsorption in various colloidal systems. It has been applied to, in addition to probing adsorption and transport at living cell membranes, other biologically relevant systems including liposomes [32-37] and neuron cells [38].

In this report we show the use of SHG for probing the MEL cell membranes. Due to the lack of a rigid cell wall, animal cells usually adopt a variety of shapes, which would bring in complexity in analyzing SHG signals; however, MEL cell is of spherical shape owing to the inner red blood cell membrane skeleton composed of a network of proteins. The spherical shape eliminates any possible defects or fluctuations that irregular shapes may cause, thus, enables straightforward analysis of the SHG signal. Moreover, the MEL cell has an average volume of $500 \mu\text{m}^3$ [39], which enables SHG signal detection in the experimentally straightforward forward-propagation direction. In this report, the molecules used for study are the positively charged hydrophobic ion Malachite Green (MG) and the neutral hydrophobic dye Bromocresol Purple (BCP). It is recognized that membrane association with various biomolecules is governed by a complex interplay of hydrophobic and electrostatic interactions. MG and BCP are hydrophobic molecules with and without charge, respectively. Therefore, they serve as model molecules for general understanding molecular interaction with cell membranes.

4.2 Experiment

The experimental setup for SHG measurement of molecular interaction with cell membrane surface is described in chapter 3.2. Murine Erythroleukemia (MEL) cells was originally obtained from Gerd Blobel's laboratory and grown at 37°C with 5% CO_2 in complete DMEM supplemented with 10% fetal bovine serum, penicillin (100 units/mL)/streptomycin (100 μg /mL), 1% L-glutamine and 1% Na-Pyruvate. Cell number was counted in Burker counting chamber. After eliminating culture medium by centrifugation, cells were then re-suspended in distilled water at neutral pH or diluted

HCl solution at pH 4.5 for SHG experiments. Cells induced with 1% DMSO for 4 days to further differentiated stage were also tested. After SHG experiments, cell density were checked in Burker counting chamber again.

In a typical experiment, the MEL cell suspension reservoir is pumped to form a continuous liquid jet through which the laser beam intersects. The liquid jet avoids window effects from any sample holder. At pH=4.5, MG exists in a cationic form (Fig. 4.1 (a)) and has an absorption peaked at 425nm [40] while BCP exists in the enol form (Fig. 4.1 (b)) and employs a strong electronic transition around 430nm [41], both of which are in resonance with the second harmonic frequency of the fundamental laser input and therefore gives resonance enhanced SHG signal. MG and BCP stock solutions at 500 μ M were respectively introduced into the MEL cell suspensions by a digital titration buret.

4.3 Results and Analysis

A certain aliquot of MG concentration (10 μ M) was mixed into the MEL cell suspension at t=0 and the signal intensity were recorded as a function of time (Fig. 4.2). As is known that MG fluorescence band extends from 425nm to 600nm with the peak at 500nm, a blank experiment without MEL cells was performed to eliminate the undesirable two photon fluorescence (TPF) from the dye molecules. After subtracted the TPF, the initial rise in SH signal indicates MG adsorption onto the MEL cell membrane surface. The time-profile shows that the observed SH signal is time independent, which means there is no subsequent transport processes following the molecular adsorption, though MG has been proven to readily transport through lipid membranes [32].

Second harmonic intensity detected as a function of the MG dye concentration in the MEL cell suspension at acidic and neutral pH values is shown in Figure 4.3 (a), (b). Adsorption isotherm of cells at a further differentiate stage was obtained as well (Fig. 4.3 (c)). The SH intensity, expressed as the number of photon counts per second, is proportional to the cell surface coverage. As the quantity of MG added into the cell suspension increases, the SH intensity increases. In a typical adsorption isotherm, the signal is expected to level off when the dye concentration reaches the maximum adsorption density of the surface. As is depicted in Fig. 4.3, a relatively large amount of MG (~30 μ M) is needed to saturate the MEL cell membrane surface. At such high MG concentration, the TPF signal from the bulk MG can no longer be neglected. The plateau of the SH intensity is clear when we subtract TPF from the original signal (Fig. 4.3).

(1) Under acidic condition (pH=4.5) when the MG exists in cationic form, the expression for cell membrane surface coverage of MG can be derived from a modified *Langmuir* adsorption model described in chapter 3.3.2 considering only the equilibrium between the MG cations in the bulk solution and those on the cell membrane surface. The adsorption equilibrium constant K can be obtained by a nonlinear least-square fit of the experimentally observed adsorption isotherms (Fig. 4.3). K can then be used to calculate the adsorption free energy of MG to MEL cell through $\Delta G = -RT \ln K$.

(2) At neutral pH, in addition to the adsorption equilibrium, the equilibrium between the neutral and cationic MG also need to be considered and the pH-adjusted *Langmuir* model was derived as described in chapter 3.3.3. In this case, a nonlinear least-square fitting of the adsorption isotherm will allow the determination of N_{\max} and αK ,

where $\alpha = \frac{[H^+]}{K_a + [H^+]}$ reflects the pH effect on the adsorption. K can then be calculated at the given pH value (pH=7.0).

The above models are used to analyze adsorption isotherms of MG on MEL cells at acidic pH and neutral pH, respectively (Fig. 4.3). For our experiments, the bulk contribution of MEL cell to the SH signal is negligible, therefore, the theoretical model described in chapter 3.3.4 can be used to analyze the adsorption isotherms. The non-linear least square fits of $I_{SH}(C_D)$ are shown as the solid lines in Figure 4.3 and the maximum adsorption densities (in different units) as well as the free energy calculated from equilibrium constant are summarized in Table 4.1. The adsorption free energy for all three conditions turned out to be approximately same within error bar: $-(10.8 \pm 1.2)$ kcal·mol⁻¹ for MEL at acidic pH=4.5, $-(11.4 \pm 5.5)$ kcal·mol⁻¹ for MEL at neutral pH, and $-(10.6 \pm 1.8)$ kcal·mol⁻¹ for further differentiated MEL at acidic pH. On the other hand, the maximum adsorption number density varies according to the conditions applied (Table 4.1). And they are found to be quite different from the literature reported value of animal's red blood cell [16], which we will discuss more in the later section.

On the other hand, a neutral dye bromocresol purple (BCP) was also tested on MEL cell membrane. As is stated that, at acidic pH=4.5, BCP has a strong electronic transition around 430 nm, which is in resonance with the SH wavelength. It was demonstrated in an earlier study that adsorption of BCP on talc in water can be monitored by SHG experiments [41]. In our experiment, the same titration procedure for MG/MEL is also performed for BCP/MEL. However, there was no detectable SH signal as was

recorded in Fig. 4.4, which means that the neutral BCP molecules do not adsorb to the MEL cell surface.

4.4 Discussion

4.4.1. Driving Force of Molecular Adsorption is Charge-Charge Interaction

It has been long recognized that cell membrane surfaces always bear net negative charges. For red blood cells this negatively charged barrier has essential importance in preventing cell-cell coagulation during blood circulation. As is depicted in Fig. 4.5, it is the external, carbohydrate-rich structure that forms the net negatively charged barrier the glycocalyx layer. A glycocalyx is a general term for any network of polysaccharide or protein containing material extending outside of the cell. On the surface of cell membranes, all kinds of antigens with various charged groups can contribute to the surface charge. In case of red blood cell and MEL cell, it has been reported that the negative surface charge is primarily due to carboxyl group (COO^-) of sialic acids rather than the phosphate groups (PO_4^-) of phospholipids [15].

Both MG and BCP are hydrophobic dyes, which may interact with the cell surface through electrostatic and/or hydrophobic interactions. Our SH experiments have demonstrated that positively charged MG adsorbs to the MEL cell while neutral BCP does not. Given the MEL cell membrane surface structure, the contrast observation of MG and BCP interaction with the MEL cell is an obvious demonstration that the dominating driving force of molecular adsorption at the MEL cell surface is charge-charge interaction between the negatively charged cell surface and the positive MG ion.

Hydrophobic interactions appear insufficient to maintain adsorption of a medium size molecule like BCP.

The adsorption free energy of MG on MEL cell quantitatively determined from the analysis of adsorption isotherms is consistent within errors for all three experimental conditions: $-(10.8 \pm 1.2) \text{ kcal} \cdot \text{mol}^{-1}$ for MEL at acidic pH=4.5, $-(11.4 \pm 5.5) \text{ kcal} \cdot \text{mol}^{-1}$ for MEL at neutral pH, and $-(10.6 \pm 1.8) \text{ kcal} \cdot \text{mol}^{-1}$ for further differentiated MEL at acidic pH, which indicates that the adsorption sites on the MEL cell membrane does not change even though the environmental conditions or the cell morphological change.

In a separate study (results shown in next chapter), we have characterized MG interaction with polystyrene PSC particles with surface termination of carboxyl groups [42]. Since the PSC particle has only one type of charged groups, carboxyl groups (COO^-), on surface, the adsorption free energy determined reflects the interaction between MG and carboxyl group only. The adsorption free energy was determined to be: $-(10.7 \pm 0.1) \text{ kcal} \cdot \text{mol}^{-1}$ [42], which agrees very well with those obtained for MG on MEL cells. This agreement further confirmed that charge-charge interactions between the positive dye and the negatively charged carboxyl group (COO^-) of sialic acids rather than any other negatively charged groups presented close to the cell surface are the driving force for molecular adsorption at MEL cell membrane surface. This deduction is consistent with the well recognized fact that the net negative charge of red blood cell is mostly composed of carboxyl group (COO^-) of sialic acids [15].

4.4.2. Adsorption Characteristics

As is demonstrated that the adsorption sites on MEL cell membrane surface are carboxyl groups (COO^-) of sialic acids, the maximum adsorption density should equal to the number density of carboxyl groups (COO^-) on the MEL surface. The number of carboxyl groups (COO^-) on human red blood cell and many other types of animal red blood cells were determined in an early study [16]. The literature recorded carboxyl group (COO^-) density of human red blood cell was $(3.2 \pm 0.3) \times 10^7 \text{ cell}^{-1}$ while those of other animal blood cells were determined to be at the order of $\sim 10^6/\text{cell}$. However, our experimental results: $(1.4 \pm 0.5) \times 10^9 \text{ cell}^{-1}$ for MEL at acidic pH=4.5, $(1.4 \pm 0.9) \times 10^{10} \text{ cell}^{-1}$ for MEL at neutral pH, and $(5.2 \pm 1.9) \times 10^9 \text{ cell}^{-1}$ for further differentiated MEL at acidic pH, are much higher than the literature results. We attribute this to the larger precursor-stage size of MEL cell than a mature red blood cell. It has been reported that erythrocyte experiences about ten times size reduction down the differentiate pathway [3]. Therefore, a hundred times reduction in cell surface area is expected from the immature stage MEL cell to its fully differentiated red blood cell, which explains the difference in the maximum adsorption density of MEL cell and red blood cell.

The pH value is a factor which is suggested to have essential effect on the cell surface characteristics. Comparing the adsorption characteristics under acidic and neutral pH, the adsorption free energy stayed almost the same within errors. This indicates the type of adsorption sites is still carboxyl group (COO^-). On the other hand, the adsorption number density is about ten times higher for neutral pH ($(4.6 \pm 2.9) \times 10^7 \mu\text{m}^{-2}$) than for acidic pH ($(4.6 \pm 1.7) \times 10^6 \mu\text{m}^{-2}$). This difference is due to the pH dependence of the equilibrium between charged and neutral form of the carboxyl groups. Studies on PSC

particles show that, at acidic pH (pH=4.5), only a small fraction (~8%) of carboxyl groups exists in its negatively charged form while at neutral pH, the negatively charged form dominates (94%)(Fig. 4.6). Calculations were based on the literature reported pKa value (5.7 ± 0.1) of carboxylated polystyrene [43].

MEL cells incubated w/ 1% DMSO for 4 days to a further differentiated state with appearance of hemoglobin but no notable size change, was also tested in order to demonstrate that the cell surface do not have distinct changes during the differentiation process. The adsorption characteristics (Table 4.1) show that the adsorption free energy remains the same while the maximum adsorption density slightly increases for the further differentiated MEL cell, which indicates that the cells grown more compact during the differentiation.

The adsorption free energy for MEL cell together with those results from other polymeric particle [42, 44] and liposome surfaces [34] are listed in Table 4.2. The results show that the adsorption free energy of MEL cell agrees very well with that of the PSC and falls in between that of the liposome and polystyrene PSS terminated with sulfate groups, which reflects that the binding with sulfate group (SO^{3-}) on PSS surface is the strongest (-12.7 ± 0.2 kcal/mol), followed by that with carboxyl group (COO^-) on MEL cell and PSC surface (-10.8 ± 1.2 kcal/mol and -10.7 ± 0.1 kcal/mol), and the binding with the phosphate group (PO^{4-}) on liposome surface is the least (-8.6 ± 0.2 kcal/mol). The results are in excellent agreement with our general understanding of the strengths of charge-charge interactions. For biomembranes, although there are many kinds of surface antigens, each of which occurs in various combinations that differ in constituents, branching, and charge density, our understanding of the collective behavior of the

complexity can be done by characterization of molecular interaction with the cell membrane surface.

4.4.3. Adsorbed Hydrophobic Ions Do Not Transport across MEL Cell Membrane

As is recorded in the time profile after addition of MG into the MEL cell suspension (Fig. 4.1), a rise in the SH signal was observed which is attributed to the adsorption of MG onto the MEL cell surface. It has been reported in the liposome study by Eisinger and coworkers [32] as well as in our *e.coli* study [30] that the transport of MG across membranes would result in the decay of SH signal. In the MEL cell experiments, no signal decay was observed following the initial rise, which indicates that MG adsorbed to the MEL cell surface do not penetrate the cell membrane. This observation is not unexpected if we consider the structure and permeability characteristics of the MEL cell membrane (Fig. 4.5). Due to the structure simplicity, ion channels and transport processes of nutritious ions and metabolites throughout the red blood cell membrane have been well characterized. The well-known Ca^{2+} -activated K^+ channel (Gardos channel) is highly selective of K^+ over Na^+ if Ca^{2+} is present at the intracellular face of the channel [45]. The non-selective cation channel (NSC) is demonstrated to be permeable to the divalent cations Ca^{2+} and Ba^{2+} , and even Mg^{2+} , but no other larger ions has been known to transport through this channel [46]. Intuitively, since MG is neither a nutritious ingredient nor a product from cellular metabolism, it is understandable that there is no specific selective channel or carrier to mediate its transport and as a result, it is excluded from the cell as foreign. On the other hand, it can be inferred from our results that the passive diffusion through lipid bilayer region of MEL cell membrane is not an alternative pathway for MG. Unlike the small, uncharged, lipid-

soluble gas molecules which have long been assumed to be the favorite uptake of the red blood cell membrane [47], MG is positively charged, not as small in size, therefore if the lateral interaction between the lipid molecules are strong enough which is most likely the case for red blood cells, the partition into the lipid bilayer region would become difficult.

4.5 Summary

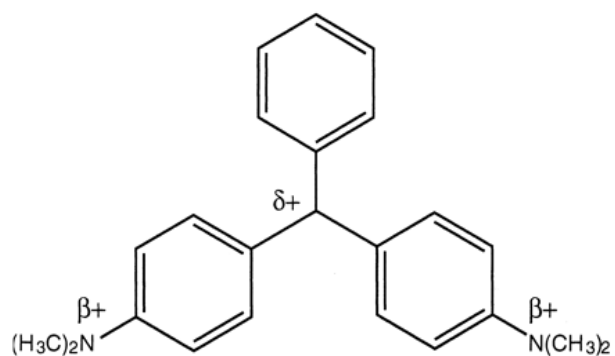
In this chapter, we use the nonlinear optical technique Second Harmonic Generation to probe molecular interactions at a eukaryotic cell – Murine Erythroleukemia cell membrane. The adsorption of a medium size hydrophobic ion malachite green onto the MEL cell surface was observed and the adsorption characteristics were determined using the modified *Langmuir* model. On the other hand, it was observed that the neutral hydrophobic molecule bromocresol purple (BCP) did not adsorb to the net negatively charged MEL cell surface, which implies the insufficiency of hydrophobic interactions to maintain adsorption of medium size molecules at MEL surface.

The results indicate that electrostatic interactions between the positively charged MG ions and the negatively charged carboxyl group (COO^-) of sialic acids are the driving force for MG adsorption at MEL cell surface. Furthermore, the observations, together with other literature reported adsorption studies, confirmed that the relative strength of interactions of MG cation with various negatively charged functional groups agrees very well with our general understanding of the strengths of charge-charge interactions: the binding with sulfate group (SO_4^{2-}) on PSS surface is the strongest, followed by that with carboxyl group (COO^-) on MEL cell and PSC surface, and the binding with the phosphate group (PO_4^{3-}) on liposome surface is the least. Based on both quantitative

results determined for further differentiated MEL cell line: the MG adsorption coverage and the adsorption free energy, it can be further inferred that the surface characteristics of MEL cell and it's fully differentiated mature stage-- red blood cell are similar.

Observations also showed that there was no further permeation of the surface adsorbed MG through the MEL cell membrane, though hydrophobic MG ions are often ready to partition into and transport through the lipid bilayer structures. For the MEL cell membrane, it is highly suggested that the lateral interactions between the lipid molecules are strong enough to exclude medium size MG ions. Also, if we consider that the primary function of the RBC is respiration, it is not unexpected that the physiological structure of the membrane only favors the transport of small, uncharged, lipid soluble gas molecules and no specific selective channels or carriers are present in the MEL cell membrane to mediate the transport of hydrophobic ions.

(a)



(b)

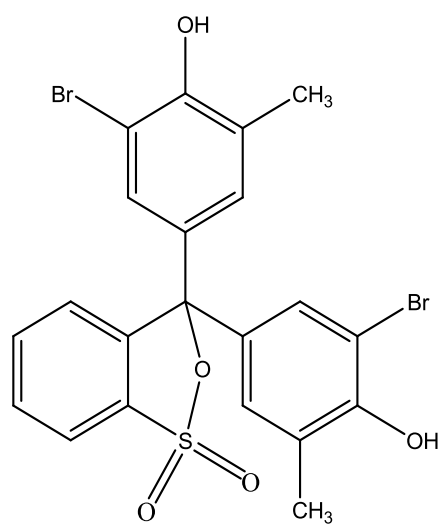


Figure 4.1 Molecular Structures of (a) Malachite Green (MG); (b) Bromocresol Purple (BCP)

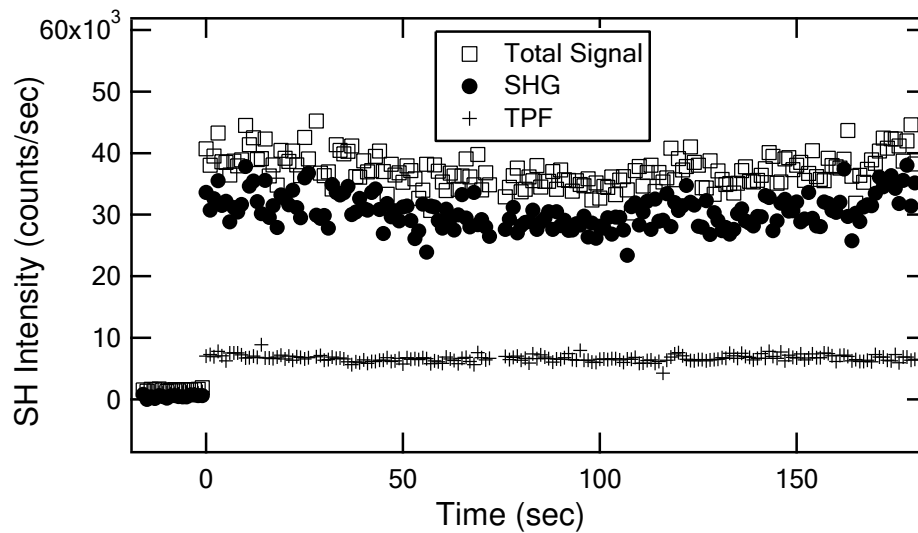
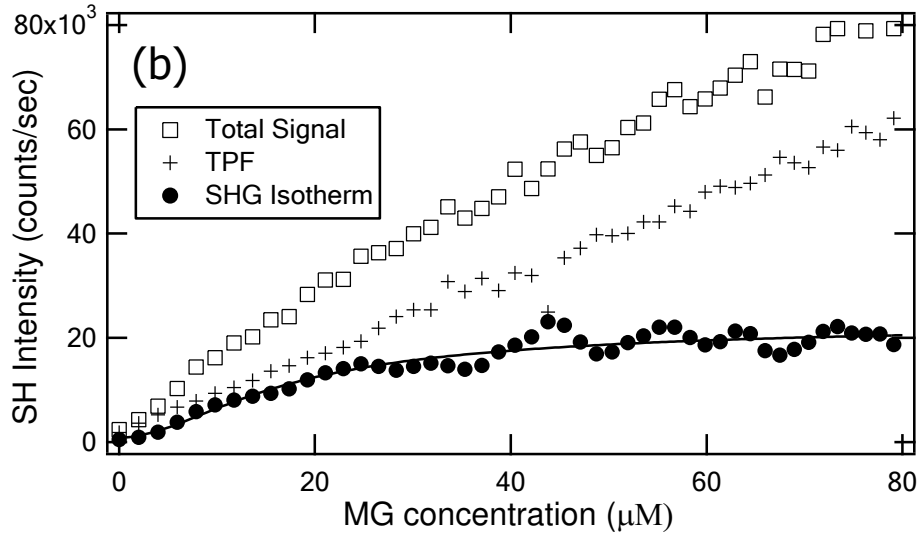
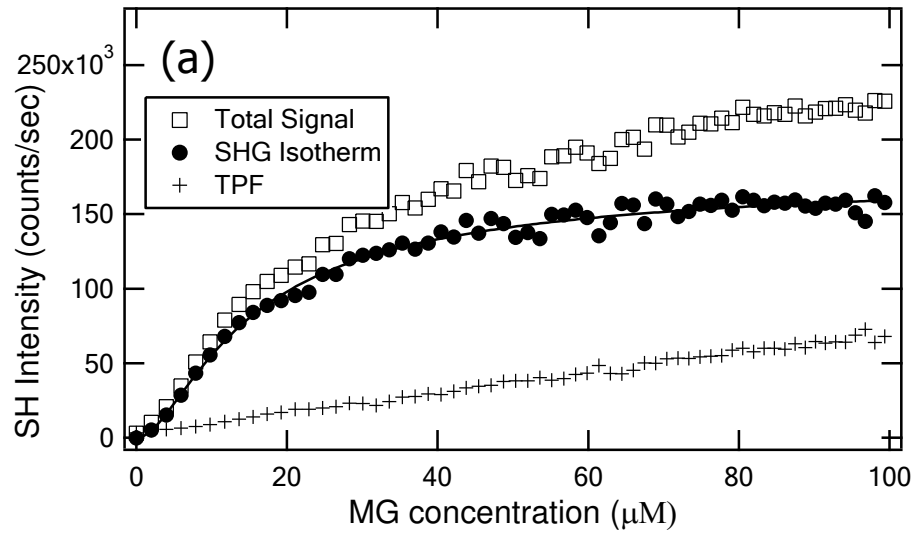


Figure 4.2: SHG signal detected as a function of time following addition of MG ions into the MEL cell solution at neutral pH. Squares (\square) represent the total intensity, crosses (+) the TPF intensity, and filled circles (\bullet) the SHG intensity.



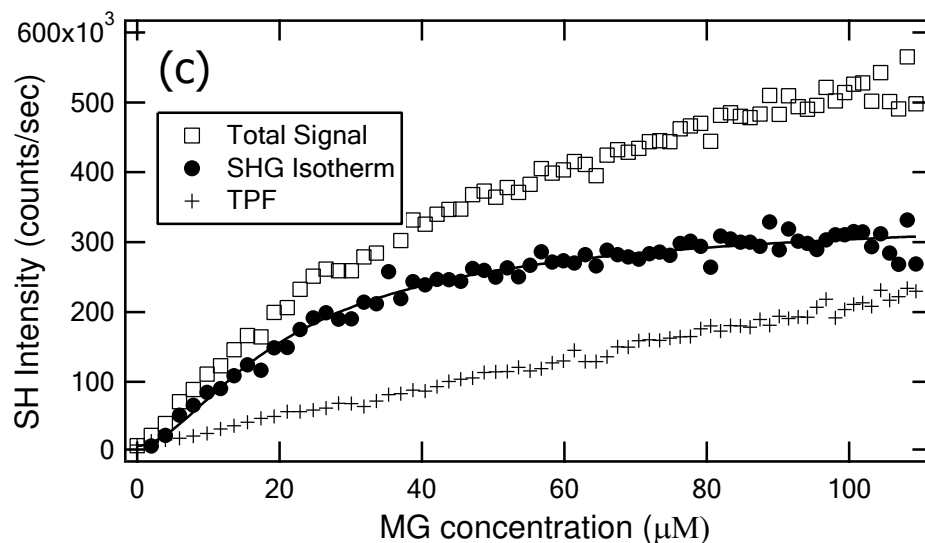


Figure 4.3: Adsorption isotherms expressed in SH intensity for MG adsorbed on MEL cell membrane surface at different conditions: (a) acidic pH value (pH=4.5); (b) neutral pH value (pH=7.0); (c) MEL cell at a further differentiated stage. Squares (\square) represent the total intensity, crosses ($+$) the TPF intensity, and filled circles (\bullet) the SHG intensity. The solid lines are nonlinear least-square fits of the modified *Langmuir* model.

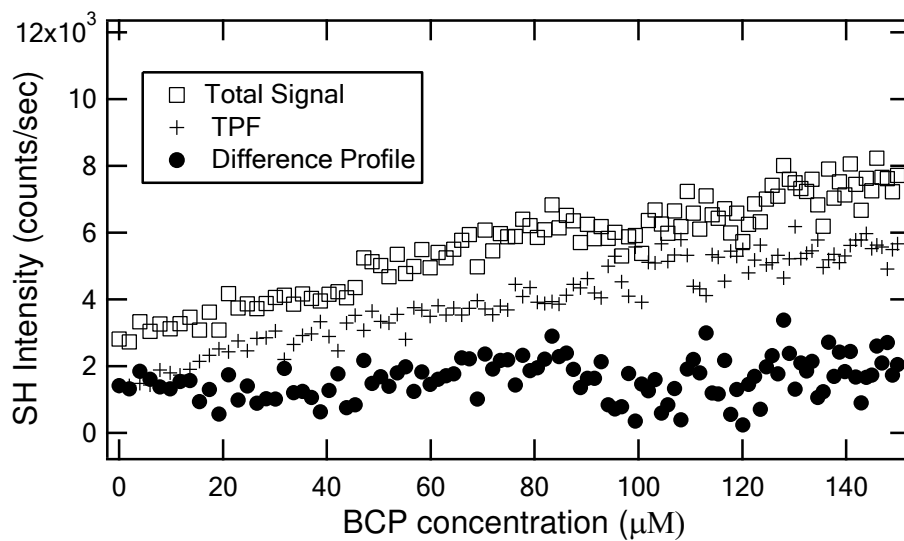


Figure 4.4: SH signal detected with increasing BCP concentration added into a solution containing MEL cells at acidic pH value (pH=4.5). Squares (\square) represent the total intensity, crosses (+) the TPF intensity, and filled circles (\bullet) the SHG intensity.

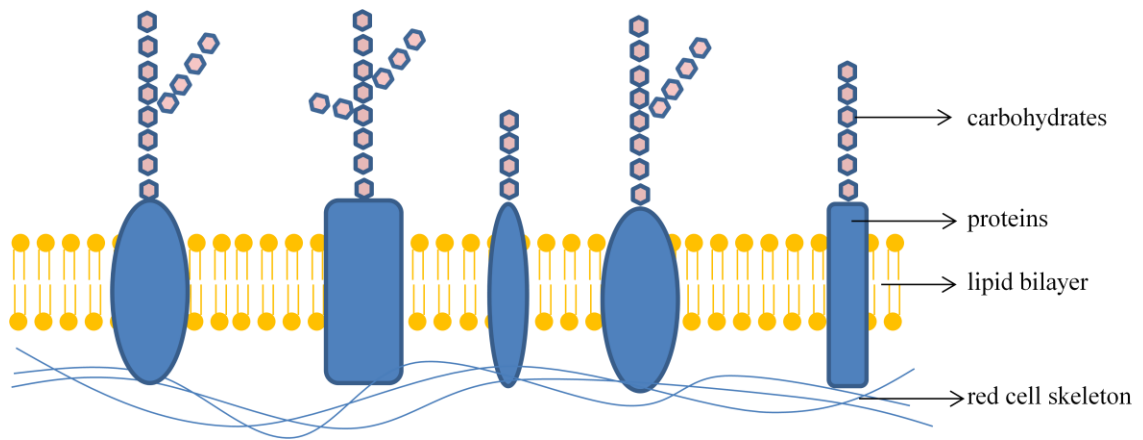


Figure 4.5: Illustration of the MEL cell membrane structure

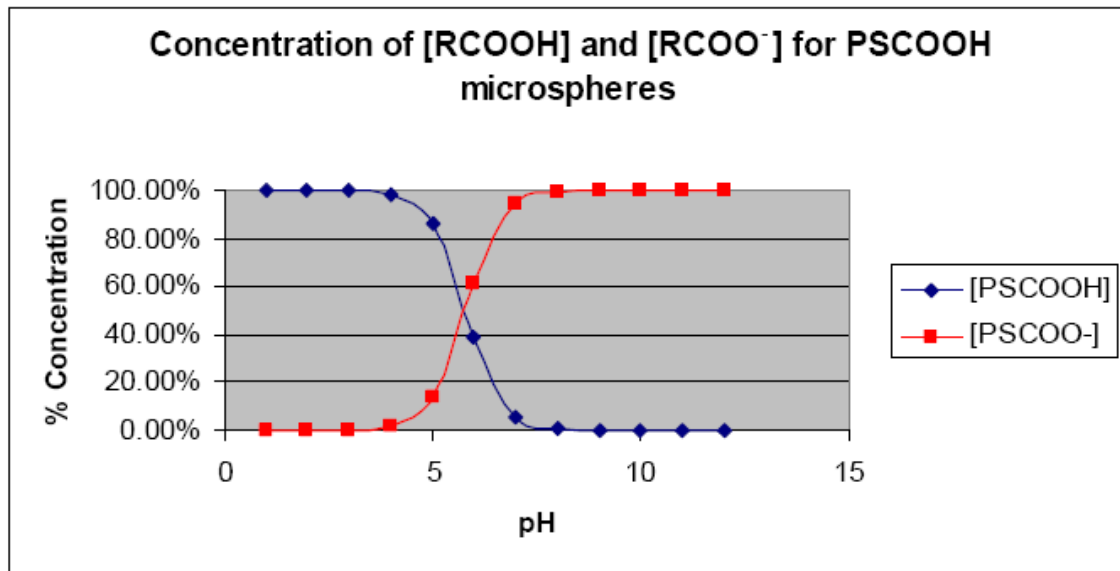


Figure 4.6 pH dependence of [COOH] and [COO⁻] of polystyrene carboxyl microspheres in water

Table 4.1: Adsorption Characteristics of MG on MEL cell under Different Conditions

	MEL Acidic pH=4.5	MEL Neutral pH	Further Differentiated MEL (Acidic pH=4.5)
N_{max} (μM)	5.3±2.0	9.7±6.3	9.6±3.5
Cell Density (mL⁻¹)	2.3×10 ⁶	4.2×10 ⁵	1.1×10 ⁶
N_{max} (cell⁻¹)	(1.4±0.5)×10 ⁹	(1.4±0.9)×10 ¹⁰	(5.2±1.9)×10 ⁹
N_{max} (μm⁻²)	(4.6±1.7)×10 ⁶	(4.6±2.9)×10 ⁷	(1.7±0.6)×10 ⁷
K (M⁻¹)	(9.8±1.1)×10 ⁷	(2.7±1.2)×10 ⁸	(7.7±1.3)×10 ⁷
-ΔG (kcal mol⁻¹)	10.8±1.2	11.4±5.5	10.6±1.8

Table 4.2: Adsorption Free Energy of MG on Polymeric Particles, Liposome and MEL Cell

	MEL	PSC[42]	PSS[44]	Liposome[48]
K (M⁻¹)	$(9.8 \pm 1.1) \times 10^7$	$(7.8 \pm 0.1) \times 10^7$	$(2.4 \pm 0.2) \times 10^9$	$(2.4 \pm 0.7) \times 10^6$
-ΔG (kcal/mol)	10.8±1.2	10.6±0.1	12.7±0.2	8.6±0.2

Bibliography

1. Harrison, P.R., *Analysis of erythropoiesis at molecular level*. Nature, 1976. **262**(5567): p. 353-356.
2. Marks, P.A. and R.A. Rifkind, *Erythroleukemic differentiation* Annu. Rev. Biochem., 1978. **47**: p. 419-448.
3. Tsiftoglou, A.S. and W. Wong, *Molecular and cellular mechanisms of leukemic hematopoietic-cell differentiation - an analysis of the Friend system*. Anticancer Res., 1985. **5**(1): p. 81-99.
4. Agre, P. and J.C. Parker, eds. *Red Blood Cell Membranes: Structure, Function, Clinical Implications*. 1989, Marcel Dekker, Inc.: New York.
5. Jensen, F.B., *Red blood cell pH, the Bohr effect, and other oxygenation-linked phenomena in blood O₂ and CO₂ transport*. Acta Physiol. Scand., 2004. **182**(3): p. 215-227.
6. Sonveaux, P., et al., *Transport and peripheral bioactivities of nitrogen oxides carried by red blood cell hemoglobin: role in oxygen delivery*. Physiology, 2007. **22**: p. 97-112.
7. Cabantchik, Z.I., P.A. Knauf, and A. Rothstein, *Anion transport-system of red blood-cell -- role of membrane protein evaluated by use of probes*. Biochimica Et Biophysica Acta, 1978. **515**(3): p. 239-302.
8. Passow, H., *Molecular aspects of Band-3 protein-mediated anion transport across the red-blood-cell membrane*. Rev. Physiol. Biochem. Pharmacol., 1986. **103**: p. 61-203.

9. Roufogalis, B.D., *Regulation of calcium translocation across the red-blood-cell membrane*. Can. J. Physiol. Pharmacol., 1979. **57**(12): p. 1331-1349.
10. Gatto, C. and M. Milanick, *Red blood cell Na pump: Insights from species differences*. Blood Cells Mol. Dis., 2009. **42**(3): p. 192-200.
11. Telen, M.J., *Erythrocyte blood-group antigens - not so simple after all*. Blood, 1995. **85**(2): p. 299-306.
12. Reid, M.E. and N. Mohandas, *Red blood cell blood group antigens: structure and function*. Semin. Hematol., 2004. **41**(2): p. 93-117.
13. Foa, C., et al., *Steric stabilization and cell adhesion*. J. Mater. Sci.-Mater. Med., 1996. **7**(3): p. 141-148.
14. Elbert, D.L. and J.A. Hubbell, *Self-assembly and steric stabilization at heterogeneous, biological surfaces using adsorbing block copolymers*. Chem. Biol., 1998. **5**(3): p. 177-183.
15. Cook, G.M.W., G.V.F. Seaman, and D.H. Heard, *Sialic acids and electrokinetic charge of human erythrocyte* Nature, 1961. **191**(478): p. 44-&.
16. Eylar, E.H., et al., *Contribution of sialic acid to surface charge of erythrocyte*. J. Biol. Chem., 1962. **237**(6): p. 1992-&.
17. Nishiguchi, E., K. Okubo, and S. Nakamura, *Adhesion of human red blood cells and surface charge of the membrane*. Cell Struct. Funct., 1998. **23**(3): p. 143-152.
18. Chambers, E. and S. Mitragotri, *Prolonged circulation of large polymeric nanoparticles by non-covalent adsorption on erythrocytes*. J. Control. Release, 2004. **100**(1): p. 111-119.

19. Chambers, E. and S. Mitragotri, *Long circulating nanoparticles via adhesion on red blood cells: mechanism and extended circulation*. *Exp. Biol. Med.*, 2007. **232**(7): p. 958-966.
20. Ermakov, Y.A., et al., *Dipole potentials indicate restructuring of the membrane interface induced by gadolinium and beryllium ions*. *Biophys. J.*, 2001. **80**(4): p. 1851-1862.
21. Mosior, M. and S. McLaughlin, *Peptides that mimic the pseudosubstrate region of protein-kinase-C bind to acidic lipids in membranes*. *Biophys. J.*, 1991. **60**(1): p. 149-159.
22. Casals, C., E. Miguel, and J. Perezgil, *Tryptophan fluorescence study on the interaction of pulmonary surfactant protein-A with phospholipid-vesicles*. *Biochem. J.*, 1993. **296**: p. 585-593.
23. Murray, D., et al., *Electrostatic properties of membranes containing acidic lipids and adsorbed basic peptides: theory and experiment*. *Biophys. J.*, 1999. **77**(6): p. 3176-3188.
24. Aisenbrey, C., B. Bechinger, and G. Grobner, *Macromolecular crowding at membrane interfaces: adsorption and alignment of membrane peptides*. *J. Mol. Biol.*, 2008. **375**(2): p. 376-385.
25. Wei, Y. and R.A. Latour, *Benchmark experimental data set and assessment of adsorption free energy for peptide-surface interactions*. *Langmuir*, 2009. **25**(10): p. 5637-5646.

26. Schwieger, C. and A. Blume, *Interaction of poly(L-lysines) with negatively charged membranes: an FT-IR and DSC study*. Eur. Biophys. J. Biophys. Lett., 2007. **36**(4-5): p. 437-450.
27. Glasmastar, K., et al., *Protein adsorption on supported phospholipid bilayers*. J. Colloid Interface Sci., 2002. **246**(1): p. 40-47.
28. Denisov, G., et al., *Binding of basic peptides to membranes produces lateral domains enriched in the acidic lipids phosphatidylserine and phosphatidylinositol 4,5-bisphosphate: an electrostatic model and experimental results*. Biophys. J., 1998. **74**(2): p. 731-744.
29. Kim, J.Y., et al., *Binding of peptides with basic residues to membranes containing acidic phospholipids*. Biophys. J., 1991. **60**(1): p. 135-148.
30. Zeng, J., H.M. Eckenrode, and H.-L. Dai, *Time-Resolved Molecular Transport across Living Cell Membranes*. Nat. Methods, Submitted.
31. Wang, H., et al., *Second harmonic generation from the surface of centrosymmetric particles in bulk solution*. Chem. Phys. Lett., 1996. **259**(1-2): p. 15-20.
32. Srivastava, A. and K.B. Eisenthal, *Kinetics of molecular transport across a liposome bilayer*. Chem. Phys. Lett., 1998. **292**(3): p. 345-351.
33. Yan, E.C.Y. and K.B. Eisenthal, *Effect of cholesterol on molecular transport of organic cations across liposome bilayers probed by second harmonic generation*. Biophys. J., 2000. **79**(2): p. 898-903.
34. Liu, Y., et al., *Surface potential of charged liposomes determined by second harmonic generation*. Langmuir, 2001. **17**(7): p. 2063-2066.

35. Shang, X.M., et al., *Effects of counterions on molecular transport across liposome bilayer: probed by second harmonic generation*. J. Phys. Chem. B, 2001. **105**(51): p. 12816-12822.
36. Liu, J., et al., *Antibiotic assisted molecular ion transport across a membrane in real time*. Faraday Discuss., 2005. **129**: p. 291-299.
37. Liu, J., et al., *Second Harmonic Studies of Ions Crossing Liposome Membranes in Real Time*. J. Phys. Chem. B, 2008. **112**(48): p. 15263-15266.
38. Jiang, J., K.B. Eisenthal, and R. Yuste, *Second harmonic generation in neurons: electro-optic mechanism of membrane potential sensitivity*. Biophys. J., 2007. **93**(5): p. L26-L28.
39. Volloch, V. and D. Housman, *Terminal differentiation of murine erythroleukemia-cells - physical stabilization of end-stage cells*. J. Cell Biol., 1982. **93**(2): p. 390-394.
40. Green, F.J., *The Sigma-Aldrich Handbook of Stains, Dyes and Indicators*. 1990, Milwaukee, WI: Aldrich Chemical Co., Inc.
41. Wang, H.F., et al., *In situ, nonlinear optical probe of surfactant adsorption on the surface of microparticles in colloids*. Langmuir, 2000. **16**(6): p. 2475-2481.
42. Zeng, J. and H.-L. Dai, *Effect of solvent ionic strength and ion specificity on molecular interactions at neutral surface in aqueous colloids*. to be submitted.
43. Bastosgonzalez, D., et al., *Carboxylated latexes for covalent coupling antibodies*. I. J. Colloid Interface Sci., 1995. **176**(1): p. 232-239.

44. Zeng, J. and H.-L. Dai, *Effect of solvent ionic strength and ion specificity on molecular interactions at negatively charged surface in aqueous colloids*. to be submitted.
45. Maher, A.D. and P.W. Kuchel, *The Gardos channel: a review of the Ca²⁺-activated K⁺ channel in human erythrocytes*. *Int. J. Biochem. Cell Biol.*, 2003. **35**(8): p. 1182-1197.
46. Kaestner, L. and I. Bernhardt, *Ion channels in the human red blood cell membrane: their further investigation and physiological relevance*. *Bioelectrochemistry*, 2002: p. 71-74.
47. Jensen, F.B., *Red cell transport of anions (Cl⁻, HCO₃⁻ and NO₂⁻) and functions in blood transport of gases (O₂, CO₂ and NO)*. *Comp. Biochem. Phys. A*, 2005. **141**(3): p. S98-S98.
48. Liu, Y., E.C.Y. Yan, and K.B. Eisenthal, *Effects of bilayer surface charge density on molecular adsorption and transport across liposome bilayers*. *Biophys. J.*, 2001. **80**(2): p. 1004-1012.

CHAPTER FIVE

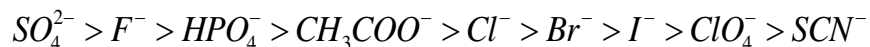
EFFECTS OF SOLVENT IONIC STRENGTH AND ION SPECIFICITY ON MOLECULE-SURFACE INTERACTIONS IN AQUEOUS COLLOIDS

5.1 Introduction

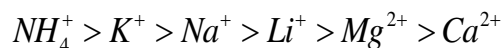
The interfacial phenomena in colloid, polymer, and bioscience depend greatly on the specific identity and concentration of the solvent salt ion presented. It has been well recognized that the interfacial association with various molecules are governed by a complex interplay of electrostatic and hydrophobic interactions. Many recent investigations have focused on characterizing the nature of the molecule-surface interactions [1-4] or the direct interactions of salt ions with the colloid/aqueous interface [5, 6]. However, in real-life environments, the two types of interactions usually intertwine with each other and can never be separated as independent processes. And in most interfacial phenomena related applications, it would be more straightforward to change the external solvent conditions rather than to modify the surface properties by changing surface structures. Therefore, it is important to understand the fundamental principles of

how the solvent ionic strength and ion specificity influence the interfacial interactions on various surfaces.

The specific ion effects on the physical behavior of a wide variety of aqueous colloidal processes exhibit a reoccurring trend first noted by Hofmeister and coworkers [7]. The typical order for the anion series is:



The species on the left side of the series salt out (precipitate) solutes, while those on the right side salt in (dissolve or denature) solutes. Analogous series, though less pronounced, can be constructed for cations:



The phenomena are over a century old and have traditionally been attributed to the influence of the salt ions on the structure of bulk water. Recent research popularity has cast doubt on the bulk water structure concept and brought up new hypothesis that direct ion interactions with surfaces and influences on hydrophobic interactions are largely responsible for most aspects of the phenomena [5, 6]. As is treated as interfacial phenomena, a lot of recent studies have been performed to test and support the new theory of direct ion-surface interactions. Spectroscopic pump-probe technique [8-10] has been applied to probe the O-H stretch mode of water and demonstrated ions had no influence on the dynamics of bulk water. Thermodynamic studies [11, 12] also disproved the change in bulk water structure. Further probe of the interfacial water structures with the vibrational sum frequency spectroscopy (VSFS) technique [13] revealed that it is the direct interaction with surface rather than indirect influence via changes in water structure

that are responsible for the ion related phenomena. However, the experiments and simulations are mostly conducted on air/water interfaces [14-18] rather than on aqueous colloidal surfaces. And problems addressed are focused on how the interfacial water structures been changed rather than how the interactions between the molecule and colloidal surface been affected. The old concept is receiving destructive challenge, while on the other hand, a variety of observations have been reported without a clear organizing constructive principle.

We report in this chapter the application of Second Harmonic Generation (SHG), to the investigation of solvent salt ion effects on molecule-surface interactions in an aqueous colloidal environment. The SHG technique is capable of quantitative, in situ characterization of molecule-surface interactions at the solid-liquid interfaces and can be used to investigate the salt ion effects on interfacial interactions occurring on buried surfaces in colloids. The lack of inversion symmetry at the surface of a centrosymmetric medium enables SHG probe of the buried surfaces of the micrometer or submicrometer particles in aqueous colloids.

Eisenthal and coworkers [19] first demonstrated that a significant SHG signal can be detected from the surface of micro-sized centrosymmetric particles upon adsorption of the molecules with optical transition in resonance with the second harmonic frequency. SHG has been used to characterize molecular adsorption in a full scope of colloidal systems, including polymer particles [4, 20-22], nanoparticles [23-26], carbon black particles [27], emulsions [20, 28, 29], and living cells [30, 31]. Versatile applications of SHG technique also include direct measurements of surface electric potential [29, 32] and transmembrane kinetics of microemulsion [20, 29], liposome vesicle surfaces [33-38] as

well as living cell membranes [30]. In our previous studies, a liquid jet sample circulation system was employed in order to make continuous in situ measurements of the particle surface adsorption processes and the complete adsorption isotherm can be recorded in a relatively short time [4, 21, 22]. Dai and coworkers also developed a displacement method so that the adsorption of molecules without large second order polarizability can be detected through competitive adsorption with dye molecules [21]. SHG studies of specific ion effects on air/aqueous salt solution interfaces [39-41] as well as solvent salt ion effects in colloidal systems [32, 36] have also been reported. However, a potential induced contribution to SHG is required and in order to achieve detection of the potential induced SHG signal, the colloidal surfaces have to bear charges while adsorbates with larger second order polarizability have to be avoided. The focus was mainly on polarized bulk water molecules by surface charges. Ions were applied only to create large surface potential in order to induce detectable SHG signal rather than to play a role in the molecule-surface interactions. As is described, the SHG studies on colloids involving solvent salt ions has been limited to the electrostatic forces dominating system with charged surfaces and Gouy-Chapman model has been extensively used to describe the dependence of surface potential of the electric double layer on the bulk salt concentration while ion specificity influence on and the ion effects on molecule-surface interactions remain unexploited.

We choose to probe the ion effects on the well characterized surface interactions between the polystyrene microparticles and the cationic dye malachite green (MG). Polystyrene with charged “head groups” are hydrophobic in nature while MG is hydrophobic dye with positive charge. As a cationic hydrophobic molecule, both

electrostatic and hydrophobic interactions can serve as driving force for MG's adsorption to colloids, depending on the surface composition. In our previous studies, the adsorption free energies and the densities of malachite green on polystyrene surfaces with different charge composition have been measured and the nature of the interaction between an adsorbate and the colloidal surfaces has been identified: a charged hydrophobic molecule get attracted to an oppositely charged colloidal surface through electrostatic interaction while for a neutral surface, adsorption occurs based on hydrophobic interaction [4]. Not only are the attractive forces between the surface and adsorbate are important, but also their interactions with the solvent is important as well. The solvent salt ion can affect the molecule-surface interactions in three ways: (1) changing the interfacial potential through electric double layer, (2) through association with surface either by attaching to head group or to hydrophobic region, (3) by solvating the adsorbate molecules both in the bulk and on the surface. Given the understanding of the nature of the molecule-surface interactions, we are now able to move one step further to investigate the solvent salt ion effects on the interactions.

In this chapter we will show that, the solvent salt ions will have great effects on the molecule-surface interactions occurring at colloids interfaces. The interactions dominated by electrostatic forces at polystyrene surface terminated with sulfate groups (PSS) are largely affected by the ionic strength of the solution but not sensitive to ion specificity while the interactions dominated by hydrophobic forces at polystyrene surface terminated with carboxyl groups (PSC) show pronounced dependence on ion specificity but less affected by ionic strength in the solution. Furthermore, we will show that how the ionic strength and ion specificity affect the adsorption free energy and maximum

adsorption number density of the electrostatic interactions as well as the hydrophobic interactions between the adsorbate molecule and colloidal surface. Both anionic and cationic series have been investigated and distinct effects have been identified.

5.2 Experiment

The experimental setup for characterization of solvent salt ion effects on molecule-surface interactions is similar to the setup for studying molecular adsorption at cell membrane surfaces, the details of which have been described in chapter 3.2. The sample was prepared in a flow/titration system. The sample solution was pumped with a small motorized liquid pump at the speed of about 200mL/min, to form a liquid jet through a nozzle made out of pressed stainless steel tubing with 1/16 in. inner diameter. The liquid sample in the reservoir, 250mL in total volume, was forced out and collected back through Nalgene tubing connected to the nozzle and was continuously stirred using a magnetic stirrer. The liquid sample volume in the circulation tubing was about 10mL or less, which was small enough compared to the total sample volume to prevent significant error of the concentration reading. The laser intercepted the center of the jet perpendicularly and passed through the jet with approximately 1mm path length. Instead of a steady cell, the flowing jet avoided SHG signals generated from the windows of the cell as well as accumulation and coagulation of particle/dye on the window walls. Aqueous solutions of dye/salt at known high concentrations were added into the aqueous colloid reservoir by a digital titrator akku-drive (Hirschmann Laboratory).

The colloids used in the experiments were monodispersed polystyrene microspheres (Molecular Probes, Inc.) with different functional groups: (1) polystyrene

sulfate microspheres (PSS) terminated with SO_3^- (diameter $1.05\pm 0.05\mu\text{m}$), (2) polystyrene carboxyl microspheres (PSC) terminated with COOH (diameter $1.12\pm 0.08\mu\text{m}$). Microspheres solutions were prepared with deionized water or salt solutions with known identity and concentrations. A small volume of colloidal stock solution (PSS with w/v concentration 8.2%, PSC with w/v concentration 4.1%) was used to reach a final concentration of $\sim 10^8$ particle/mL in a 250 mL reservoir. 0.01N HCl was added to adjust the pH of the solution to 3.5 ± 0.2 . Under this condition, PSS surface bearing SO_3^- (pKa ~ 2) was negatively charged while PSC surface bearing COOH (pKa ~ 5.8) was neutral. All experiments reported in this chapter were performed at pH 3.5 ± 0.2 .

Inorganic salt solutions for studying anion series were sodium iodide (NaI), sodium chloride (NaCl) and sodium sulfate (Na_2SO_4); while those for studying cation series were lithium chloride (LiCl), sodium chloride (NaCl), potassium chloride (KCl) and ammonium chloride (NH_4Cl). All salts were purchased from Fisher Scientific and used as received. Chloride series were prepared at 4M concentration for cationic titration experiments while sodium series were prepared at 2M concentrations for anionic titration experiments due to the relatively low solubility of sodium sulfate in water.

In a typical experiment, the colloidal surface was firstly covered by MG dye molecules and then titrated by aqueous salt solutions to monitor SHG signal change upon salt ion addition. Titration isotherms of MG dye on colloids under different ion identities and concentrations were then obtained by varying salts and salinities.

5.3 Standard *Langmuir* Adsorption Model

5.3.1 Standard *Langmuir* Adsorption Model

The modified *Langmuir* adsorption model has been described in chapter 3.3. The modified *Langmuir* model is actually the complete form of *Langmuir* model without further assumptions. It is more accurate only when there is substantial depletion of adsorbate molecules from the solution due to adsorption, which is usually the case for molecular adsorption to micro-surfaces, where the effective surface area is very large so that the surface density N can be comparable to C most of the time and cannot be neglected from the $(C-N)$ term in equation 3.2 of chapter 3.3. However, this is not always the case. A theoretical simulation of the modified *Langmuir* model with the adsorption equilibrium constant set to a small value ($5 \times 10^7 \text{M}^{-1}$) for different maximum surface adsorption densities ($1 \mu\text{M}$ and $5 \mu\text{M}$) is shown in Fig. 5.1. The simulation clearly demonstrated that when the adsorption equilibrium constant is small, an extremely large bulk concentration of molecules is needed to sustain a relatively small surface coverage; therefore, the surface density N depleted from the bulk solution due to adsorption is no longer comparable to C , i.e., $C \gg N$. The complete form of modified *Langmuir* model can no longer give reliable determination of N_{max} . Instead, the standard *Langmuir* form should be used. For the standard *Langmuir* model, the term $(C-N)$ is actually replaced by C . Thus equation 3.2 of chapter 3.3 becomes:

$$\frac{dN}{dt} = k_1 \frac{C}{55.5} (N_{\text{max}} - N) - k_{-1} N \quad (5.1)$$

And at equilibrium, the surface coverage θ is given as:

$$\theta = \frac{1}{1 + \frac{55.5}{KC}} \quad (5.2)$$

It should also be recognized that the intrinsic principle of the standard *Langmuir* model will not allow determination of N_{\max} . In order to meet the conditions of using modified *Langmuir* model for determination of N_{\max} , a simple way is to increase the concentration of the colloidal particles in the solution to achieve substantial depletion in the lower adsorbate concentration region. At the same time, we also need to consider that, in concentrated colloidal solutions, particles tend to coagulate and inter-particle interactions will come into play and can bring more complexity to the system. Therefore, colloidal solutions with high concentrations are not preferred in the experiments, and only smallest amount of colloids necessary for measurements should be used to make proper size of reservoir.

5.3.2 General Application of the Modified *Langmuir* Model by Global Fitting

As is described in the previous sections, both the complete form of modified *Langmuir* model and the simplified form of standard *Langmuir* model have limitations in applications. We prefer to use the complete form of *Langmuir* model to analyze the obtained experimental isotherms since it will allow the determination of maximum surface density as well as the adsorption free energy while the simplified standard *Langmuir* model can only provide the free energy information. In this section, we propose a practical analysis method that would allow general application of the modified *Langmuir* model without restrictions of sufficient depletion of molecules from bulk due to adsorption.

Illustrated in Fig. 5.2 are the theoretical simulations of the modified *Langmuir* isotherms expressed in SH intensity as a function of molecule concentration. Fig. 5.2(a) represents isotherms at a fixed value of adsorption equilibrium constant ($K = 10^{10}$) by varying maximum adsorption density while Fig. 5.2(b) represents isotherms at a fixed value of maximum adsorption density ($N_{\max} = 0.2\mu M$) by varying adsorption equilibrium constant. As is shown by Fig.5.2 (a), the “S” shape of the adsorption isotherm is clearer when the maximum adsorption density is larger and therefore, the determination of N_{\max} is more reliable. On the other hand, if the maximum adsorption density is relatively small as is used in the simulations in Fig.5.2 (b), it is not possible to obtain isotherm curves with clear “S” shape by changing the value of adsorption equilibrium constant and therefore, the determined N_{\max} is less reliable, usually with high error bars.

Given a colloidal system and a specific molecule as adsorbate, the adsorption equilibrium constant is the system’s intrinsic characteristic that cannot be changed. However, the maximum adsorption density as an ensemble total can be monitored by changing the total concentration of colloidal particle applied. However, as was discussed in the previous section, increasing the colloidal concentration can increase the depletion of molecules from bulk at the lower molecule concentration region but may have undesired side-effects if the particle concentration is too high. Here we propose to improve the analysis by monitoring a set of adsorption isotherms, with fixed ratio of adsorption number densities. The analysis software Igor Pro provides the so called Global Fitting function which allows the fitting of a group of curves sharing global fitting parameters. Figure 5.3 is an example of analyzing a set of adsorption isotherms of malachite green

(MG) molecules on polystyrene sulfate (PSS) surface (the detailed description of the experiments and materials has been elaborated in chapter 3.2) with a fixed ratio of PSS concentrations: 1:2:4:8. The global fitting results are compared to the individual fitting results listed in Table 5.1. The results did confirm that the global fitting gives more reliable adsorption characteristics while the individual fitting clearly suffers from a concentration effect.

5.4 Results and Discussion:

5.4.1 Adsorption of MG on PSS/PSC Surfaces without Solvent Salts

Before the ion effects are investigated, the adsorption isotherms of the dye molecules on the model polystyrene particle surfaces in aqueous solution without applying salts need to be established first. The adsorption isotherms, expressed in the form of SH intensity as a function of MG concentration, of PSS and PSC particle surfaces at pH= 3.5±0.2 were measured (Fig. 5.4).

The adsorption isotherm of MG at PSS surface was analyzed using the modified *Langmuir* model described in chapter 3.3. For negatively charged PSS surface, N_{\max} and K are determined to be $(1.60 \pm 0.02) \times 10^5 \mu\text{m}^{-2}$ and $(5.59 \pm 0.65) \times 10^9 \text{M}^{-1}$, respectively. The adsorption free energy ΔG , calculated from the equilibrium constant K using $\Delta G = -RT \ln K$, is 13.16 ± 0.06 kcal/mol.

As is observed, the curve shape of the adsorption isotherm of PSC is quite different from that of the PSS: less “S” shape is obtained in the lower concentration region and much higher bulk dye concentration is needed to saturate the PSC surface.

The seemingly slight difference of the isotherm curves actually requires quite different analysis model.

As is shown in Fig. 5.4 (b), the isotherm curve of PSC showed obscure “S” shape in the lower concentration region and a substantial amount of MG was required to reach saturation, which imply small adsorption equilibrium constant for MG adsorption at PSC surface and a relatively small maximum adsorption density on PSC surface. In this case, there was not sufficient depletion from the bulk due to adsorption; therefore, the standard *Langmuir* form described in chapter 5.3 should be used.

A nonlinear least-square fit of $I_{SH}(C)$ yielded the equilibrium constant $K = (7.82 \pm 0.10) \times 10^7 \text{M}^{-1}$ which at 22°C corresponding to adsorption free energy of $10.66 \pm 0.14 \text{ kcal/mol}$, which is definitely much smaller than that of MG adsorption to PSS surface. The results in turn proved the validity of the use of standard *Langmuir* form to analyze the adsorption curve of PSC. It should also be recognized that the intrinsic principle of the standard *Langmuir* model will not allow determination of N_{\max} . In order to meet the conditions of using modified *Langmuir* model for determination of N_{\max} , a simple way is to increase the concentration of the colloidal particles in the solution to achieve substantial depletion in the lower dye concentration region. We did try to make measurements by employing higher concentrations of PSC particles; however, the depletion was still not sufficient to allow determination of N_{\max} by using modified *Langmuir* model. We also need to consider that, in concentrated colloidal solutions, particles tend to coagulate and inter-particle interactions will come into play and can bring more complexity to the system. Therefore, colloidal solutions with high

concentrations are not preferred in the experiments, and only smallest amount of colloids necessary for measurements should be used to make proper size of reservoir.

A large difference in magnitude of the free energies determined for MG adsorption to PSC and PSS surfaces has been observed, which is due to different dominating driving force for the molecular adsorption processes on the surfaces. For sulfate terminated PSS surface, it is well recognized that the adsorption is dominated by opposite charge attractive interaction [4], while for neutral carboxyl terminated PSC surface, we believe it is the hydrophobic (van der Waals) interaction between hydrophobic regions of dye and particle surface that contribute most to the adsorption, which results in a much smaller magnitude of free energy value.

5.4.2 Salt Ion Effects on MG Adsorption to Charged PSS Surface

With the adsorption process free of salts quantitatively characterized, we now investigate the salt ion effects on MG adsorption to charged PSS surface. Firstly, sufficient amount of MG dye ($1\mu\text{M}$ MG for 1.5×10^8 particles/mL PSS) was added to achieve a full coverage of PSS surface as the maximum adsorption density is known. An instantaneous shoot up of SH signal was recorded as a respond to surface saturation of dye. The dye covered colloids was then titrated with concentrated NaCl solution. The SH signal showed a continuous decay and leveled off as more NaCl was added to the reservoir. The titration profile of SHG intensity as a function of NaCl concentration was recorded (Fig. 5.5). In order to confirm that the observed decay process was caused by the addition of NaCl, a control experiment was performed by titrating with blank solution without NaCl, the profile of which is also shown in Fig. 5.5. Compared to the salt titration profile, the SH intensity of the control experiment did not show as prominent

decay. The hardly noticeable slight decay is attributed to coagulation of colloidal particles in the reservoir and was included in the correction of salt titration profiles.

As was illustrated in the last section, the SH signal is proportional to the dye coverage on the surface. Therefore, the decay of SH signal should be a direct reflection of decreasing surface density of adsorbed MG molecules. There are two possible mechanisms that may cause the decrease of MG density on surface: (1) an instinct thinking would be the displacement of the surface adsorbed MG by Na^+ ion, which should result in decreased dye coverage hence decreased SH response. Similar observation of surfactant/biopolymer titration of MG saturated polystyrene has been reported previously and successfully interpreted by the compete adsorption between MG molecules and surfactant/biopolymers [21, 22]. (2) The addition of NaCl may cause changes to the characteristics of the MG adsorption process, resulting in different free energy and maximum number density from those without addition of salt. In this way, we consider the intertwined influence of the salt ions on molecular adsorption rather than treating them as independent competing processes not affecting each other as is described in the displacement model. Further experiments have been done to determine between the above two models. MG adsorption isotherms on PSS surfaces at different NaCl concentrations were obtained and analyzed using modified *Langmuir* model (Fig. 5.6). Dependence of adsorption free energy ΔG and maximum density N_{max} on NaCl concentration was summarized in Table 5.2 and plotted in Fig. 5.7. Figure 5.7 shows that as the ionic strength of the solution increases, both adsorption free energy ΔG and maximum density N_{max} decrease, and level off when the ionic strength is sufficiently

high. Both models predict the decrease of maximum adsorption density N_{\max} , however, the dramatic change in ΔG (from $13.16 \pm 0.06 \text{ kcal/mol}$ to $11.82 \pm 0.05 \text{ kcal/mol}$) is obviously contradictory to the assumption of the displacement model that salt cations and MG compete to adsorb to the PSS surface without affecting each other's process. The observations, on the other hand, strongly supported the principles of the second model that salt ions will influence the characteristic of molecular adsorption. Therefore, the second model is more appropriate for describing the salt ion effects on molecular adsorption at colloidal particles. This is not surprising if we consider the relative size of sodium ion and MG molecule, as well as ΔG of sodium ion adsorption at PSS surface. Sodium ion can be considered a point charge compared to MG with a much larger size ($\sim 10 \text{ \AA}$). It has been reported that the free energy of sodium ion adsorption onto negatively charged surfaces can be as low as 1 M^{-1} [42]. The compete adsorption model doesn't actually take place, and it is the significant drop in adsorption free energy ΔG upon addition of NaCl that results in decreasing surface density of MG. Also need to mention that since ΔG is becoming smaller as NaCl concentration increases, a higher density of PSS particle ($6 \times 10^8 \text{ particle/mL}$) was used in this series of experiment to ensure sufficient depletion of MG from bulk solution in order to determine maximum adsorption density N_{\max} (see discussion in previous section). The plot of isotherms therefore has different x-axis scale in Fig. 5.4 and Fig. 5.6 due to this reason.

In addition to ionic strength effect, ion specificity on molecular adsorption at charged PSS surface has also been studied. A series of inorganic salt with different cations were tested. As was done similarly for NaCl, PSS colloids pre-covered with MG molecules were titrated with a series of chloride salts: LiCl, NaCl, KCl, NH_4Cl . The

titration profiles (Fig. 5.8) are almost identical for all four chlorides used which implies that they all have same effect on the free energy ΔG of MG adsorption at PSS surface. No ion specificity effects have been observed for molecule-surface interaction at charged PSS surface.

The free energy ΔG of MG adsorption at charged PSS surface will have significant change by varying solvent ionic strength but will not be affected by ion specificity. A molecule adsorbing from a bulk salt solution onto a charged colloidal surface will have to pass through the electric double layer of the interfacial region. The observed adsorption free energy for MG cation moving through the electric double layer can be expressed as [43-47]:

$$\Delta G = \Delta G_{electrostatic} + \Delta G_{chemical} \quad (5.3)$$

where $\Delta G_{electrostatic}$ is the electrostatic contribution due to the purely charge-charge interactions while $\Delta G_{chemical}$ is the nonelectrostatic contribution associated with the adsorption process (i.e., hydrogen bonding, dipole-dipole interactions, etc.). Here the electrostatic interaction as the dominating driving force for bringing a charged molecule to a charged colloidal surface is related to the electrostatic interfacial potential φ of the electric double layer:

$$\Delta G_{electrostatic} = N_A z e \varphi \quad (5.4)$$

where N_A is the Avogadro's number, z is the ion valency, and e is the elementary charge. Further, the Gouy-Chapman theory describes the exponential decay of the interfacial potential φ from a charged surface through an electric double layer. The

expression of the Gouy-Chapman model describes the dependence of the potential φ on the bulk electrolyte concentration c :

$$\varphi = \frac{2k_B T}{ze} \sinh^{-1} \left(\sigma \sqrt{\frac{\pi}{2\epsilon k_B T c}} \right) \quad (5.5)$$

where k_B is the Boltzmann constant, T is the Kelvin temperature, z is the valence of the electrolyte, σ is the surface charge density, and ϵ is the dielectric constant of the medium. Therefore, the adsorption energy can be expressed as the follows:

$$\Delta G = 2RT \sinh^{-1} \left(\sigma \sqrt{\frac{\pi}{2\epsilon k_B T c}} \right) \quad (5.6)$$

It is known that for hyperbolic function:

$$\sinh^{-1} x = \ln(x + \sqrt{x^2 + 1}) \quad (5.7)$$

And when $x \geq 4$, the expression can be approximated with $\leq 1\%$ error by:

$$\sinh^{-1} x = \ln(2x) \quad (5.8)$$

In our experimental conditions, the value of $\sigma \sqrt{\pi / 2\epsilon k_B T c}$ is always greater than 4.

Therefore, the approximation can be applied to the ΔG expression in equation 5.4:

$$\Delta G = 2RT \ln(2\sigma \sqrt{\frac{\pi}{2\epsilon k_B T}}) - RT \ln c \quad (5.9)$$

The surface charge density σ is modeled as the sum of the initial surface charge density of the sulfate group on PSS surface $N_{PSS}^{SO_3^-}$ and the maximum charge density established by the adsorbed MG at each given salt concentration $N_{PSS}^{MG^+}$:

$$\sigma = N_{PSS}^{SO_3^-} - N_{PSS}^{MG^+} \quad (5.10)$$

The PSS surface was fully covered by MG in the salt free situation so that $N_{PSS}^{MG^+}(c=0) = N_{PSS}^{SO_3^-}$. According to our fitting results (Table 5.2), the maximum adsorption density for MG decreased from about 90% of $N_{PSS}^{MG^+}(c=0)$ to about 55% when the salt concentration c had a 50 times increase from 1mM to 50mM. The change in magnitude of adsorption free energy Δ (ΔG) can be estimated by equation 12 to be 0.54kcal/mol, which is comparable to the difference of our fitting results (0.65 ± 0.07) kcal/mol.

5.4.3 Salt Ion Effects on MG Adsorption to Neutral PSC Surface

Similar salt titration experiments were performed to investigate salt ion effects on the molecule-surface interactions at the neutral PSC surface. Large amount of MG ($10\mu\text{M}$ MG for 1.1×10^8 particle/mL PSC) was added to maintain a relatively small surface coverage of PSC. An initial rise in SH signal showed as expected, however, when the MG saturated PSC was titrated with NaCl solution, the observation was shocking different from those titration profile curves obtained for PSS surface. The SH signal first increased as the salt concentration increased, once reached maximum, started to decrease and level off as the salt concentration further increase (Fig. 5.9 (a)). Similar to the PSS study, a blank titration control of PSC was also performed to ensure that the observed SH signal changes were caused by the NaCl applied (Fig. 5.9 (a)).

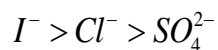
The changes of the SH signal reflect the changes of dye coverage on the surface in the same trend: the rise of SH signal indicates an increasing surface density of MG on PSC while the following decay of SH signal should be the result of a decreasing MG coverage. However, in the case of PSS, maximum adsorption densities can be determined

by using modified *Langmuir* model, while for PSC surface, standard *Langmuir* form has to be used due to insufficient depletion from bulk and maximum adsorption densities can no longer be obtained. As to the free energy values, intuitively, we might think that the addition of NaCl changed the free energy ΔG of MG adsorption at PSC surface in an opposite way to the changes on PSS surface. MG adsorption isotherms of PSC (1) without NaCl (0mM), (2) at NaCl concentration where SH intensity reaches peak value (44mM), (3) at NaCl concentration where SH intensity levels off (150mM), were obtained and analyzed by standard *Langmuir* model (Fig. 5.9 (b)). The fitting results summarized in Table 5.3 show that the free energy ΔG of MG adsorption at neutral PSC surface is independent of ionic strength of the solution. Therefore, the rise-decay observation of SH signal for neutral PSC surface cannot be attributed to ΔG change as was the case for charged PSS surface, which is understandable if we consider the dominant driving forces for the two distinct colloidal surfaces. As was discussed in the previous sections, for neutral PSC surface, the driving force for molecular adsorption is hydrophobic interactions rather than electrostatic interactions. The ionic strength, though may have great effect on electric potential, should have little influence on the hydrophobic driving force. Therefore, the nonelectrostatic hydrophobic contribution to the free energy for MG adsorption at neutral PSC surface should not be affected by the solvent ionic strength.

It has been well recognized that interfacial hydrophobic interactions are sensitive to specific ion effects, known as Hofmeister series. In order to understand the observed rise-decay in SH signal, ion specificity experiments were performed. Neutral PSC colloids pre-saturated with MG molecules were titrated with sodium salts of different

anions: I^- , Cl^- , SO_4^{2-} and chlorides with different cations: Li^+ , Na^+ , K^+ , NH_4^+ . The SH intensities as function of salt concentrations are plotted in Fig. 5.10. This time the SH intensity showed different response upon application of different ions. The observation of the difference in ion behavior due to ion identity is more prominent for anion series than for cation series, which is usually the case for most Hofmeister phenomenon.

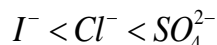
For the anion series, the I^- trail had most rise and least decay in SH signal while the SO_4^{2-} trail showed least rise but most decay. Since the SH signal is a direct reflection of the surface adsorbed MG density, we attribute the rise of SH intensity to the increased surface adsorption sites established by surface acquired anions. Colloidal interfaces more easily acquire a negative than a positive charge [48]. One of the reasons is that anions tend to bind unspecifically to interfaces, which follows Hofmeister series. Large inorganic anions like I^- , ClO_4^- , SCN^- adsorb to most interfaces [48]. Our experimental observation demonstrated that I^- trail had the most SH signal rise, followed by Cl^- , and SO_4^{2-} had the least rise, which exactly follows the Hofmeister series of decreasing surface affinity for the three anions:



However, the decay of the SH signal here is not due to decreasing surface adsorption sites, but due to the most well known ability of Hofmeister anions: to salt in (solublize) /salt out (aggregate) proteins by influencing hydrophobic interactions. Anions to the left of the series, like I^- , tend to salt in the proteins while anions to the right side of the series, like SO_4^{2-} , tend to cause aggregations and precipitate the proteins. Our anion titration profiles showed clearly that I^- trail had the least signal decay, followed by Cl^- , and SO_4^{2-} had

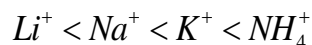
the most decay, which can be well interpreted by the positions of the ions in Hofmeister series: I^- is located at the very left of the whole Hofmeister series (see chapter 5.1) and tends to stabilize the colloids; while SO_4^{2-} is located at the very right side and tends to precipitate the colloids.

To further confirm the interpretation, MG adsorption isotherms on PSC surfaces at featured ionic strengths for the anion and cation series were obtained and analyzed using standard *Langmuir* form (Fig. 5.11). The fitting results of adsorption free energies are listed in Table 5.4. For both ionic strengths, 50mM where SH intensities reached peak values and 150mM where SH intensities showed prominent decreases, the magnitude of ΔG increases through the series:



The changes in ΔG for different anions indicated electrostatic contribution resulting from the interactions between MG and the surface acquired anions. It is not surprising that MG has strongest binding with the divalent anion SO_4^{2-} .

Similar experiments and analysis were performed for the cation series (Fig. 5.10 (b), Fig. 5.11 (c) (d)). Since it is the surface acquired anions that are responsible for the SH intensity rises, varying the identity of cations has little further influence on the signal rise (Fig. 5.10 (b)). On the other hand, the Hofmeister cations also have the abilities to salt in/salt out proteins and the ability to precipitate proteins follows:



In the cation series experiments, the SH signal decay of the titration profiles indicates the ability of cations in precipitating colloids. Observations in Figure 5.10 (b) demonstrated

that the decay effect of the SH intensity did follow the Hofmeister cation series, where NH_4^+ has the most effect on precipitating colloids, followed by K^+ , Na^+ , Li^+ , sequentially. The adsorption free energy under the influence of cation series were also obtained and summarized in Table 5.5. For both featured ionic strengths, the ability to reduce the magnitude of ΔG follows the series:

$$NH_4^+ > K^+ > Na^+ > Li^+$$

Though the effects are less prominent for cation series, the trend is still quite clear.

5.5 Summary

Both PSS and PSC colloidal particles are hydrophobic in nature but with charged and neutral terminations, respectively, therefore can serve as comparable colloid models. MG can be used as an SHG indicator to study salt ion effects on the molecule-surface interactions.

For MG adsorption at charged PSS surface, the adsorption isotherm was obtained and modified *Langmuir* analysis yields the adsorption free energy as well as the maximum adsorption number density. The dominant driving force is electrostatic interactions between MG cation and negatively charged sulfate termination. In this case, the electrostatic contribution of the adsorption free energy depends on the interfacial electric potential, which can be related to ionic strength of the solvent salts through Gouy-Chapman model. Therefore, for electrostatic force dominating molecule-surface interactions, ionic strength, rather than ion specificity, will have significant effects on the magnitude of the free energy. The higher the ionic strength, the smaller the magnitude of adsorption free energy, and the smaller the maximum adsorption density, as a result.

For MG adsorption at neutral PSC surface, the situation is completely different. Analysis of adsorption isotherm using standard *Langmuir* form only allows determination of adsorption free energy, while maximum adsorption density cannot be obtained due to insufficient depletion from bulk solution. The dominating driving force in this case is hydrophobic interactions between hydrophobic regions of the dye and particle surface. The nonelectrostatic hydrophobic contribution to the adsorption free energy will no longer be affected by ionic strength of the solution. Specific ion effects, the Hofmeister series, are highly responsible for the observed ion behaviors on molecule-surface interactions. Salt anions tend to bind unspecifically to the PSC colloidal surface and the surface acquired anions will provide more adsorption sites for MG cations. The interpretation is confirmed by the fact that the anion affinity to surface exactly follows the Hofmeister series. And furthermore, anion identity will influence the adsorption free energy and the change in ΔG for different anions reflects electrostatic interaction between MG and anion. At the same time, the salt ions also have salt out effects on colloids that will cause aggregation and precipitation. The experimental observations agree very well with both Hofmeister anion and cation series in the ability to precipitate. The trend is more prominent for anions than for cations.

In summary, MG can be used as a SHG indicator to study salt ion effects on the molecule-surface interactions and distinct effects have been identified for different colloidal surfaces.

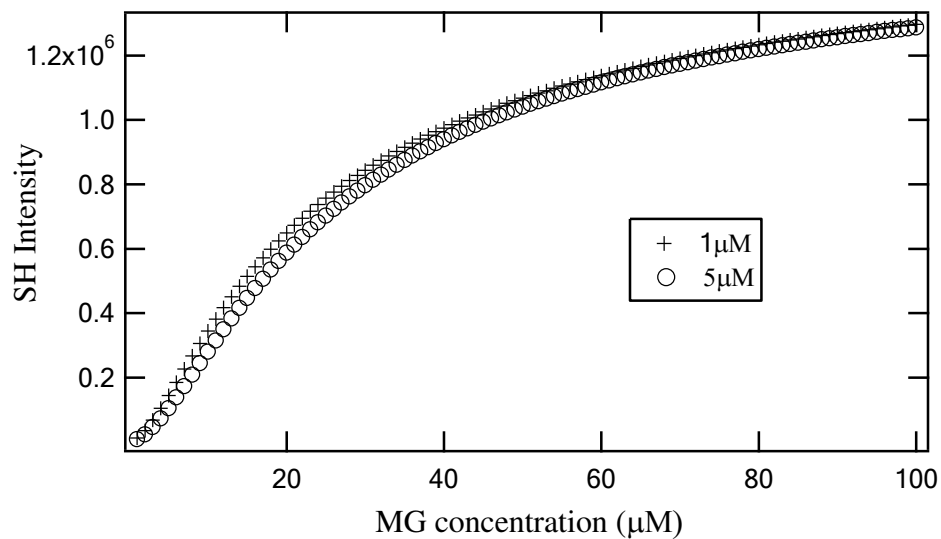
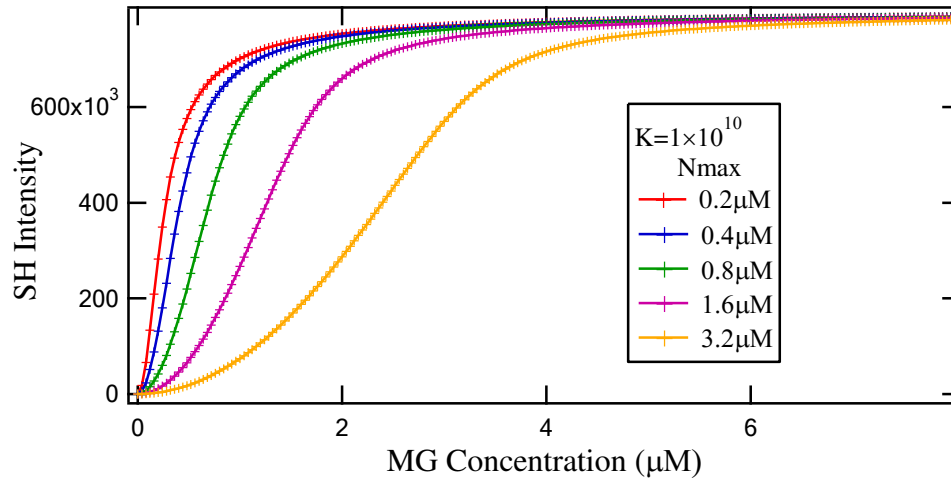


Figure 5.1: A theoretical simulation of the modified *Langmuir* model with the adsorption equilibrium constant set to a small value ($5 \times 10^7 \text{M}^{-1}$) for different maximum surface adsorption densities ($1 \mu\text{M}$ and $5 \mu\text{M}$).

(a)



(b)

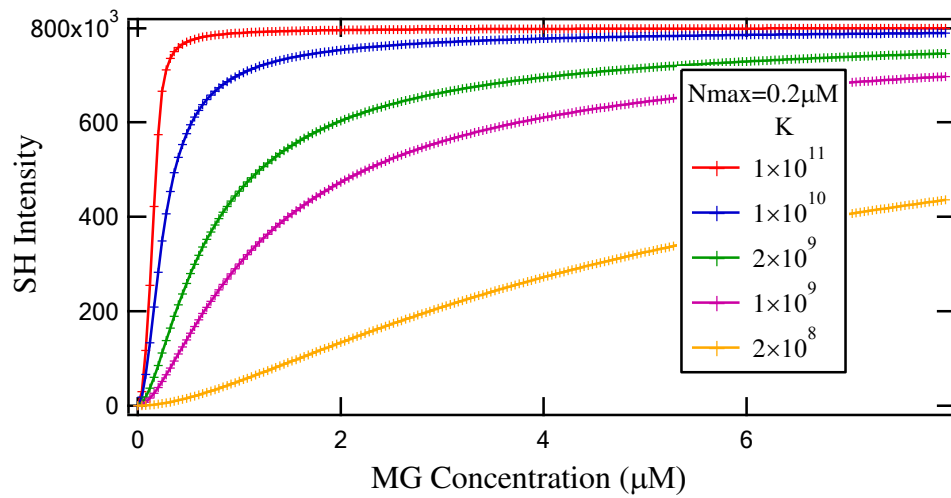


Figure 5.2: Theoretical simulations of the modified *Langmuir* isotherms expressed in SH intensity as a function of MG concentration: (a) isotherms at a fixed value of adsorption equilibrium constant ($K = 10^{10}$) by varying maximum adsorption density; (b) isotherms at a fixed value of maximum adsorption density ($N_{\text{max}} = 0.2 \mu\text{M}$) by varying adsorption equilibrium constant.

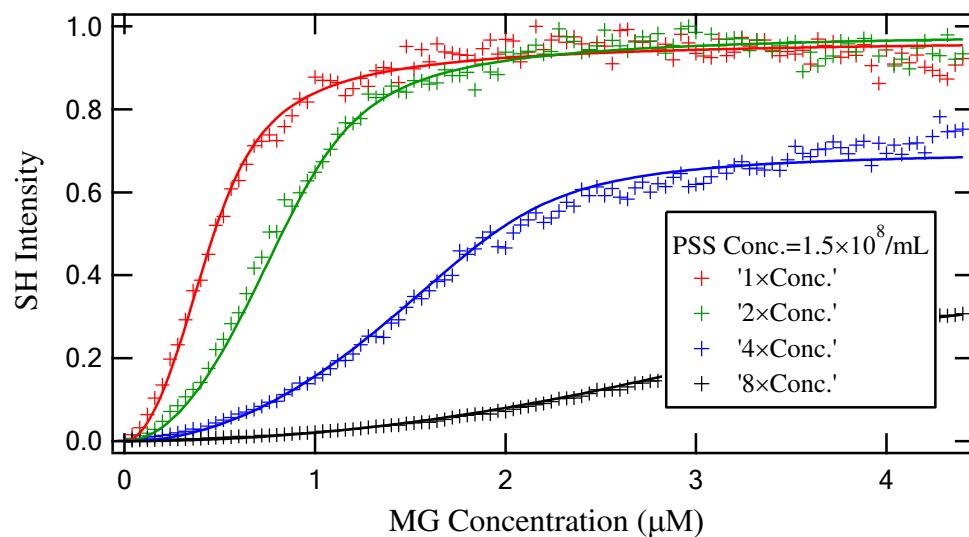
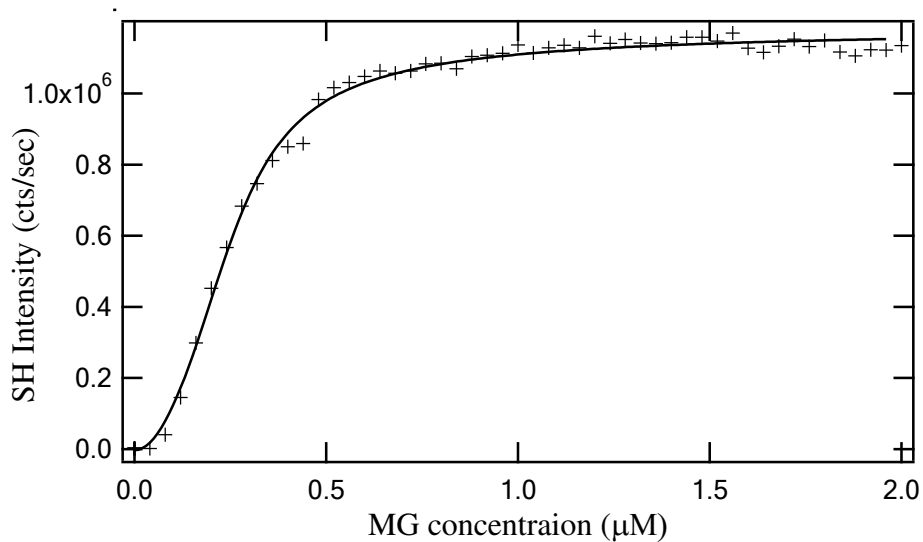


Figure 5.3: An example of analyzing a set of adsorption isotherms of malachite green (MG) molecules on polystyrene sulfate (PSS) surface by Global Fitting. The concentrations of the colloids were fixed with ratios: 1:2:4:8. The solid lines are the fitting results.

(a)



(b)

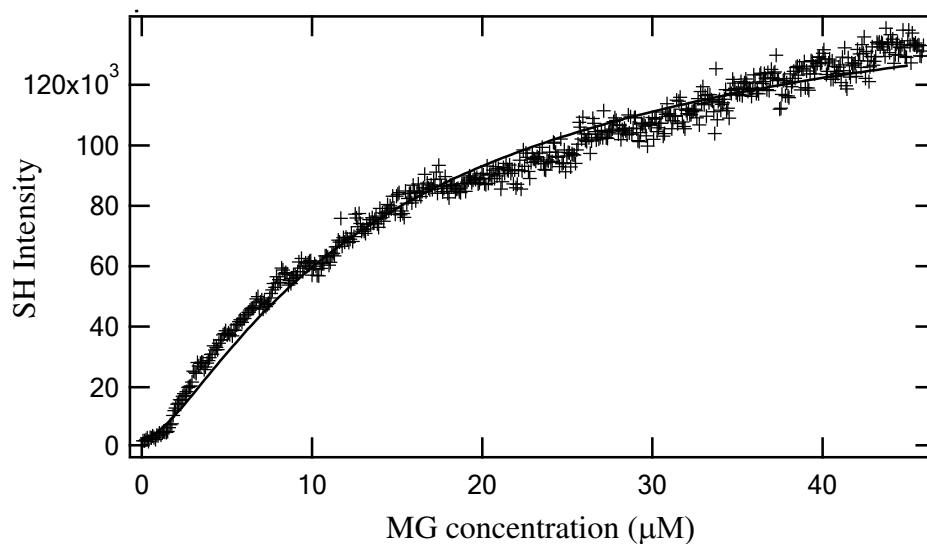


Figure 5.4: SH intensity detected as a function of MG concentration added in the colloidal solution of (a) charged polystyrene sulfate microspheres (PSS); and (b) neutral polystyrene carboxyl microspheres (PSC) particle surfaces, at $\text{pH} = 3.5 \pm 0.2$. The solid line is a nonlinear least-square fit of (a) a modified *Langmuir* model; and (b) a standard *Langmuir* model.

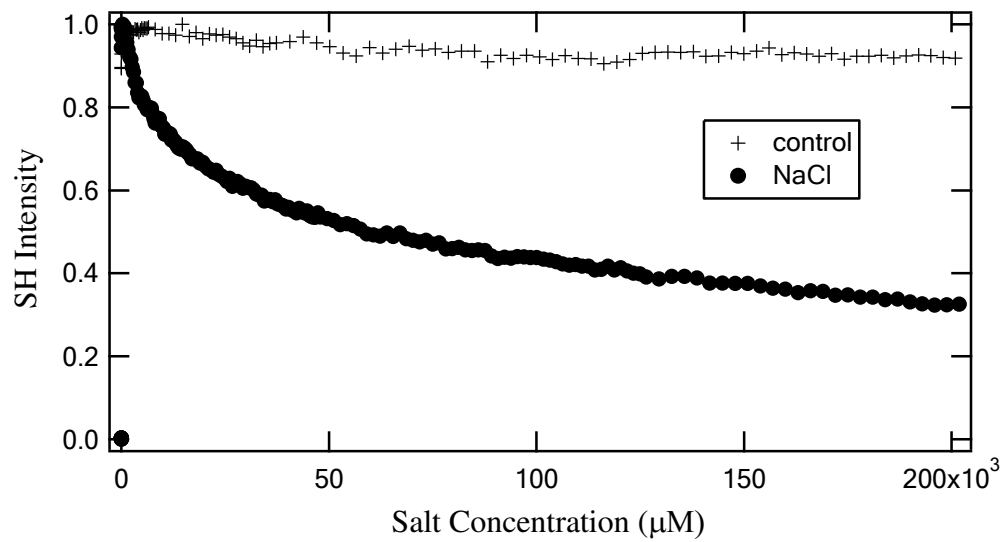


Figure 5.5: SH intensity recorded as a function of NaCl concentration added in the MG fully covered PSS colloidal solutions. Also displayed is the control trial titrated with blank solution without NaCl.

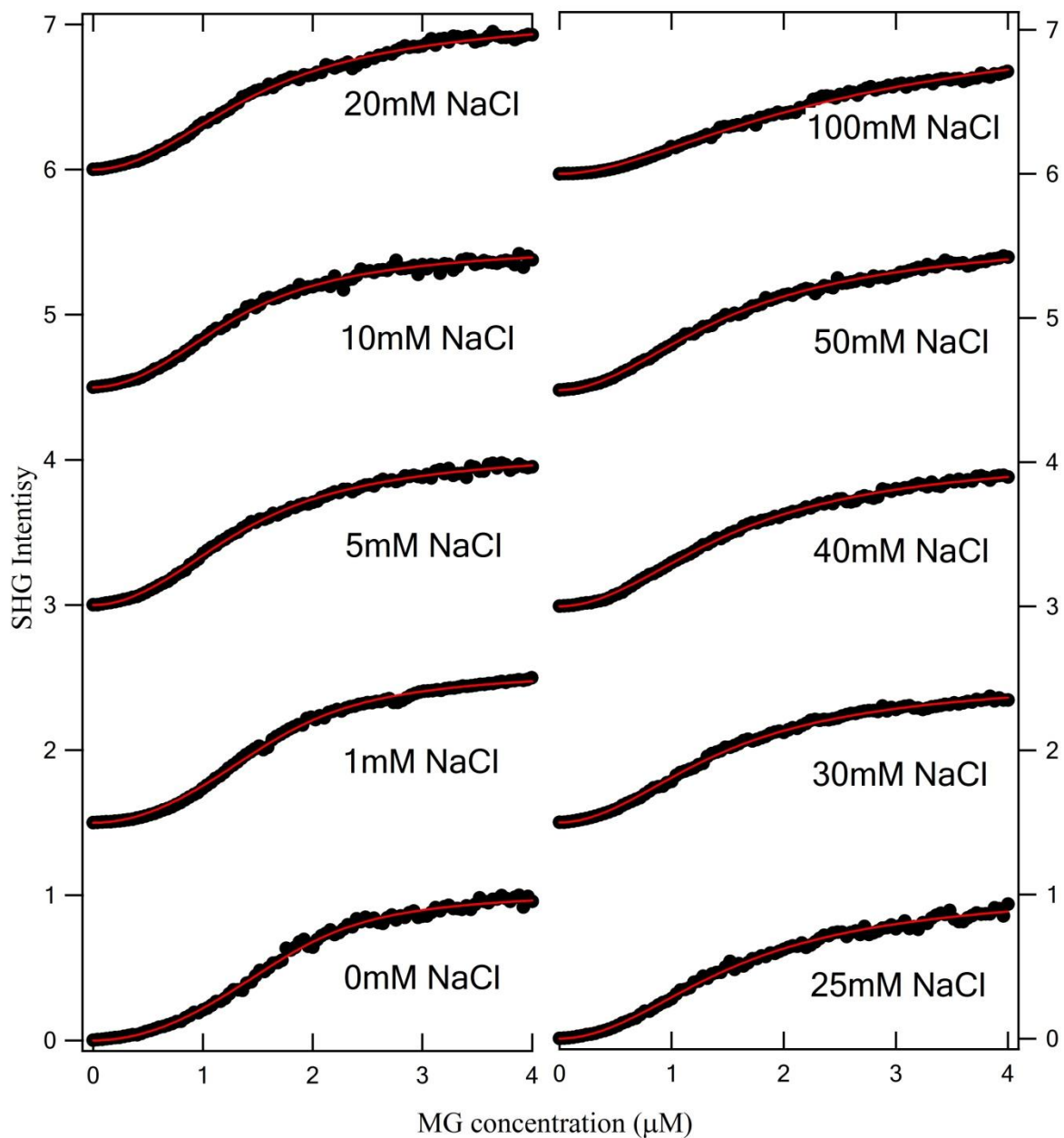
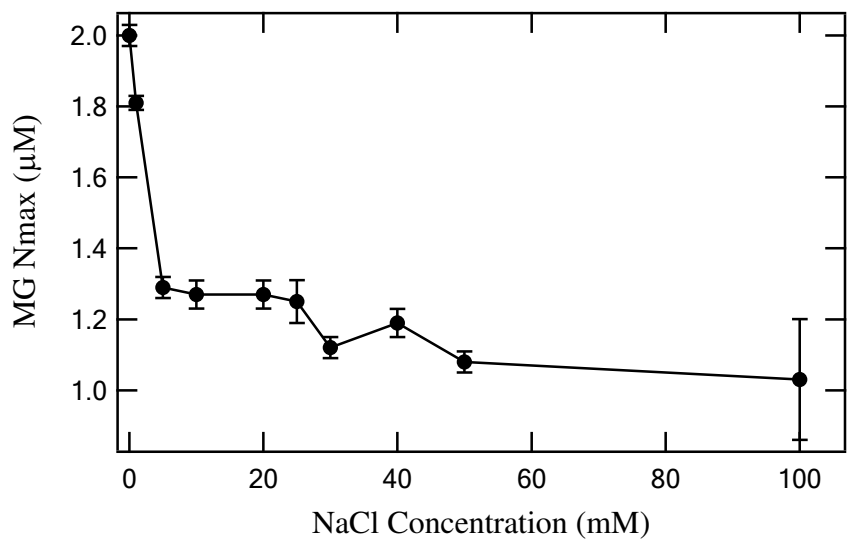


Figure 5.6: MG adsorption isotherms on PSS surfaces at different NaCl concentrations.

The solid red lines are nonlinear least-square fits of the modified *Langmuir* model.

(a)



(b)

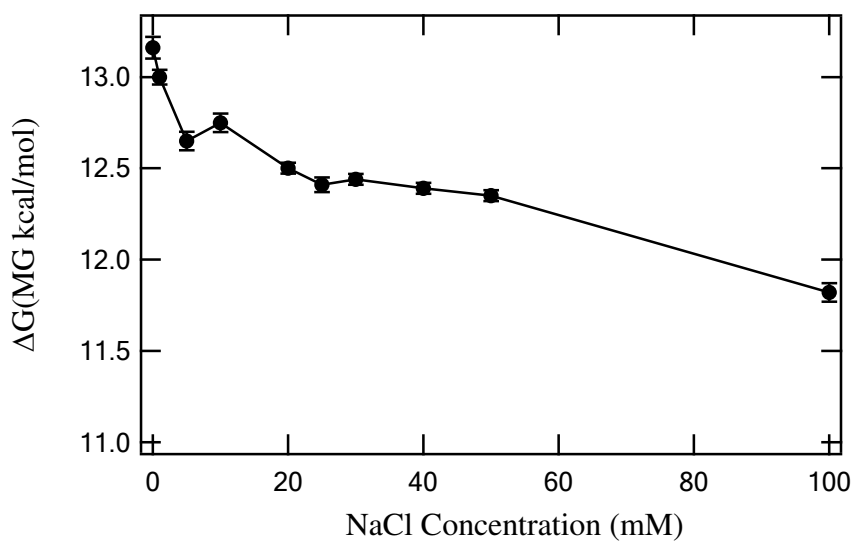


Figure 5.7: Dependence of (a) adsorption maximum density N_D^{\max} and (b) free energy ΔG on NaCl concentration.

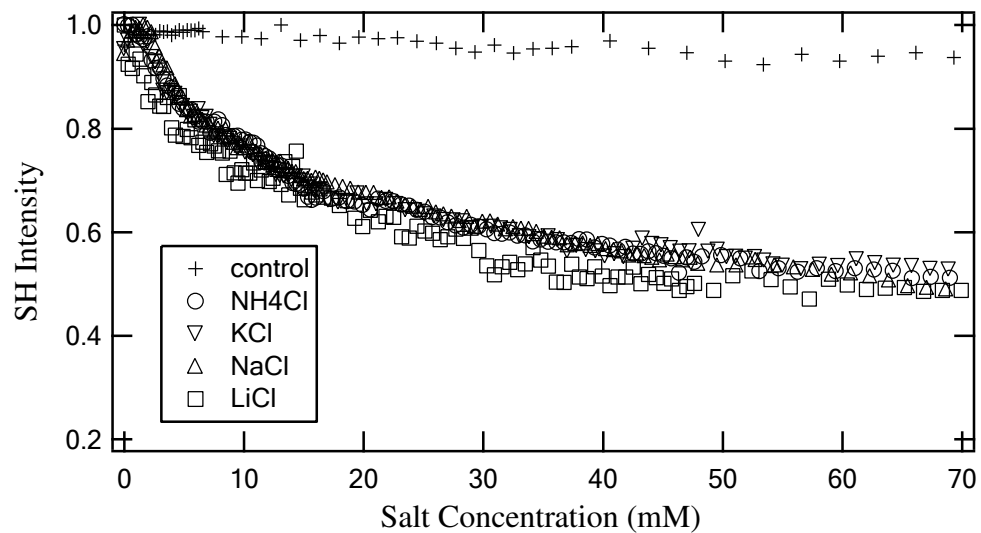


Figure 5.8: Titration profiles of a series of chloride salts: LiCl, NaCl, KCl, NH₄Cl into PSS colloids pre-covered with MG.

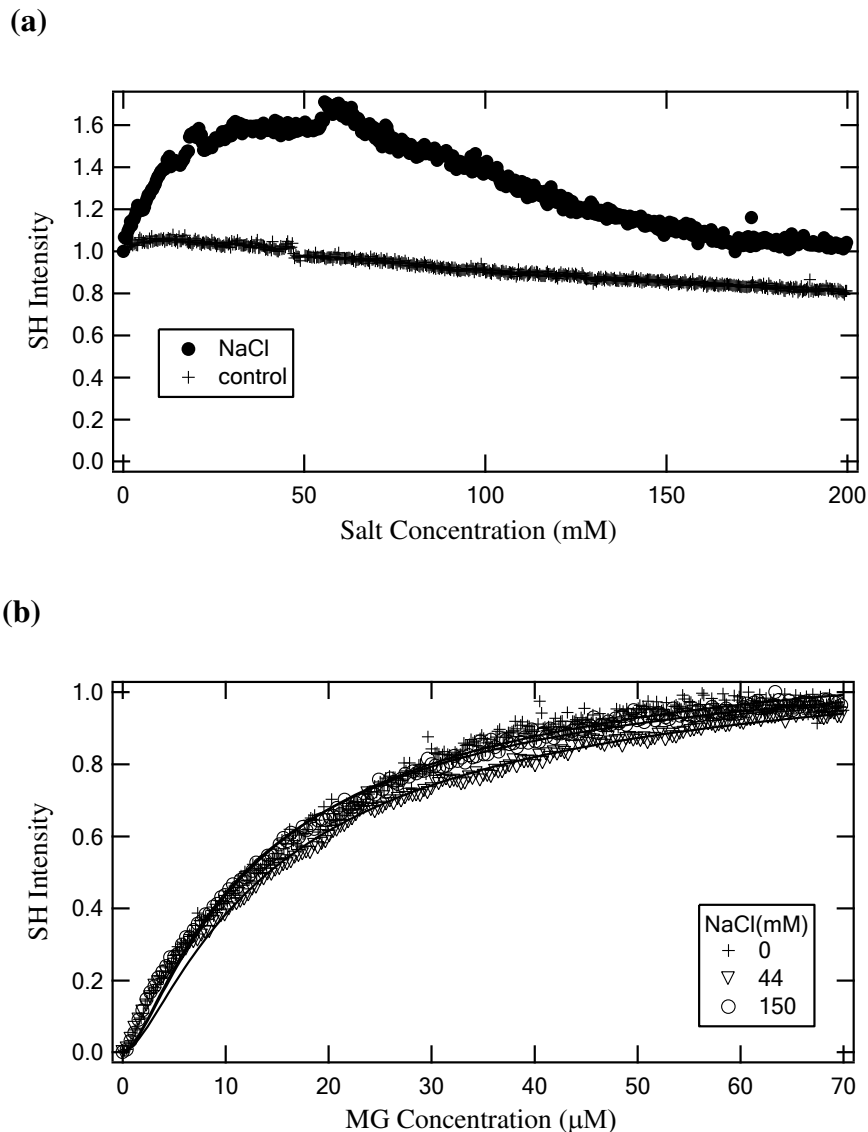


Figure 5.9: (a) SH intensity recorded as a function of NaCl concentration added in the MG fully covered PSC colloidal solutions. Also displayed is the control trial titrated with blank solution without NaCl. (b) MG adsorption isotherms of PSC (1) without NaCl (0mM); (2) at NaCl concentration (44mM) where SH intensity reaches peak value; (3) at NaCl concentration (150mM) where SH intensity levels off. The solid lines are nonlinear least-square fits of the standard *Langmuir* model.

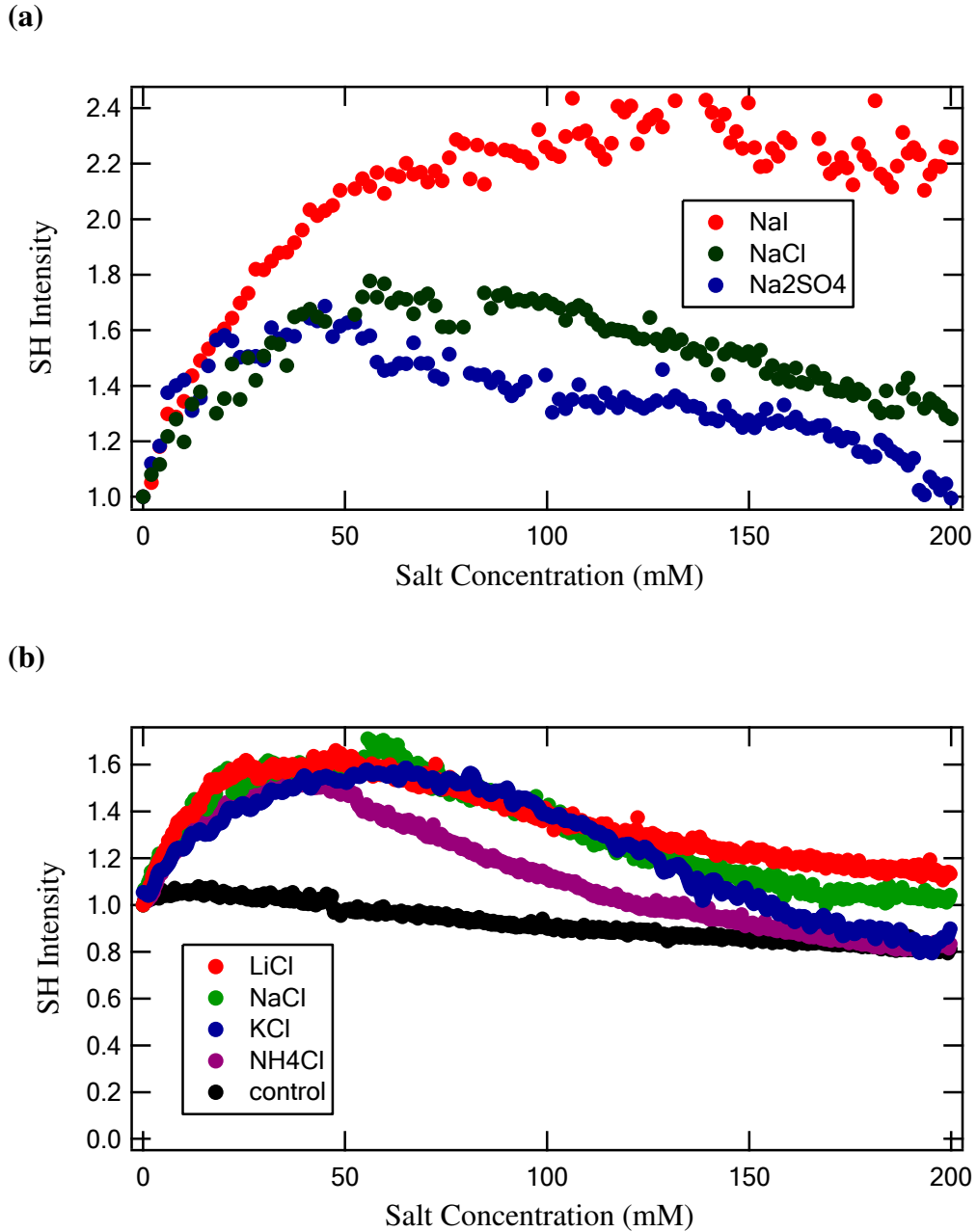
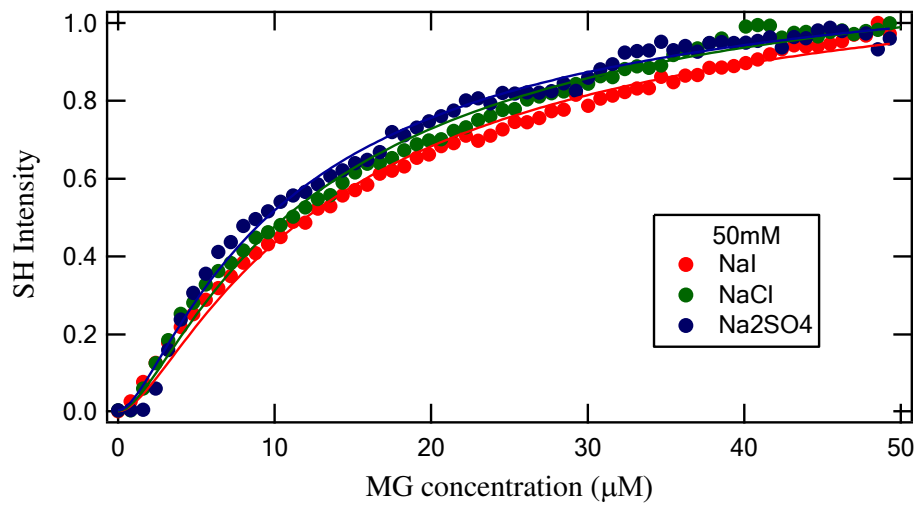
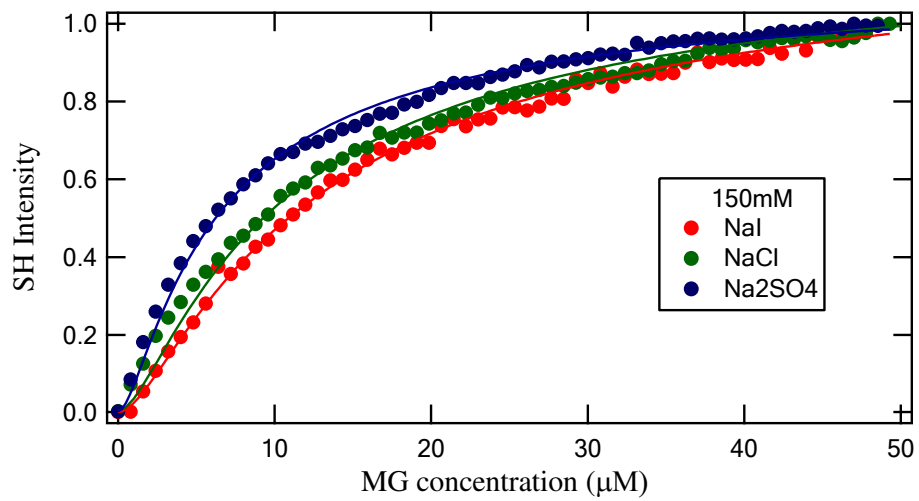


Figure 5.10: SH intensities as function of salt concentrations of (a) sodium salts of different anions: I^- , Cl^- , SO_4^{2-} ; and (b) chlorides with different cations: Li^+ , Na^+ , K^+ , NH_4^+ ; applied into PSC colloids pre-saturated with MG molecules.

(a)



(b)



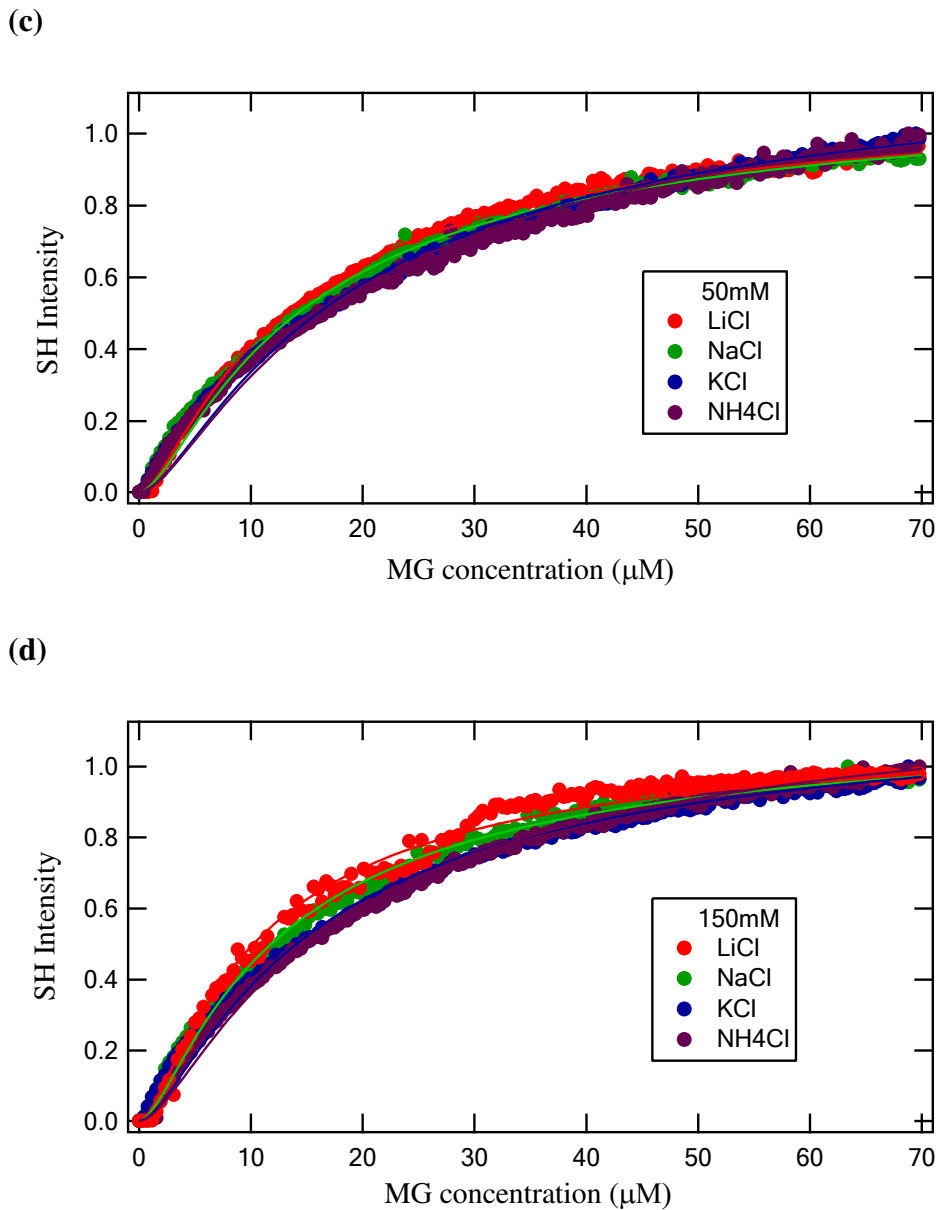


Figure 5.11: MG adsorption isotherms on PSC surfaces at featured ionic strengths for the anion series: I^- , Cl^- , SO_4^{2-} at (a) 50mM; (b) 150mM; and the cation series: Li^+ , Na^+ , K^+ , NH_4^+ at (c) 50mM; (d) 150mM. The solid lines are nonlinear least-square fits of the standard *Langmuir* model.

Table 5.1: Global fitting results versus individual fitting results of MG adsorption at PSS surface

	Global Fitting	Individual Fitting
N_{max} (1×Conc.)	(0.49±0.01)μM	(0.52±0.02)μM
N_{max} (2×Conc.)	(0.95±0.01)μM	(0.97±0.02)μM
N_{max} (4×Conc.)	(2.14±0.02)μM	(1.50±0.05)μM
N_{max} (8×Conc.)	(4.26±0.17)μM	(6.40±0.25)μM
K (1×Conc.)	(1.2±0.1)×10 ¹⁰ M ⁻¹	(1.2±0.1)×10 ¹⁰ M ⁻¹
K (2×Conc.)	(1.2±0.1)×10 ¹⁰ M ⁻¹	(1.2±0.1)×10 ¹⁰ M ⁻¹
K (4×Conc.)	(1.2±0.1)×10 ¹⁰ M ⁻¹	(1.2±0.1)×10 ¹⁰ M ⁻¹
K (8×Conc.)	(1.2±0.1)×10 ¹⁰ M ⁻¹	(1.2±0.1)×10 ¹⁰ M ⁻¹

Table 5.2: Dependence of adsorption maximum density N_D^{\max} and free energy ΔG on NaCl concentration.

NaCl (mM)	N_{\max} (μM)	ΔG (kcal/mol)
0	2.00 ± 0.03	13.16 ± 0.06
1	1.81 ± 0.02	13 ± 0.04
5	1.29 ± 0.03	12.65 ± 0.05
10	1.01 ± 0.02	12.75 ± 0.05
20	1.27 ± 0.04	12.50 ± 0.03
25	1.25 ± 0.06	12.41 ± 0.04
30	1.12 ± 0.03	12.44 ± 0.03
40	1.19 ± 0.04	12.39 ± 0.03
50	1.08 ± 0.03	12.35 ± 0.03
100	1.03 ± 0.17	11.82 ± 0.05

Table 5.3: Adsorption equilibrium constant and free energy of MG on PSC surface (1) without NaCl (0mM); (2) at NaCl concentration (44mM) where SH intensity reaches peak value; (3) at NaCl concentration (150mM) where SH intensity levels off.

NaCl (mM)	K (M⁻¹)	-ΔG (kcal/mol)
0	(8.5±0.1)×10⁷	10.7±0.1
44	(7.6±0.1)×10⁷	10.6±0.1
150	(9.1±0.1)×10⁷	10.7±0.1

Table 5.4: Adsorption equilibrium constant and free energy of MG on PSC surface at featured ionic strengths: (a) 50mM and (b) 150mM, for the anion series: I^- , Cl^- , SO_4^{2-} .

(a)		
50mM	K (M^{-1})	$-\Delta G$ (kcal/mol)
NaI	$(8.2 \pm 0.2) \times 10^7$	10.7 ± 0.1
NaCl	$(8.6 \pm 0.2) \times 10^7$	10.7 ± 0.1
Na₂SO₄	$(10.4 \pm 0.3) \times 10^7$	10.8 ± 0.1
(b)		
150mM	K (M^{-1})	$-\Delta G$ (kcal/mol)
NaI	$(8.9 \pm 0.2) \times 10^7$	10.7 ± 0.1
NaCl	$(10.7 \pm 0.2) \times 10^7$	10.8 ± 0.1
Na₂SO₄	$(18.1 \pm 0.4) \times 10^7$	11.2 ± 0.1

Table 5.5: Adsorption equilibrium constant and free energy of MG on PSC surface at featured ionic strengths: (a) 50mM and (b) 150mM, the cation series: Li^+ , Na^+ , K^+ , NH_4^+ .

(a)		
	K (M⁻¹)	-ΔG (kcal/mol)
LiCl (37.0mM)	(8.4±0.1)×10⁷	10.7±0.1
NaCl (44.0mM)	(7.6±0.1)×10⁷	10.6±0.1
KCl (54.5mM)	(6.0±0.1)×10⁷	10.5±0.1
NH4Cl (33.5mM)	(5.7±0.1)×10⁷	10.4±0.1
(b)		
150mM	K (M⁻¹)	-ΔG (kcal/mol)
LiCl	(1.1±0.1)×10⁸	10.9±0.1
NaCl	(9.1±0.1)×10⁷	10.7±0.1
KCl	(7.2±0.1)×10⁷	10.6±0.1
NH4Cl	(6.3±0.1)×10⁷	10.5±0.1

Bibliography

1. Radovic, L.R., et al., *An experimental and theoretical study of the adsorption of aromatics possessing electron-withdrawing and electron-donating functional groups by chemically modified activated carbons*. Carbon, 1997. **35**(9): p. 1339-1348.
2. Matijevic, E., *Interactions of solutes with monodispersed colloids - practical aspects*, in *Adsorption and Its Applications in Industry and Environmental Protection, Vol I: Applications in Industry*. 1999, Elsevier Science Publ B V: Amsterdam. p. 847-878.
3. Aray, Y., et al., *Electrostatics for exploring the nature of water adsorption on the laponite sheets' surface*. J. Phys. Chem. B, 2003. **107**(34): p. 8946-8952.
4. Eckenrode, H.M., et al., *Adsorption of a cationic dye molecule on polystyrene microspheres in colloids: Effect of surface charge and composition probed by second harmonic generation*. J. Phys. Chem. B., 2005. **109**(10): p. 4646-4653.
5. Zhang, Y.J. and P.S. Cremer, *Interactions between macromolecules and ions: the Hofmeister series*. Curr. Opin. Chem. Biol., 2006. **10**(6): p. 658-663.
6. Tobias, D.J. and J.C. Hemminger, *Chemistry - Getting specific about specific ion effects*. Science, 2008. **319**(5867): p. 1197-1198.
7. Hofmeister, F., *Zur Lehre von der Wirkung der Salze*. Arch Exp Pathol Pharmacol 1888. **24**: p. 247-260.
8. Omta, A.W., et al., *Negligible effect of ions on the hydrogen-bond structure in liquid water*. Science, 2003. **301**(5631): p. 347-349.

9. Kropman, M.F. and H.J. Bakker, *Dynamics of water molecules in aqueous solvation shells*. Science, 2001. **291**(5511): p. 2118-2120.
10. Kropman, M.F. and H.J. Bakker, *Effect of ions on the vibrational relaxation of liquid water*. J. Am. Chem. Soc., 2004. **126**(29): p. 9135-9141.
11. Batchelor, J.D., et al., *Impact of protein denaturants and stabilizers on water structure*. J. Am. Chem. Soc., 2004. **126**(7): p. 1958-1961.
12. Chalikian, T.V., *Structural thermodynamics of hydration*. J. Phys. Chem. B, 2001. **105**(50): p. 12566-12578.
13. Gurau, M.C., et al., *On the mechanism of the Hofmeister effect*. J. Am. Chem. Soc., 2004. **126**(34): p. 10522-10523.
14. Jungwirth, P. and D.J. Tobias, *Specific ion effects at the air/water interface*. Chem. Rev., 2006. **106**(4): p. 1259-1281.
15. Gopalakrishnan, S., et al., *Air-liquid interfaces of aqueous solutions containing ammonium and sulfate: Spectroscopic and molecular dynamics studies*. J. Phys. Chem. B, 2005. **109**(18): p. 8861-8872.
16. Gopalakrishnan, S., et al., *Vibrational spectroscopic studies of aqueous interfaces: Salts, acids, bases, and nanodrops*. Chem. Rev., 2006. **106**(4): p. 1155-1175.
17. Petersen, P.B. and R.J. Saykally, *Comment on "Interfacial pH at an isolated silica-water surface"*. J. Phys. Chem. B, 2006. **110**(30): p. 15037-15038.
18. Ghosal, S., et al., *Electron spectroscopy of aqueous solution interfaces reveals surface enhancement of halides*. Science, 2005. **307**(5709): p. 563-566.

19. Wang, H., et al., *Second harmonic generation from the surface of centrosymmetric particles in bulk solution*. Chem. Phys. Lett., 1996. **259**(1-2): p. 15-20.
20. Wang, H.F., et al., *Energetics and population of molecules at microscopic liquid and solid surfaces*. J. Phys. Chem. B, 1998. **102**(23): p. 4446-4450.
21. Wang, H.F., et al., *In situ, nonlinear optical probe of surfactant adsorption on the surface of microparticles in colloids*. Langmuir, 2000. **16**(6): p. 2475-2481.
22. Eckenrode, H.M. and H.L. Dai, *Nonlinear optical probe of biopolymer adsorption on colloidal particle surface: Poly-L-lysine on polystyrene sulfate microspheres*. Langmuir, 2004. **20**(21): p. 9202-9209.
23. Malvezzi, A.M., et al., *Melting-induced enhancement of the second-harmonic generation from metal nanoparticles*. Phys. Rev. Lett., 2002. **89**(8).
24. Russier-Antoine, I., et al., *Multipolar contributions of the second harmonic generation from silver and gold nanoparticles*. J. Phys. Chem. C, 2007. **111**(26): p. 9044-9048.
25. Jen, S.H. and H.L. Dai, *Probing molecules adsorbed at the surface of nanometer colloidal particles by optical second-harmonic generation*. J. Phys. Chem. B, 2006. **110**(46): p. 23000-23003.
26. Jen, S.H., G. Gonella, and H.L. Dai, *The effect of particle size in second harmonic generation from the surface of spherical colloidal particles. I: experimental observations*. J. Phys. Chem. A, 2009. **113**(16): p. 4758-4762.

27. Wang, H.F., et al., *Adsorption at a carbon black microparticle surface in aqueous colloids probed by optical second-harmonic generation*. J. Phys. Chem. C, 2007. **111**(25): p. 8708-8715.
28. Langevin, D., *Optical methods for studying microemulsions and microemulsion interfaces*. Ber. Bunsen-Ges. Phys. Chem. Chem. Phys., 1996. **100**(3): p. 336-343.
29. Yan, E.C.Y., Y. Liu, and K.B. Eisenthal, *New method for determination of surface potential of microscopic particles by second harmonic generation*. J. Phys. Chem. B, 1998. **102**(33): p. 6331-6336.
30. Zeng, J., H.M. Eckenrode, and H.-L. Dai, *Time-Resolved Molecular Transport across Living Cell Membranes*. to be submitted.
31. Zeng, J., H.M. Eckenrode, and H.-L. Dai, *Molecular interaction with murine erythroleukemia (MEL) cell membrane probed by second harmonic generation*. to be submitted.
32. Liu, Y., et al., *Surface potential of charged liposomes determined by second harmonic generation*. Langmuir, 2001. **17**(7): p. 2063-2066.
33. Srivastava, A. and K.B. Eisenthal, *Kinetics of molecular transport across a liposome bilayer*. Chem. Phys. Lett., 1998. **292**(3): p. 345-351.
34. Yan, E.C.Y. and K.B. Eisenthal, *Effect of cholesterol on molecular transport of organic cations across liposome bilayers probed by second harmonic generation*. Biophys. J., 2000. **79**(2): p. 898-903.
35. Liu, Y., E.C.Y. Yan, and K.B. Eisenthal, *Effects of bilayer surface charge density on molecular adsorption and transport across liposome bilayers*. Biophys. J., 2001. **80**(2): p. 1004-1012.

36. Shang, X.M., et al., *Effects of counterions on molecular transport across liposome bilayer: probed by second harmonic generation*. J. Phys. Chem. B, 2001. **105**(51): p. 12816-12822.
37. Liu, J., et al., *Antibiotic assisted molecular ion transport across a membrane in real time*. Faraday Discuss., 2005. **129**: p. 291-299.
38. Liu, J., et al., *Second Harmonic Studies of Ions Crossing Liposome Membranes in Real Time*. J. Phys. Chem. B, 2008. **112**(48): p. 15263-15266.
39. Petersen, P.B. and R.J. Saykally, *On the nature of ions at the liquid water surface*. Annu. Rev. Phys. Chem., 2006. **57**: p. 333-364.
40. Bian, H.T., et al., *Increased interfacial thickness of the NaF, NaCl and NaBr salt aqueous solutions probed with non-resonant surface second harmonic generation (SHG)*. Phys. Chem. Chem. Phys., 2008. **10**(32): p. 4920-4931.
41. Bian, H.T., et al., *Specific Na⁺ and K⁺ cation effects on the interfacial water molecules at the air/aqueous salt solution interfaces probed with nonresonant second harmonic generation*. J. Chem. Phys., 2009. **130**(13): p. 11.
42. Gennis, R.B., *Biomembranes: Molecular Structure and Function*. 1989, New York: Springer-Verlag.
43. Langmuir, D., *Aqueous Environmental Geochemistry*. 1997, Upper Saddle River, NJ: Prentice Hall.
44. Morel, F.M.M. and J.G. Hering, *Principles and Applications of Aquatic Chemistry*. 1993, New York: John Wiley & Sons, Inc.
45. Stumm, W. and J.J. Morgan, *Aquatic Chemistry*. 3rd ed. 1996, New York: John Wiley & Sons, Inc.

46. Castro, A., K. Bhattacharyya, and K.B. Eisenthal, *Energetics of adsorption of neutral and charged molecules at the air/water interface by second harmonic generation: hydrophobic and solvation effects*. J. Chem. Phys., 1991. **95**(2): p. 1310-1315.
47. Malin, J.N., J.G. Holland, and F.M. Geiger, *Free energy relationships in the electric double layer and alkali earth speciation at the fused silica/water interface*. J. Phys. Chem. C, 2009. **113**(41): p. 17795-17802.
48. Evans, D.F. and H. Wennerström, *The Colloidal Domain- where physics, chemistry, biology, and technology meet*. 2nd ed. 1999, New York: Wiley-VCH.

CHAPTER SIX

CONCLUDING REMARKS

6.1 Perspective Applications

Membrane transport has long been an intriguing concentration of study and a substantial knowledge base has been established through experimental observations and theoretical interpretations. Besides the small essential metal ions, it is highly desired to study the transport of drug molecules in order to understand the pharmacokinetics and to achieve appropriate drug formulations. The exploit of amino acid-based drugs [1], peptide-based drugs [2], antibody drugs [3] as well as small molecule drugs [4] are closely associated to the quantitative determination of membrane adsorption and transport kinetics of amino acids, peptides, proteins as well as small molecules. It has been reported that approximately 40% of the small molecules that are emerging as new drug candidates have poor aqueous solubility and are hydrophobic ions [4]. In this thesis we proposed an experimental means based on the nonlinear optical phenomenon – second harmonic generation -- to study time-resolved membrane transport kinetics of small hydrophobic molecular ions. The molecular probe we used was the hydrophobic ion

malachite green dye. The molecular structure, size, as well as its hydrophobicity are a good mimic of small molecule drug candidates.

In addition, the SHG technique can also be applied as a useful method to study various factors that may affect membrane transport kinetics. In this thesis, we've initiated the study of salt ion effects on modulating colloidal/protein behaviors in solutions using SHG technique. Adsorption processes at both neutral and charged colloidal particles employed as globular protein models have been characterized and ion concentration effects as well as ion identity effects have been identified. As has been demonstrated, SHG technique can serve as a powerful experimental means to probe in-situ adsorption processes occur at biological surfaces and all kinds of environmental factors can be investigated, such as the gating effect of ion channels upon applied transmembrane voltages, the channel blocker mechanism, as well as the changing of in-situ solution conditions (i.e. pH values, ionic strength, ion identity, viscosity, isotonicity) across the biological membrane.

6.2 Feasibility

The surface specific SHG technique can be feasible as long as two conditions are satisfied: an intense laser pulse source and a nonlinear medium. According to the SHG principle (chapter two), when the incident fundamental or the generated second harmonic frequency is in resonance with that of a molecular transition, the magnitude of the second order susceptibility will be greatly enhanced, which allows easy detection of SHG signal. It is obvious that most of the drug candidates are lack of center of inversion symmetry, therefore, will have non-zero second order molecular polarizability which is the radiation source of second harmonic generation. Adsorption spectra can be easily obtained for

these candidate drug molecules. Therefore, the application of the SHG technique in studying membrane surface adsorption processes and cross-membrane drug delivery mechanisms can be applied to almost all kinds of small molecule drug candidates as long as an appropriate incident laser wavelength is chosen.

Bibliography:

1. Kanai, Y. and H. Endou, *Heterodimeric amino acid transporters: Molecular biology and pathological and pharmacological relevance*. *Current Drug Metabolism*, 2001. 2(4): p. 339-354.
2. Herrera-Ruiz, D. and G.T. Knipp, *Current perspectives on established and putative mammalian oligopeptide transporters*. *Journal of Pharmaceutical Sciences*, 2003. 92(4): p. 691-714.
3. Fesinmeyer, R.M., et al., *Effect of Ions on Agitation- and Temperature-Induced Aggregation Reactions of Antibodies*. *Pharmaceutical Research*, 2009. 26(4): p. 903-913.
4. Liu, J., H. Lee, and C. Allen, *Formulation of drugs in block copolymer micelles: Drug loading and release*. *Current Pharmaceutical Design*, 2006. 12(36): p. 4685-4701.